STUDIES OF A VERTICAL FALLING FILM REACTOR

by

Jose Manuel Guzman Bello

A thesis submitted to the University of Aston in Birmingham for the degree of Doctor of Philosophy.

Department of Chemical Engineering
The University of Aston in Birmingham

Studies of a Vertical Falling Film Reactor

by

Jose Manuel Guzman Bello

Ph.D. July 1981

Summary

An extensive review of literature has been carried out on the hydrodynamics of falling films and the mass transfer from the gas phase into the liquid film.

The experimental work has been divided into three parts mainly: (1) Entrance region, droplet entrainment and minimum wetting rate; (2) Measurements have been made of the film thickness, when flowing cocurrently with a turbulent gas stream, using an ultrasonic probe; (3) Mass transfer rate of dilute ammonia gas into water and into an aqueous sulphuric acid solution.

A vertical tubular film reactor was built to study the above, consisting of a 2.04 m long "perspex" tube with an I.D. of 0.3 m, and a concentrically arranged stainless steel pipe with an O.D. of 0.22 m.

The behaviour of the falling film was investigated using five different liquids, with viscosities ranging from 10^{-3} Ns/m^2 to 6.10^{-2} Ns/m^2. Gas flowrates in the range from 175 Kg/h to 1000 Kg/h and liquid flowrates from .1 m^3/s to .4 m^3/s were studied. The experimental data has been correlated with distance along the length of the column and the flow parameters. The behaviour of the liquid film at the entry region was investigated and good agreement was obtained between the Nusselt's Theory and the experimental results.

A mathematical model of the hydrodynamics of the system has been derived, taking into consideration the shear at the interface. This was solved numerically by an appropriate computer program. The simulation results were analysed by a semiempirical relationship to predict the surface velocity, friction factor at the interface and the velocity profile in the liquid film. Flow conditions, under which droplet entrainment or film rupture occurred were experimentally determined and have been compared with existing criteria.

Physical and chemical absorption experiments were carried out under the same hydrodynamic condition to determine the mass transfer coefficients, $k_g a$ and $k_l a$. The effect on the hydrodynamics on the interfacial area and the enhancement were analysed theoretically.

Keywords

Film thickness, droplet entrainment, mass transfer coefficients, vertical falling film reactor, 2-phase cocurrent flow.

ACKNOWLEDGEMENTS

The author wishes to express his thanks to his Supervisor, Professor G.V. Jeffreys, for his encouragement and for providing the facilities for research. He also wishes to thank Mr. P. Murray and the rest of the technical staff for their assistance in fabricating the equipment and in the photographic work. Ministerio de Energia y Minas de Venezuela for their financial support, Miss L. Bryan for her help, and Mrs. N. Armstrong for her diligence in typing the thesis.

C O N T E N T S

LIST OF APPENDICES

LIST OF FIGURES

LIST OF TABLES

CHAPTER I

INTRODUCTION

Chemical engineering process involving two-phase gas-liquid flow are encountered in industrial operations such as gas-absorbing distillation towers, packed columns, evaporators, boilers, chemical reactors, etc. The obvious importance of this subject has resulted in a substantial amount of research literature. Annular two-phase flow is perhaps the simplest case of two-phase flow. In this type of flow a thin liquid film flows either down or up a solid wall with a gas stream adjacent to the liquid surface. This topic has been extensively studied by several authors including Hewitt and Taylor (1), Wallis (2) and Duckler (3). However, in spite of this, no reliable information is available for the design of plant scale cocurrent gas-liquid downward flow systems. The attention of most research workers have concentrated on the study of counter-current flow, which is the one that is most commonly found in heat exchangers.

The study of falling films have been generally concerned with its stability and flow pattern. Falling film absorbers have been used as standard laboratory equipment for the determination of the mass transfer coefficients (see Morris and Jackson (4), Norman (5) and Sherwood, Pigford and Wilke (6)). A comprehensive analysis of the hydrodynamics of falling films and its effect on the rate of heat andmass transfer has not been possible because of the complexity of the surface motion. The design of this type of absorber-reactors has been so far based largely on empirical correlations, obtained in small diameter (up to 2.5cm) systems, and generally assuming a

simple model for the hydrodynamics, using a parabolic velocity distribution in the liquid and a constant film thickness, as described by Nusselt (7,8)

The advantages of using a cocurrent downward system have been listed by Alves (9) as follows:

1. Continuous operation
2. Relative simplicity in its design
3. Low liquid hold-up
4. Good temperature control
5. Large interfacial area
6. No flooding, even at high gas flowrates
7. High mixing in the liquid film as a result of the surface motion
8. Easy contact-time control

Its main disadvantages are the long length of the column and the inherent instability of the film flow.

The principal aspects of the design of a vertical falling film reactor were investigated in this study following a semi-empirical approach. These were: entry effects, critical flowrates, hydrodynamic characteristics of the falling film when subject to high interfacial shear, and the effect of the above variables in the rate of absorption of a dilute gas into the liquid film, with and without chemical reaction.

In order to carry out the investigation a falling film reactor was designed and built, of the same size as most columns used in industry. The length of the contacting section of the column was 2.0 m with an inside diameter

0.3 m wide. The inside pipe had an outside diameter of 0.22 m. The liquid and gas phase were fed continuously into the top of the reactor and the liquid flowed downwards forming a thin film on the wall of each pipe or both as desired. The external pipe consisted of a "perspex" tube, enabling visual observation of the flow behaviour. The problem of determining the film thickness, without interfering with the flow, was solved by developing an ultrasonic probe technique. The efficiency of this kind of equipment depends to a large extent in obtaining an even and uninterrupted distribution of the liquid film; therefore great care was taken to guarantee that the column was vertical, the smoothness of its walls, and the determination of the flow parameters under which the liquid film would brake into rivulets or droplets would be sheared off by a cocurrent turbulent gas stream.

The complexity of the two-phase flow system must dictate a semi-empirical approach to this study. The film thickness was considered to be the characteristic parameter of the film flow. Experimental data on the thickness of the liquid film under conditions of high interfacial shear, have been related to reactor length, gas velocity and liquid flowrate and physical properties. A mathematical model of the hydrodynamics has been proposed, based on a phenomenological description of the flow. The model has been solved numerically, using experimental data to determine the boundary conditions.

The rate of transport across the interface has been previously found to be affected by the hydrodynamics of the falling film, i.e. Fulford (10), Hobler (11). The mass transfer coefficients for falling films have been experimentally determined by numerous researchers. For those conditions under which the liquid-side resistance can be neglected, most of the published literature agree with the work of Gilliland and Sherwood (12). They proposed an empirical correlation for k_g in terms of the Schmidt and Reynolds number of the gas phase, from the experimental data obtained using a column having an I.D. of 2.54 cm. However, Shilimkan (13,14) recently demonstrated the effect of pipe diameter on the rate of mass transfer. Liquid-side residual controlled absorption has been generally described by the penetration theory or by the surface removal theory developed by Danckwerts (15). Most of the previous works in this area, explained the increase in mass transfer as a consequence of the increase in the interfacial area; however, it has been suggested by several authors; i.e. Astarita (16), that the increase is due primarily to increases in the mixing at the interface, caused by the turbulent conditions in the gas stream. The existing uncertainty on the reliability of previous studies for the design of an industrial size absorber-reactor, has resulted in a need to carry out experimental studies on the effect of the film hydrodynamics rate of mass transfer, using a pilot plant reactor.

CHAPTER II

LITERATURE SURVEY

The systematic study of the flow of liquid films over solid vertical surfaces has been the subject of a vast number of experimental and theoretical investigations over the last 70 years. In 1964, Fulford (10) presented an extensive survey, listing the more significant results of the studies of the behaviour of liquid film flow, and of heat and mass transfer to films.

2.1 Hydrodynamics

As early as 1910, Hopf (18) made observations of the film thickness, surface velocity and wave formation in gravity induced film flow. Later; in 1916 van Nusselt (7, 8) produced what has become one of the most influential studies of the flow of smooth laminar films. Assuming that there are no surface waves, and that the falling film thickness is constant along the length of the wetted wall; he developed expressions for the film thickness and the directional velocity profile, as functions of the distance from the interface, the liquid flow rate per unit of wetted perimeter and its physical characteristics, density and absolute viscosity.

Nusselt reduced the Navier-Stokes equation of motion to the two-dimensional simplified form:

$$\frac{d^2u}{dy^2} + g\rho/\mu = 0 \qquad (2.1)$$

which, assuming no slip at the wall and no drag at the interface, gives rise to the following relationships:

The film thickness:

$$\delta_N = \left(\frac{3\Gamma\mu}{\rho g}\right)^{1/3} \tag{2.2}$$

Surface velocity,

$$u_s = \frac{g\delta^2}{2\nu} \tag{2.3}$$

and the velocity distribution

$$u = \frac{2u_s}{\delta}\,(y - y^2/2\delta) \tag{2.4}$$

That is, the velocity profile is assumed to be parabolic. However, the appearance of waves at the free surface greatly limits the applicability of Nusselt's theory. Kapitza (19) in 1943 was the first to try to solve this problem, by proposing an approximate steady periodic solution for the film thickness he obtained from an integral solution of the boundary layer momentum equation. Kapitza's theory has been proved to be inadequate for high flow rates by the experimental work of Jones and Whitaker (20), Stainthorp and Allen (21) and Tailby and Portalski (22, 23).

A large number of theoretical attempts have been made to predict the conditions under which waves are likely to occur. The common approach followed is to set up the main equations of flow, usually the Navier-Stokes equation or its simplified version by Nusselt, on which small perturbations are imposed. This leads to the formulation of an

Orr-Sommerfeld type of equation, Schlichting (23).

Benjamin (24) in 1957, concluded that films on vertical surfaces are always unstable, but he introduced the stabilizing effect of the surface tension, his results were later corroborated by the work of Yih (25).

In more recent years, considerable work has been undertaken to solve the Orr-Sommerfeld equation by several authors, among them, Lin (26), Krantz (27) Anhus (28) and Solesio (29), by introducing various approximations. However, all these treatments are lengthy and the most that has been obtained is a description of film flow under very limited conditions, such as very low Reynolds number. Therefore, they have very little relevance to this investigation.

Whitaker and Cerro (30), studied the effects of surface active materials on wave formation. They analysed the effects of properties such as "surface viscosity", "surface diffusion", and "surface elasticity", and concluded that "surface elasticity", which is related to the variations in the surface tension brought about by the surfactant, stabilizes the behaviour of falling vertical film. Their theoretical work consisted of the numerical integration of the Orr-Sommerfeld integration.

The presence of a free surface and the appearance of waves at relatively low flow rates, greatly complicates the definition of "the regimes of falling film flow". A commonly accepted classification, in the order of increasing

Reynolds number, is smooth laminar, wavy laminar and turbulent. The boundary between these regimes have been described in terms of Reynolds numbers; this has originated a large number of 'critical Reynolds numbers', as listed by Fulford (10).

A more realistic division for the falling film regimes takes into consideration the changing properties of the film not only with respect to the Reynold's number, but also with respect to distance in the direction of the flow.

Three zones are defined: the acceleration region, the smooth region and the wavy region. The acceleration zone is characterized by having a film thickness larger than that predicted by Nusselt, with a smooth surface. The flow is steady but non-uniform.

The zone of stabilized flow is governed by Nusselt's equations, therefore, it is steady and uniform, with a smooth surface.

The wavy region is characterized by its non-uniformity and instability. The inertia forces and the surface drag determine the behaviour of the film.

The combined length of the first two zones is relatively short with respect to the total length of the reactor. Considerable efforts have been made to understand the behaviour of the falling film in the wavy region. The most common methods found in the literature are: periodic steady state models, semi-empirical models and statistical analysis.

The first to attempt to describe the film behaviour using an oscillatory steady state solution of the equation of motion was Kapitza (19). His method is described by Levich (31), and has been further developed by Bushmanov (32). The model describing the hydrodynamics of the film is:

$$\frac{\sigma\bar{\delta}_o}{\rho}\frac{d^3\emptyset}{dx^3} + (c - \bar{u}_o)\left(c - \frac{9}{10}\bar{u}_o\right)\frac{d\emptyset}{dx} - \frac{3\nu}{h_o^2}(c - 3\bar{u}_o)\emptyset +$$

$$g - \frac{3\nu\,\bar{u}_o}{h_o^2} = 0 \qquad (2.5)$$

where $\emptyset$ is the free surface deformation function defined by

$$\delta = \bar{\delta}_o\,(1 + \emptyset) \qquad (2.6)$$

where $\bar{\delta}_o$ is the film thickness averaged over a wavelength, c wave celerity, and $\bar{u}_o$ is the average velocity for a cross section of width $\bar{\delta}_o$.

$\emptyset$ is a function of the celerity, the wavelength and the wave amplitude. Several values are found in the literature for the dimensionless ratio $c/\bar{u}_o$, and there is still disagreement whether it is constant or not.

Portalski (34), by applying Kapitza's theory, explained the generation of circulating eddies in a liquid falling film. This particular problem was further analyzed by Massot, Irani and Lightfoot (35), whose work differs from

Kapitza's by including a term $\nu(\delta^2 u/\delta x^2)$ from the Navier-Stokes equation and by deriving v, the y component of velocity as a function of distance, time and film thickness. An attempt was made to determine mathematically the streamlines of the wavy motion. An interesting feature of this model is that it does not pressupose a surface shape.

Semiempirical methods to describe the behaviour of falling films consist of using a model developed for single phase flow in pipes, neglecting the effect of waves on the free surface. Duckler and Bergelin (36) in 1952, used the universal velocity profile to describe the falling film behaviour. The U.V.P. was developed by von Karman (37) and Nikuradse (38) to describe the flow of liquid in pipes. Duckler (3) discarded the notion that falling film flow could be either laminar or turbulent and stated that "any theory studying momentum must consider combined mechanisms at all points in the film".

The basic equation in Duckler's approach:

$$\tau = \frac{1}{g} (\mu + \varepsilon\rho) \frac{du}{dy} \qquad (2.7)$$

which relates the shear stress to the velocity gradient. In the region near the wall, the eddy viscosity is very small and the shear stress becomes proportional to the velocity gradient. Away from the wall, as turbulence develops, the term $\varepsilon\rho$ increases with respect to the viscosity.

The eddy viscosity is defined for $0 < u_w y/\nu < 20$, by Deissler's empirical equation:

$$\varepsilon = n^2 uy(1 - e^{-n^2 uy/\nu}) \tag{2.8}$$

and for $u_w y/\nu > 20$, by von Karman's equation:

$$\varepsilon = \kappa \left(\frac{du}{dy}\right)^3 / \left(\frac{d^2u}{dy^2}\right)^2 \tag{2.9}$$

where n and κ are numerical constants.

The velocity profile, based on equation 2.8, was calculated numerically since there is no analytical solution for it.

The following expressions were developed by Duckler for the dimensionless film thickness (δ^+) and the Reynolds number

$$\delta^+ = g^{\frac{1}{2}} \rho \, \delta^{3/2} / \mu \tag{2.10}$$

$$Re = \delta^+(3.0 + 2.5 \ell n \, \delta^+) - 64 \tag{2.11}$$

Since the Reynold's number can be calculated, the film thickness can then be estimated by simultaneous solution of these two equations.

The most important contribution of Duckler's work is that, for the first time, the film velocity is not a unique function of the distance from the wall, but it does depend on the interfacial shear.

Kulov, Vorolitin, Malyusov and Zhavorankov (39) modified Duckler's theory to include the distribution of tangential stress in their description of the liquid film flow. Their expression for the average film thickness is:

$$\bar{\delta} = (\nu^2/g)^{1/3} \eta_\delta \qquad (2.12)$$

where η_δ is a dimensionless term, a function of the Reynolds number, and the dimensionless average discharge velocity of the liquid film $(\bar{u}/\sqrt{g\delta})$.

$$\eta_\delta = \frac{Re}{4(\bar{u}/\sqrt{g\delta})} \qquad (2.13)$$

Telles and Duckler (40) and Chu and Duckler (42,41) investigated the statistical characteristics of falling wavy films. Experiments were conducted for a wide range of gas and liquid Reynolds numbers and measurements of film thickness were taken using conductance probes. Duckler and his co-authors provided an excellent description of wavy flow and its behaviour under different conditions and a number of conclusions were drawm from their studies:

1. These are two types of waves, a large less frequent wave and a small regular wave (see figure 2.1).

2. The film is always thicker than a substrate. This minimum film thickness is independent of the gas rate.

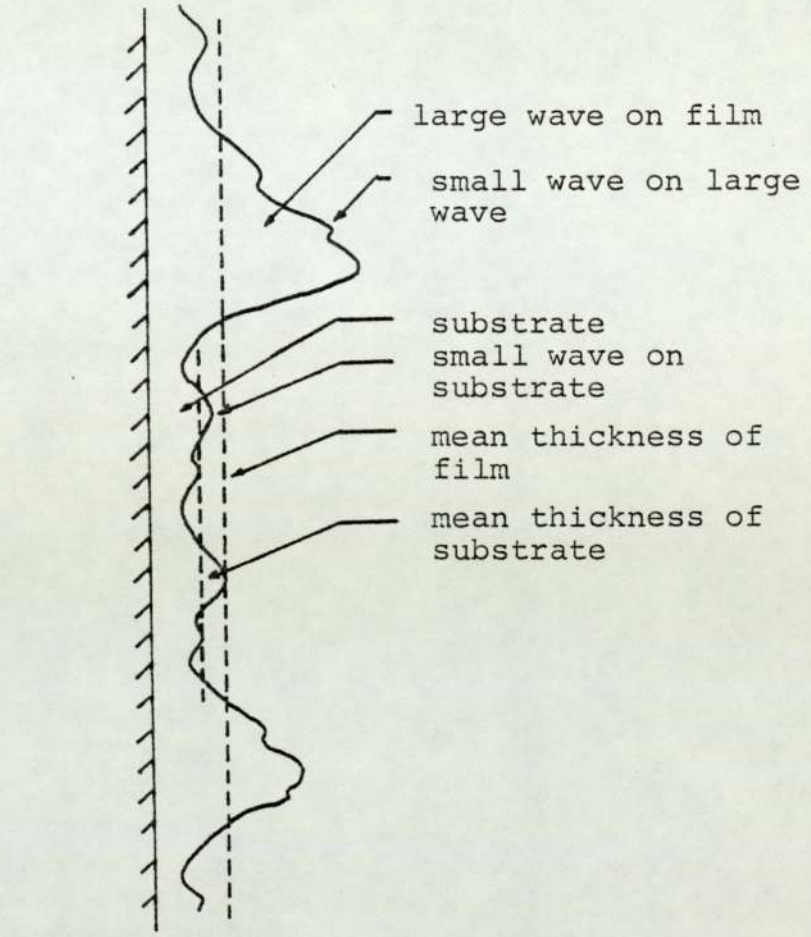

Figure 2.1 - Duckler's Wave Model

3. The large wave structures contribution to the total interfacial shear never exceeds 4%. Therefore, the increase pressure drop that takes place during two-phase flow is due to the small waves on the inter-phase.

4. As the velocity of the gas-phase is increased, the interfacial shear causes acceleration, spreading and thinning of the waves.

Salazar and Marschall (43) studied the variation of the statistical properties, not only with Reynolds number, but also with distance along the direction of the flow. The film thickness data was obtained using an optical method, described by Salazar (44). A decrease in the film thickness, as distance from the entry increased, was observed.

2.1.1 Film Thickness

The most obvious characteristics of the falling film is its thickness and a large amount of experimental work has been carried out to determine this, with many techniques described in the literature for the measurement of the film thickness. These techniques have been classed by Fulford as either direct or indirect, depending on whether they make direct contact with the liquid, such as electrical probes, or not such as photographic or light refraction methods.

Direct methods are undesirable, since any interference with the flow of such a thin film would create disturbances. Therefore, the accuracy of direct methods are questionable.

Extensive surveys on most of these techniques, including discussion of their advantages or disadvantages have been made by Portalski (45) and Hewitt (1). A confusing aspect found in the literature is the definition of what is actually being measured as "film thickness", and the interpretation of such measurements. There are, however, several possible meanings to this term;

1. The maximum height of the wave peak.

2. The average film thickness of the substrate.

3. The average film thickness taken over the entire surface of the film, at any particular time.

4. The time averaged thickness at any point on the column.

Early experimental data on the thickness of falling films were reported as a function of the Reynolds number only. Reducing the applicability of such correlations, when the film thickness of liquids, other than the one used by the investigator were estimated.

Two correlations were proposed by Fulford. The first is the film friction factor correlation, which is expressed as

1. Nusselt - eq. 2.2
2. Kapitza - eq. 2.5
3. Duckler (U.V.P.) - eq. 2.10
4. Kulov - eq. 2.12
5. Portalsk: (experimental measurements)

Figure 2.2 - Prediction of the Film Thickness

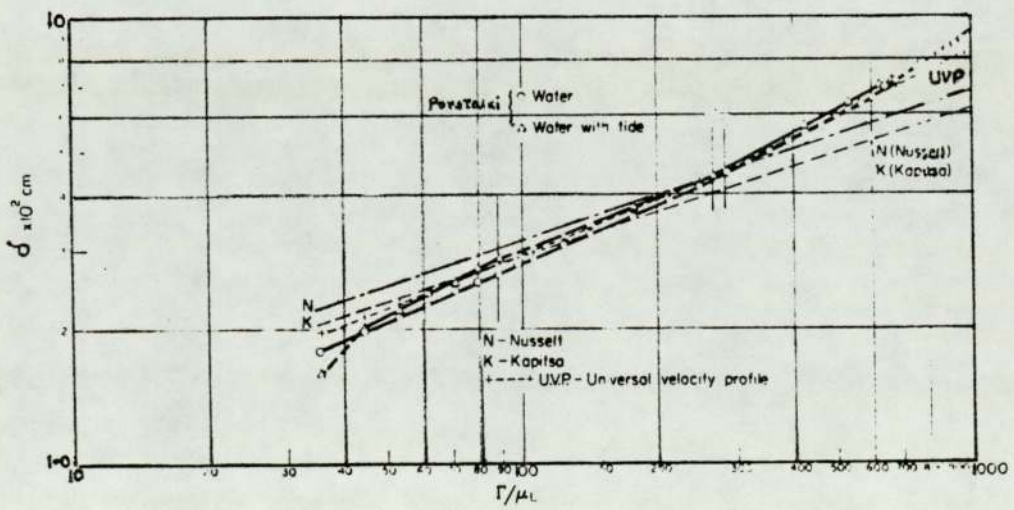

Figure 2.3 - Comparison of Predicted Film Thickness

$$f = \frac{2\delta^3 g}{\Gamma^2} \qquad (2.14)$$

Brauer (46) suggested that an expression of the friction factor as a function of the Reynolds number should correlate the film thickness. However, as Fulford (10) indicated, equation 2.14 represents the friction factor only when the falling film is steady and uniform.

The second correlation, which seems more realistic, uses a dimensionless film thickness defined as the Nusselt film thickness parameter (T):

$$T = \delta(g/\nu^2)^{1/3} \qquad (2.15)$$

Several correlations are found in the literature for the film thickness. The more relevant ones are listed in figure 2.2.

A comparison of such estimates with the theoretical predictions of Nusselt, Kapitza and Duckler is illustrated in figure 2.3.

2.1.2 Hydrodynamics of Falling Liquid Film with a Cocurrent Turbulent Gas Stream

Most of the above mentioned literature ignored the effect of the gas-phase fluid dynamics upon the liquid phase. However, several recent studies have clearly indicated the strong dependance of the mean film thickness and the wave surface structure on the interfacial shear stress.

The first systematic attempt to describe the effect of interfacial shear was made by Duckler (47) in 1959, who used the actual shear distribution and a two region eddy viscosity model in the momentum equation. Hewitt (1) in 1961, used Duckler's approach to relate the interfacial drag τ_i to the frictional pressure gradient.

$$\tau_i = \frac{(D - 2\delta)}{4} \frac{dP_F}{dx} \qquad (2.16)$$

where D is the pipe diameter. The frictional pressure drop was obtained using empirical correlations, such as the one proposed by Lockhart and Martinelli (117) in 1949. However, these empirical correlations have shown poor reliability when used beyond the range of data from which they were obtained, as shown by Duckler, Wicks and Cleveland (48) in 1964.

More recently, Henstock and Hanratty (49) proposed a model to predict the film thickness of the falling film and the interfacial drag, following the work of Duckler and Hewitt. A dimensionless group F was introduced, very similar to Martinelli's flow parameter.

$$F = \frac{\gamma}{Re_g^{\cdot 9}} \frac{\nu_{\cdot}}{\nu_g} (\rho_{\cdot}/\rho_g)^{\frac{1}{2}} \qquad (2.17)$$

where

$$\gamma = ((.707Re^{\cdot 5})^{2\cdot 5} + (.0379Re^{\cdot 9})^{2\cdot 5})^{\cdot 4} \qquad (2.18)$$

The ratio of the film thickness to the pipe diameter was found to be

$$\frac{\delta}{D} = \frac{6.59F}{(1 + 1400F)^{.5}} \qquad (2.19)$$

However, the main limitation of this model, as stated by its authors, is that the correlation is based entirely on measurements with the air-water system, this needs to be extended to other systems.

Recent experimental data has been reported by Kulov (50). Measurements were taken of the mean film thickness, pressure drop and interface film velocity using a 2.5 cms diameter pipe, with air velocities up to 50m/sec. Two regions were identified. The first one is characterized by a weak interaction between the phases, with the gas flow not affecting either the film thickness or the wavy surface. The second region is characterized by gas velocities over 5m/sec when the dimensionless film thickness was described by the equation

$$T = .266\ Re^{.6}\ Re_g^{-.1} \qquad (2.20)$$

A different approach to analyse data for frictional pressure drop is by correlation with a simplified physical mode; for example, the homogeneous flow model, which has the advantage of treating the two-phases as a single phase with averaged properties. However, no significant attempt to use this approach has been found in the literature. Duckler and co-workers (3) examined an approach through similarity analysis to correlate data for

frictional pressure drop. The approach consisted of obtaining a correlation based on the data for one single phase system, for the relationship between friction factor and Reynolds number. Once the relationship was found, the condition of dynamic similarity required the same relationship to apply for the two-phase system.

Several authors (51,52,53) have measured the interfacial shear and reported it in terms of the interfacial friction factor f_i

$$\tau_i = f_i \tfrac{1}{2} u_g^2 \rho_g \qquad (2.21)$$

Davies, Van Ouwerkerk and Venkatesh (54) developed an analytical solution, using a mathematical model based on the Navier-Stokes equation, assuming that the shear force is much larger than the gravitational force

$$\tau_i >> \rho g - (dP/dx) \qquad (2.22)$$

The film thickness was defined as

$$\delta = \left(\frac{2\Gamma\mu}{f_i \rho_g}\right)^{\frac{1}{2}} \frac{1}{u_g} \qquad (2.23)$$

where f_i is defined as in equation 2.21.

Hikita and Ishimi (55,56) described the hydrodynamics of a falling liquid film in the presence of either a laminar or turbulent gas stream. They used the equations of motions for gas and liquid, using the Prandtl mixing length model, as modified by Gill and Scher (57) to

describe the velocity profile in transition and fully developed turbulent gas flow

$$\tau = \mu_g \frac{du_g}{dy} + \rho_g (\ell \frac{du}{dy})^2 \qquad (2.24)$$

where ℓ is the mixing length as expressed by Gill and Sheer:

$$\ell = \kappa\, y(1 - e^{-\emptyset 2y/D})$$

were

$$\emptyset = \{(\sqrt{\sigma_i \rho_g}(R-\delta)/\mu_g) - 60\ /22 \qquad (2.25)$$

Using the above equations, a relationship was found to describe the friction factor, f_i, which was highly complex and could only be solved numerically.

Zhivaikin (58) proposed an empirical correlation for the film thickness, assuming a linear dependence on the gas velocity,

$$\delta = [1 - 0.022(ug-4)]\,\delta_N \qquad (2.26)$$

where ug is the gas velocity measured in ms^{-1}, which only affects the film thickness when it is greater than $4ms^{-1}$. The predicted results were in good agreement with the experimental data obtained using liquids in the range of $1cP < \mu < 8cP$, in a vertical tube of diameter 21mm and length 830mm.

Chung and Murgatroyd (59) and others considered the effect of the high interfacial shear on the surface of the liquid, forming rolling waves, and eventually leading to the entrainment of liquid drops by the gas stream. These studies are further analysed in Chapter 5 of this work.

2.2 Mass Transfer With or Without Chemical Reaction

Gas absorption in a liquid phase has been extensively studied in the past by several authors. Usually the study has been made of packed or plate columns or wetted walls down which the liquid flows under laminar conditions. However, the development of a reliable theoretical model for all these situations has been made difficult by the existance of a free interface, whose hydrodynamics are not fully understood. The classical approach to describe mass transfer across an interface are:

1. Whitman's film model (60), which assumed that resistance to mass transfer occurs only across a thin layer of stagnant liquid, of thickness h, at the surface. The bulk flow is assumed to be well mixed. The mass transfer coefficient was defined as

$$K_w = D/h \qquad 2.27$$

2. Higbie's penetration model (61), which is based on a surface-renewal argument. The concentration at the interface is kept constant for a fixed time τ_h, before being removed by the bulk flow. The time averaged mass transfer coefficient is described as

$$K_H = 2(D/\pi\tau_h)^{.5} \qquad 2.28$$

3. Danckwert's surface renewal theory (15) is a modification of the penetration model, the fresh elements of liquid are in contact with the gas phase for variable lengths of time, allowing for a random distribution of surface renewal, S. The mass transfer coefficient

is given by the expression

$$K_D = (DS)^{.5} \qquad 2.29$$

All three models described above involve the prediction of arbitrary parameters h, τ_H or S. This is done either experimentally or deduced from a physical representation of the system.

2.2.1 Laminar Film Flow

Ever since Vyazovov (62) first considered the problem in 1940, most of the published literature on gas absorption into a falling liquid film, with or without chemical reaction, have been for laminar flow, assuming a smooth surface, constant film thickness and a parabolic velocity profile as predicted by the Nusselt's theory. In the case of gas absorption accompanied by a first order chemical reaction, the distribution of the absorbed component in the liquid phase has the following form:

$$D \frac{\delta^2 c}{\delta y^2} = u(y) \frac{\delta c}{\delta x} + K_r C \qquad 2.30$$

For the case when only physical absorption takes place, the reaction rate constant, K_r, is zero. In 1954, Emmert and Pigford (63) studied the absorption of oxygen and carbon dioxide into water in a wetted wall column, a surfactant was added to eliminate the waves at the interface. They solved equation 2.30 and obtained the following expression for the logarithmic mean mass transfer coefficient in the liquid phase

$$K_{l,m} = \left(\frac{6D\Gamma}{\pi L \delta_N}\right)^{.5} \qquad 2.31$$

Emmert and Pigford were the first to demonstrate the increase in the mass transfer rate due to a wavy surface when the waves were surpressed by the addition of a surfactant, the data obtained was slightly higher than values predicted by the penetration theory. Kamei and Oishi (64) corroborated this, using a 2m. long vertical column to absorb carbon dioxide into water. They concluded that the effect of surface tension on the mass transfer coefficient was negligible. However, the conditions used in the experiment and the lack of sufficient data tends to invalidate such a conclusion. Other authors such as Nguiyjen-Li Carbonell and McCoy (65), Whitaker and Pigford (66), and Pelvan and Quinn (67) have extended the early work by Pigford (68,63) on the effect of surfactants on the resistance to mass transfer at the interface. Davidson and Cullen (69) used the same theoretical approach to measure diffusion coefficients using a wetted wall sphere. Olbrich and Wild (70) generalised Davidson and Cullen's approach and solved equation 2.30 for the ten sets of eigenvalues and eigenfunction coefficients. In 1971, Tamir and Taipel (71) analysed the same problem but made allowances in their model for the effect of a constant surface resistance. An earlier attempt to describe the gas absorption by a falling film, using the penetration theory was made by Lynn, Straatemeier and Kramer (72) in 1955, their major contribution was their observation on the entry and exit effects on the experimental determination of the mass

transfer coefficient.

Broetz (73) used the mass transfer coefficient as defined by the penetration theory (2.28), substituting τ_h as follows

$$\tau_h = \frac{1}{1.5} \frac{L\delta}{\Gamma} \qquad 2.32$$

Up to the Reynolds number 2360, Broetz assumed δ to be defined by Nusselt's equation reducing equation 2.32 to Pigford's equation (equation 2.31). Above such Reynolds number, Broetz defined the film thickness by his own empirical correlation. The introduction of the mixing coefficient, K_M gives relevance to this approach to be used instead of the diffusion coefficient for Reynolds numbers above 1200.

$$K_M = D \frac{Re}{1200} \qquad 2.33$$

In a recently published paper, Best and Horner (74) solved equation 2.30 for the case of gas absorption with chemical reaction, using Kummer's function (confluent hypergeometric). This method consists of substituting into the dimensionless form of equation 2.34.

$$\frac{\delta^2\alpha}{\delta z^2} = (1 - z^2) \frac{\delta\alpha}{\delta\theta} + \psi\alpha \qquad 2.34$$

Where α is the dimensionless concentration (c/c_i), z is the dimensionless distance from the interface $((\delta-y/\delta))$ θ is the dimensionless time of exposure $(LD/u_s\delta^2)$ and ψ is the dimensionless reactor parameter $(K_r\delta^2/D)$.

The boundary conditions are

$$\text{B.C.1} \quad \theta=0, \quad 0 < z < 1 \quad \alpha = 0 \qquad 2.35$$

$$\text{B.C.2} \quad \theta>0, \quad z = 0 \quad \alpha = 1 \qquad 2.36$$

$$\text{B.C.3} \quad \theta>0, \quad z = 1 \quad \frac{\delta\alpha}{\delta z} = 0 \qquad 2.37$$

Kummer's technique introduces T and Z, function of $\emptyset$ and z only. Eigenvalues and coefficients were found for a range of the reaction parameter. They concluded that the film thickness and velocity profile affect the mass transfer rate only when $\psi < 5$.

In 1980, Kalthod and Ruckenstein (75) analysed and compared the increase in the rate of mass transfer due to the mixing created by the wavy motion of the fluid with the increase due to rapid drop in concentration at the interface, as the absorbed component disappears by chemical reaction. An equation similar to Danckwert's was obtained for the mass transfer coefficient, K_L

$$K_L \sim \sqrt{D\omega + DK_r} \qquad 2.38$$

where ω is the wave frequency. Kapitza's theory is used to describe the motion of waves and the resulting velocity profile. The equation of convective-diffussion with first order reaction was solved by the penetration theory. This work is based on previous studies by Ruckenstein (76) and Ruckenstein and Barbente (77). They concluded that for

fast reaction rates, the mixing due to the wave motion has no effect on the rate of mass transfer.

A solution based on the boundary layer theory was proposed by Brauer (46,78) who used the definition for the mass transfer coefficient to describe Whitman's model, assuming that the resistance to mass transfer takes place across the whole film. So equation 2.27 can be written as

$$K_L = D/\delta \qquad 2.39$$

As we know, the boundary layer theory assumes a rectilinear velocity profile which relates the film thickness to the superficial shear stress. Brauer's work was reviewed by Hobler and Kedzierski (79) in their state of the art published in 1967; Brauer's mass transfer coefficients were reported in the form of the Sherwood number as functions of the Reynolds number. However, Hobler concluded that Brauer's equation were derived by using "somewhat artificial" assumptions. A more recent attempt to apply the boundary layer theory to describe gas absorption a a moving interface was made by Boyadiev and Mitev (80), the Sherwood number are expressed as functions of the phase linear velocities and the solubility of the absorbed component. The film thickness is not taken into consideration in their analysis, reducing the adequacy of their approach when applied to systems other than deep channels.

With the exception of Ruckenstein and co-workers, all the above reviewed literature fails to include in their analysis the increase in the rate of mass transfer due to

the existence of waves at the interface, which, as has been previously mentioned, happens at even very small Reynolds number. Howard and Lightfoot (81) developed a model predicting rates of gas absorption in terms of the tangential surface velocity, using the surface stretch modification of the penetration theory as first expressed by Angelo, Lightfoot and Howard (82). The waves are assumed to have a constant height and a uniform motion, independent of the distance from the origin, which is in disagreement with experimental fundings reported in the literature. Most of the above mentioned work assumed that the gas penetrates only a short distance into the liquid; but since the film is very thin, the above assumption is no longer valid and the finite thickness of the film should be taken into consideration as well as the velocity profile.

In 1980, Yih and Seagrave (83) analysed mass transfer into a finite falling film with accompanying heat and interfacial shear, with and without chemical reaction. They concluded that an increase in gas shear decreased the film thickness and increased the absorption rate.

Experimental work done in the area has been concentrated on the gas absorption into smooth films. The waves are surpressed by adding surfactants to the liquid, as in the case of Emmert and Pigford (63), or by using a very short column, as in the work by Vivian and Peaceman (84), who used columns up to 4.25cm height. Experimental work without surpressing the wave formation was carried out by Hikita, Nakanishi and Katoaka (85), who studied the absorption of

several pure gases in liquids with surface tensions from 23 to 75 dynes/cm. Hobler and Kidzierski (79) reviewed the above work and that of several others. However, from the survey carried out in this work, it is evident that there is a need for experimental work with columns of large diameters and sufficient height.

2.2.2 Turbulent Film Flow

The liquid controlled mass transfer into a turbulent liquid film has been studied by several authors. The two most common approached used are the integration of the convective-diffusion equation using an eddy diffusivity model, and the development of hypothetical models where the mass transfer coefficients are found by using empirically determined parameters.

Levich (31) first developed the concept of eddy diffusivity, assuming damping of the turbulent motion by surface tension at the interface. Levich's work was further analysed and generalised by Davies (53) and King (86). The eddy diffusivity was described as:

$$\varepsilon_D = a\ z^n \qquad 2.40$$

where z is the distance from the interface, n is a constant determined experimentally and a is a proportionality constant defined by King as

$$a = .0064\ (g^4/\nu^5)^{1/3}\ Re^{2/3} \qquad 2.41$$

The governing differential equation for gas absorption is rewritten as:

$$u(y)\ \frac{dc}{dx} = \frac{d}{dy}\ ((D + \varepsilon_D)dc/dy) \qquad 2.42$$

with the boundary conditions

$$\text{B.C.1}\quad x = 0 \qquad c = c_o \qquad 2.43$$

$$\text{B.C.2}\quad y = \delta \qquad c = c_s \qquad 2.44$$

$$\text{B.C.3}\quad y = 0 \qquad dc/dy = 0 \qquad 2.45$$

King solved the equation for the cases of either very short or long contact times. The contact time is defined as the length of the reactor divided by the interface velocity. For very short contact times, King assumed that the absorbed gas did not penetrate deeply enough into the falling film for the eddy diffusivity to be significant, therefore he concluded that in this case, the process was well described by the classical penetration theory. For long contact times King's theory is in agreement with Danckwert's surface renewal theory.

Lamourelle and Sandall (87) experimentally analysed the eddy diffusivity model. They conducted experiments on the absorption of helium, hydrogen, oxygen and carbon dioxide into water. The mass transfer coefficient was expressed as

$$K_L = 5.65\ 10^{-3}\ Re^{.839}\ D^{.5} \qquad 2.46$$

They compared their data with Dankwert's theory with the random surface renewal rate deduced from equation 2.29 and equation 2.46 as

$$S = 3.2\ 10^{-5}\ Re^{1.678} \qquad 2.47$$

Using King's theory, assuming n = 2, they expressed the eddy diffusivity as

$$\varepsilon_D = 7.9\ 10^{-5}\ Re^{1.678}\ z^2 \qquad 2.48$$

Sandall (88) solved the eddy diffusivity model for intermediate contact times. Subramanian (89) and Gottifredi and Quiroga (90) extended Sandall's work and found analytical solutions to King's model. However, these solutions are based on a small penetration depth in comparation with the film thickness. Menez and Sandall (91), and Kayihan and Sandall (92) used the eddy diffusivity model to study gas absorption with first order reaction in turbulent liquid films, using the numerical finite difference method to solve equation 2.42, with equation 2.40 as defined by Lamourelle and Sandall. Good agreement between the experimental dat and the numerical results was claimed. Recently Yih and Seagrave (93) presented an analytical solution, using a method of separation of variables, obtaining the first ten eigenvalues.

A different approach first introduced by Fortescue and Pearson (94), consisted of assuming idealised eddy structures unaffected by interfacial forces. Fortescue assumed that the energy associated with a large eddy

controlled the mass transfer. Banerjee, Scott and Rhodes (95) proposed a small eddy model, which they compared with their experimental data. Assuming a stagnant gas, they expressed the mass transfer coefficient as

$$K_L = \kappa D^{\frac{1}{2}} Re \qquad (2.49)$$

where κ is constant, which must be determined experimentally. The data was analysed by correlating the interfacial area vs an energy dissipation parameter (E) defined in terms of the pressure drop.

$$E = \Delta P \Gamma \qquad (2.50)$$

By following the penetration theory, they expressed t as the time scale of the turbulent eddies at the waves.

$$t = (E_e/J)^{\frac{1}{2}} \qquad (2.51)$$

where J is the mass flux and E_e is the viscous rate of dissipation of energy per unit mass, defined by Batchelor (96) by the following relationship

$$E_e = \omega^2 \qquad (2.52)$$

where ω is the vorticity.

In 1979, Henstock and Hanratty (97) extended their earlier work on falling film hydrodynamics (49). They analysed gas absorption into falling films by assuming that the mass transfer rate was controlled by eddies. The length and velocity of these eddies were determined by the

characteristics of the bulk flow, with dampening at the interface due to viscosity. Experimental mass transfer coefficients were measured absorbing oxygen into water using a 30ft long and 1 inch I.D. vertical pipe. They reported an increase in the mass transfer coefficient due to the increase in the gas flow rate, which was expressed in terms of the flow parameter F (equation 2.17).

$$I = 1 + 1.8\, e^{-30F} \qquad (2.53)$$

Where I is the ratio of measured Sherwood numbers to that predicted by the following equation, obtained from their theoretical analysis.

$$Sh = .0077\gamma^{1.5}\, Sc^{.5}$$

Where Sc is the Schmidt number (ν/D) and γ is defined by equation 2.18 as a function of the liquid phase Reynolds number. The authors predicted a decrease in the mass transfer rate related to droplet entrainment at high gas flow rates.

All the above models incorporated a constant film thickness, introducing the effect of the wavy motion in the form of an empirically found turbulent diffusivity. However, as expressed by Henstock and Hanratty, the relation between eddy diffusivity and eddy viscosity has never been formally stated, although momentum transfer characteristics, such as velocity, are used to define the eddy diffusivity.

Brumfield, Houze and Theofanus (98) adopted a more realistic approach, using the statistical model for the film hydrodynamics developed by Telles and Duckler (40), and breaking down the mass transfer mechanism in two transfer regimes. The mass transfer to the laminar region was described by a surface renewal theory, where the contact time was related to the frequency and celerity of the waves. For the turbulent wavy flow which slides at a higher velocity over the laminar substrate, Fortescue and Pearson large eddy model was used. However, there is no physical justification for their assumption of two separate regimes, and the effect of surface tension has been ignored.

Chung and Mills (99,100) studied the effect of liquid velocity on the rate of mass transfer. They carried out experiments measuring the absorption of carbon dioxide by water and glycerol solutions. The mass transfer coefficient was found to increase with the increase in viscosity. More recently, the effect of surface tension on the rate of mass transfer was investigated by Won (101). The liquid side mass transfer coefficient was found to increase with increase of surface tension, contrary to the prediction of the Levich theory.

2.2.3 Gas-Phase Controlled Mass Transfer Rate

There are a number of studies of gas-phase controlled mass transfer in gas liquid contacting apparatus. Morris and Jackson (4) recommended the falling film tower as the most suitable type of equipment for the study of absorption processes in which the gas-phase is the source of almost all of the resistance to mass transfer. The dimensionless ratio ρ_s/HP where ρ_s is the density of the disolved gas, H is the solubility coefficient and P is the total pressure, was used as a criterion to determine the relevant magnitude of the resistance in both phases. At atmospheric pressure in the absence of any chemical reaction, they suggested the following guide:

1. $\rho_s/HP < 5 \times 10^{-4}$, gas phase controlled
2. $5 \times 10^{-4} < \rho_s/HP < .2$, resistance in both phases are significant.
3. $.2 < \rho_s/HP$, liquid phase controlled.

The following equation for the gas coefficient, for turbulent gas flow and based on experimental data on the absorption of ammonia from air into water, was given by the above mentioned authors.

$$K_g = .04\ (u_r \rho_s/P)\ \ Re_g^{-.25}\ Sch^{-.5}\ (DF) \qquad (2.55)$$

where u_r is the gas velocity relative to the liquid surface velocity as estimated by equation 2.3, and DF is the drift factor defined as the ratio of the total

pressure to the log mean partial pressure of insoluble gas ($P-P_s$). The drift factor was introduced to allow for the displacement of the bulk gas flow towards the gas liquid interface as a result of the removal of soluble gas by the liquid.

Byers and King (102) analysed the problem, theoretically and experimentally for the case of horizontal flow. The major contribution of their work was that they considered the influence of the liquid surface velocity, which is considerably increased by the drag at the interface at relatively high gas flow rates.

Hikita and Ishimi (103,104,105,106) followed Byers and King's analysis to the heat and mass transfer laminar and turbulent gas streams in vertical wetted walls with countercurrent and cocurrent gas-liquid flows. For mass transfer into a laminar gas stream the following relationship was found for the average Sherwood number

$$Sh_g = -(Gz_g/\pi)\ \ell n\left[\sum_{n=1}^{\infty} B_n \exp(-\pi\lambda_n^2/Gz_g)\right] \qquad (2.56)$$

where Gz_g is the gas-phase Graetz number for mass transfer defined as

$$Gz_g = \frac{Q_g}{D_G L} \qquad (2.57)$$

B_n and λ_n are the average expansion coefficients and eigenvalues, which were given in a previous work by the authors (55,56).

The gas-phase mass transfer rate into a turbulent stream was investigated by carrying out experiments on adiabatic vaporization of water, with and without surfactants. They concluded that the rippling had very little effect on the mass transfer rate. Their experimental results obtained with the absorption system ammonia-air (less than 2% in volume) and a 1.5 molal solution of sulphuric acid showed a dependence. The Sherwood number on both Reynolds numbers.

Kasturi and Stepanek (107) measured the mass transfer coefficient by absorbing sulphur dioxide into a sodium hydroxide solution and found that the gas-phase mass transfer coefficient increased with a higher gas velocity and decreased with a higher liquid velocity. This was explained by the increase in the interfacial liquid velocity; therefore they concluded that the gas side mass transfer coefficient is a function of the relative velocity of the gas against the velocity of the liquid at the interface. An empirical correlation for the values of Kg was proposed in terms of the Sherwood and Euler numbers.

2.2.4 Horizontal Flow

Relevant studies on mass transfer in horizontal two-phase flow, which could be of interest to this study are the work of Anderson, Bollinger and Lamb (108), who obtained experimental data on the gas film controlled absorption of ammonia, carried by an air stream, into water. Hughmark (109) analysed Anderson's data by means of an analogybetween mass transfer and momentum transfer. Heuss, King and Wilke (110) used a similar ammonia-air-water system for the determination of the interfacial area. Wales (111) measured all three parameters, the interfacial area, volumetric liquid and gas side mass transfer coefficients. He carried out annular and dispersed flow in a 1 inch ID horizontal tube, and observed how the mass transfer coefficients decreased when the gas velocity exceeds the entrainment inception point. Gregory and Scott (112), Cichy and Russell (113) and Jepsen (114) and Kasturi (115) revised Wales work and expressed doubts about the correctness of his data on interfacial area, for which he reported values well above any theoretical estimate.

In 1971, Cibrowski and Rychlicki (116) reviewed previous works on horizontal two-phase flow and concluded that the existing theories for mass transfer into falling films were inappropriate to describe horizontal two-phase wavy flow mass transfer phenomena.

CHAPTER III

EXPERIMENTAL EQUIPMENT AND MEASURING TECHNIQUES

3.1 Vertical Tubular Reactor

The apparatus designed for this study was a vertical annular reactor, with a diameter of 30cm and a height of 204cm. It consisted of three interconnected units: The Absorption-Reaction Unit, The Liquid Circulation Unit, and The Gas-phase Flow Unit. A schematic diagram of the whole apparatus is presented in figure 3.1, and the photographs in figures 3.2 and 3.3 show the apparatus as built.

3.1.1 The Absorption-Reaction Unit

This unit consisted of an outer perspex tube, of diameter 30cm and length 204cms, with a stainless steel tube, 22cm outside diameter, arranged concentrically. Both tubes have been machined smooth and the outer surface of the inner tube polished to provide even distribution of the liquid film on walls.

The outer pipe transparency enables direct observations of the flow phenomena ocurring, such as wave formation, liquid entrainment and rupture of the film to be seen.

The two phases are fed separately into the top of the reactor. The liquid forms a thin film on the wall of either one or both pipes. While the gas flows co-currently between both falling films or a falling film and a dry tube. This produces a large contacting surface area and a continuous process.

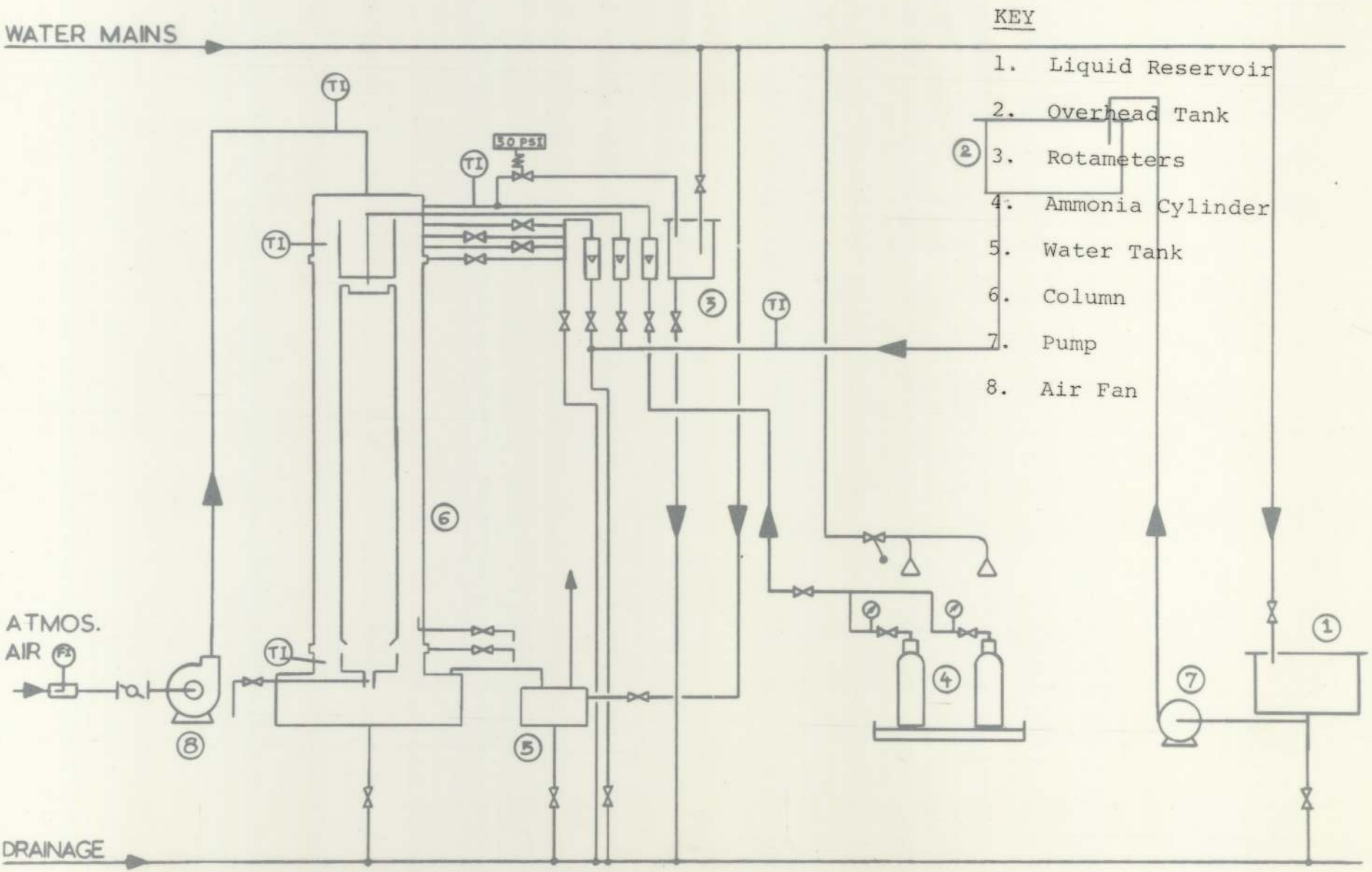

Figure 3.1 - Flow Diagram of Experimental Apparatus

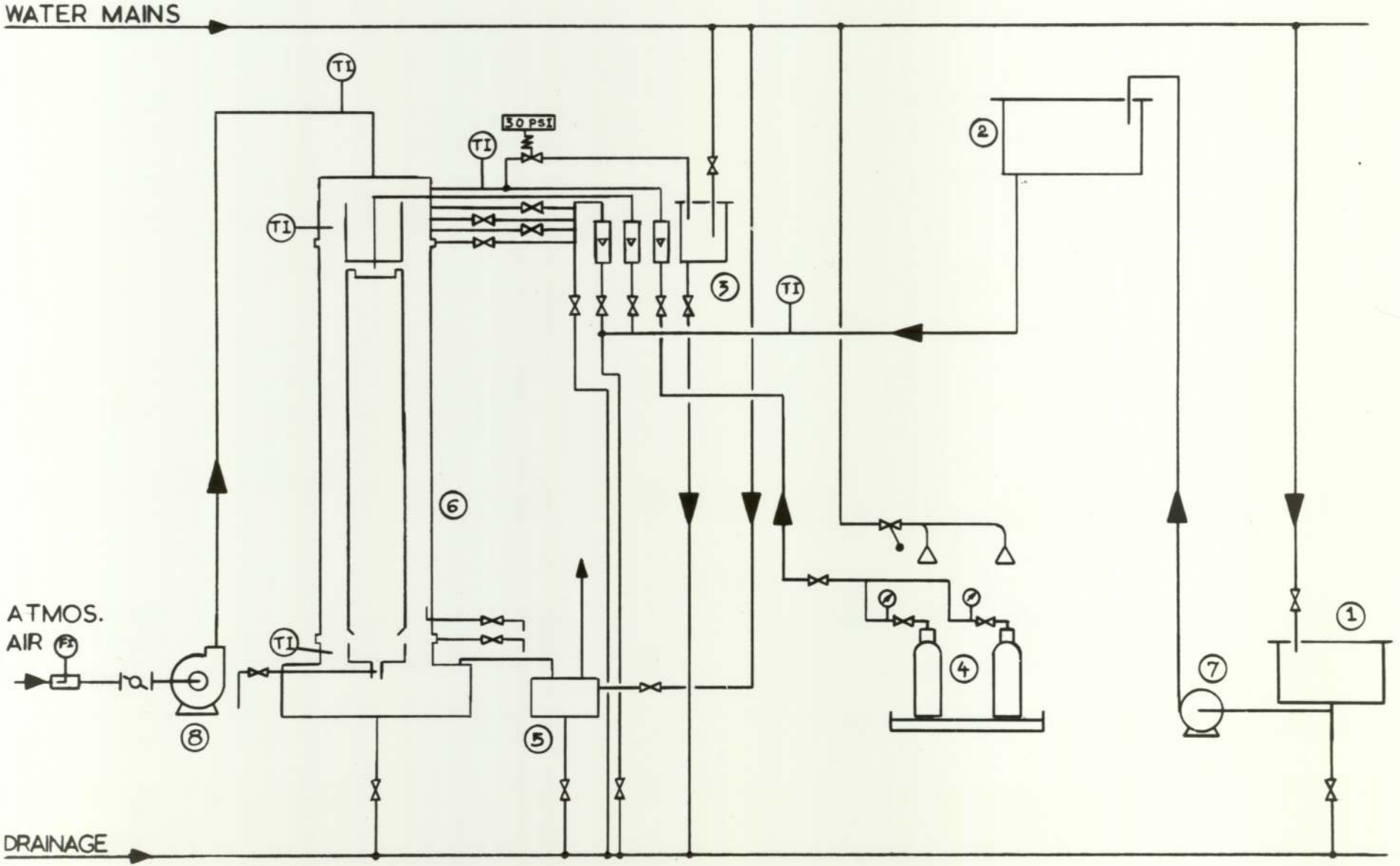

Figure 3.1 - Flow Diagram of Experimental Apparatus

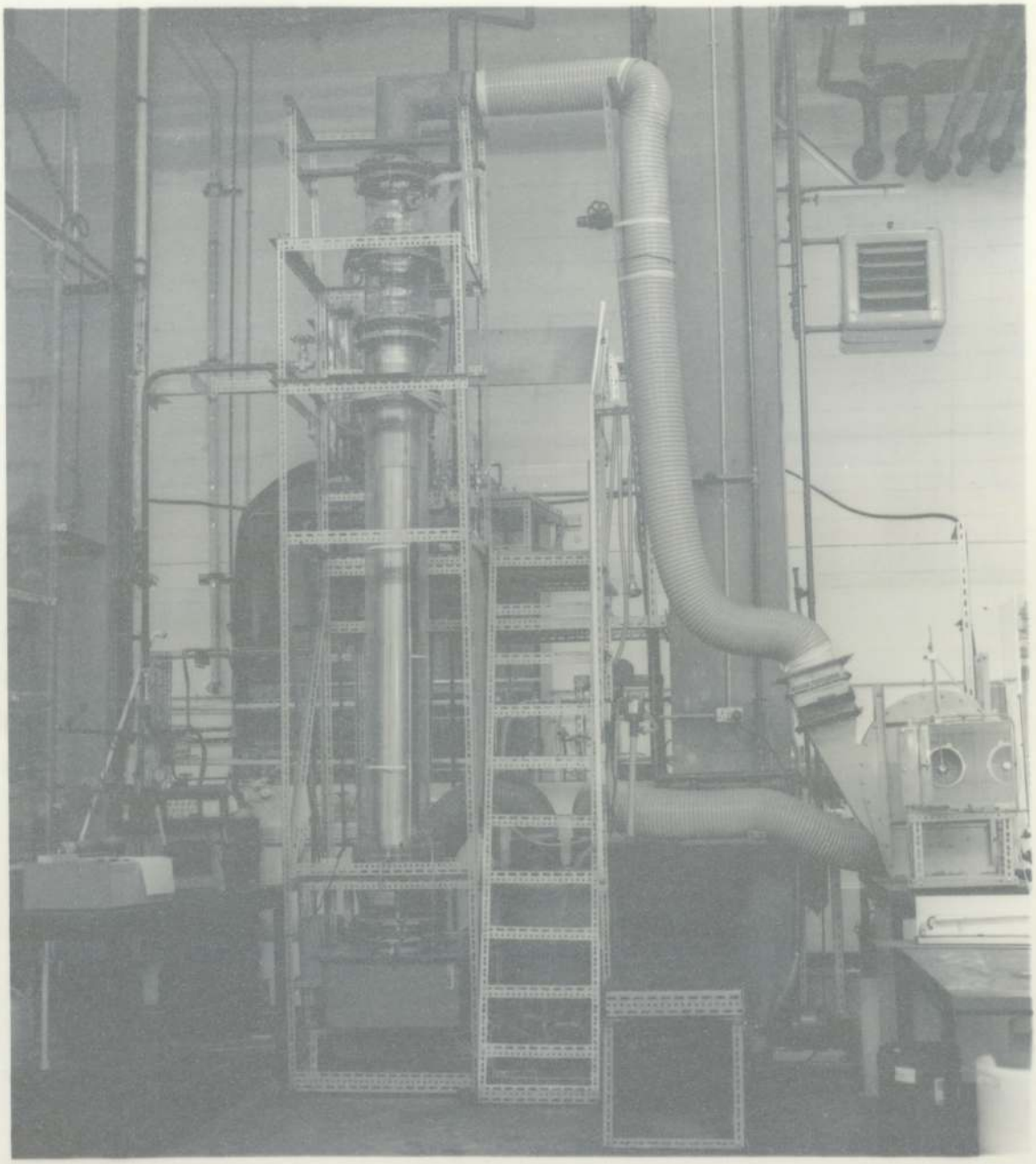

Figure 3.2 - Vertical Tubular Reactor, Front View

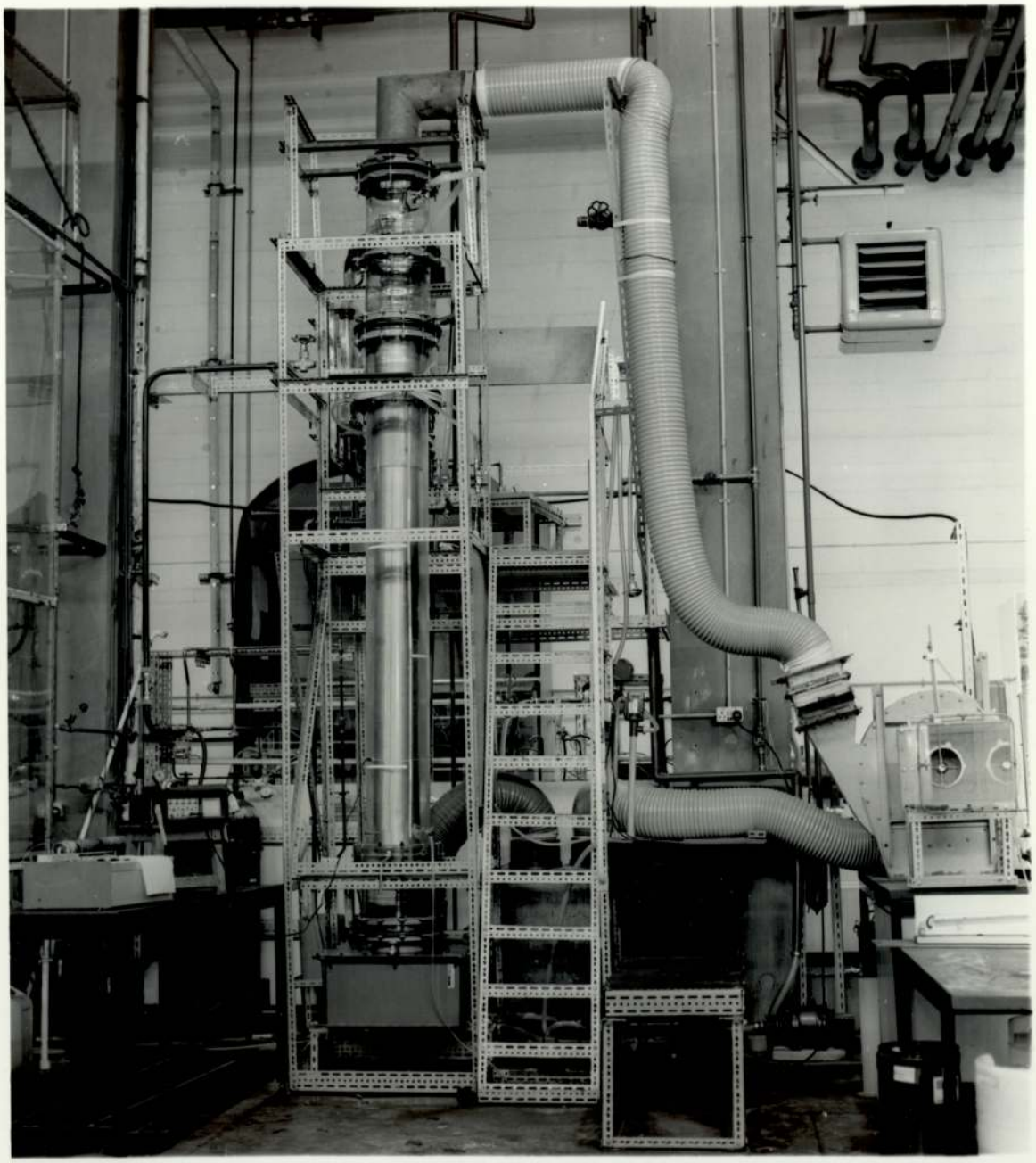

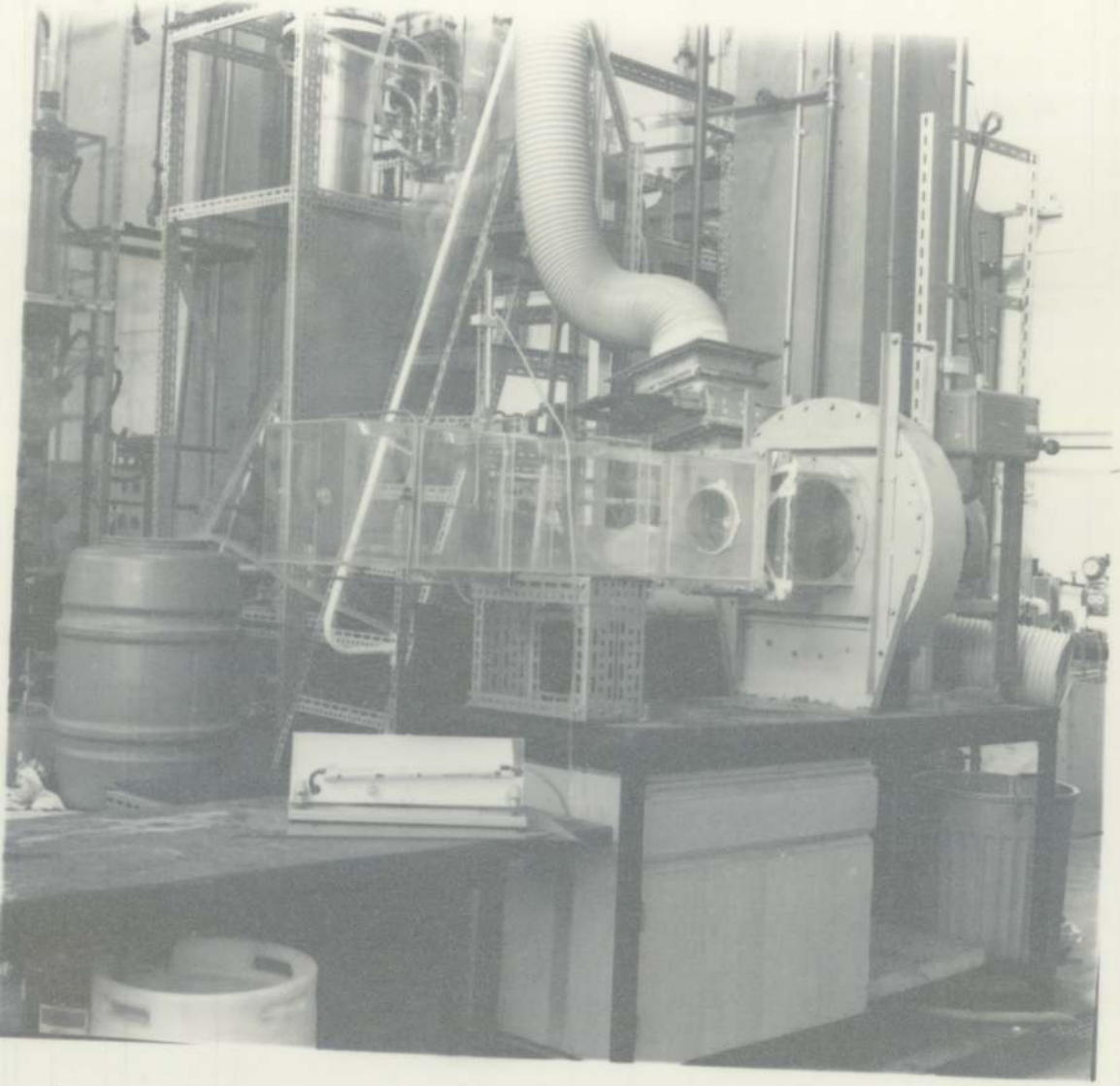

Figure 3.3 - Vertical Tubular Reactor, Side View

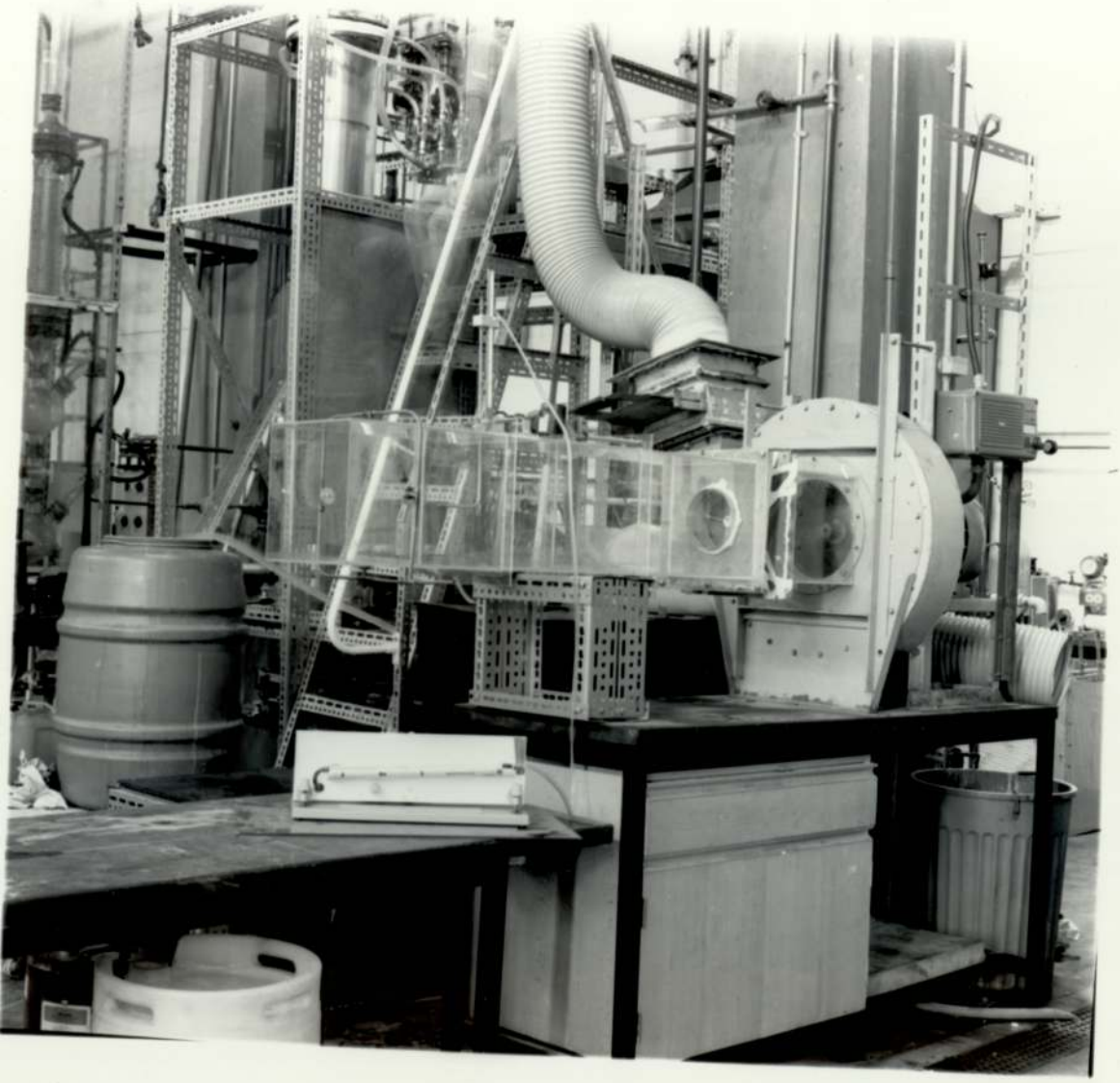

3.1.2 The Liquid Circulation Unit

The liquid is stored at ground level in a 50 gallons P.V.C. tank and is transported, by means of a centrifugal pump, from the reservoir to a constant head tank situated 10 meters above the floor. The overhead tank eliminates any disturbance introduced by the pump to the flow. The liquid flows from the overhead tank to the inlet and distribution system of each tube and the liquid flow rate to each inlet is controlled by two diaphragm valves and measured by two rotameters, tube size 24, fitted with stainless steel floats. The pipework of the circulation unit was 4.0cm diameter and made of P.V.C.

Falling film flow is highly sensitive to entry conditions and great care must be taken to ensure that the liquid flow is evenly distributed and that the falling film develops before contact is made with the gas-phase. The liquid inlet and distribution systems are shown in figure 3.4. Detailed representation of each distributor is shown in figures 3.6 and 3.7. The distributor to the outer system consisted of two perspex rings, with a channel in the bottom section. The liquid enters this channel through four equidistant orifices; flow to each of these points is controlled manually by individual diaphragm valves. After the liquid fills the channel, it discharges through the outside slot, as shown in figure 3.4. A protective shield prevents the liquid from any disturbance for 8cms before making contact with the gas-phase.

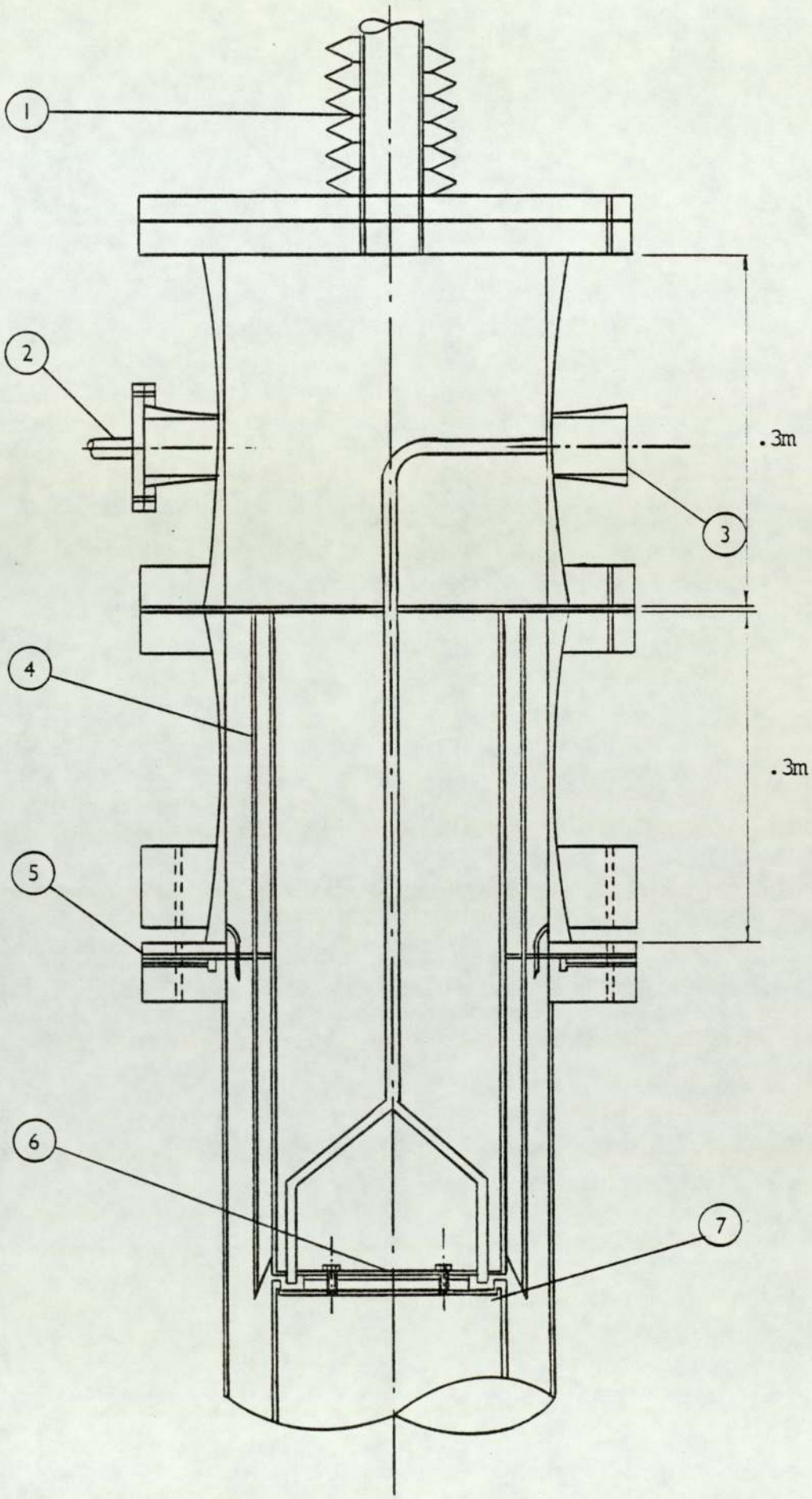

Figure 3.4 - Upper Section of the Column

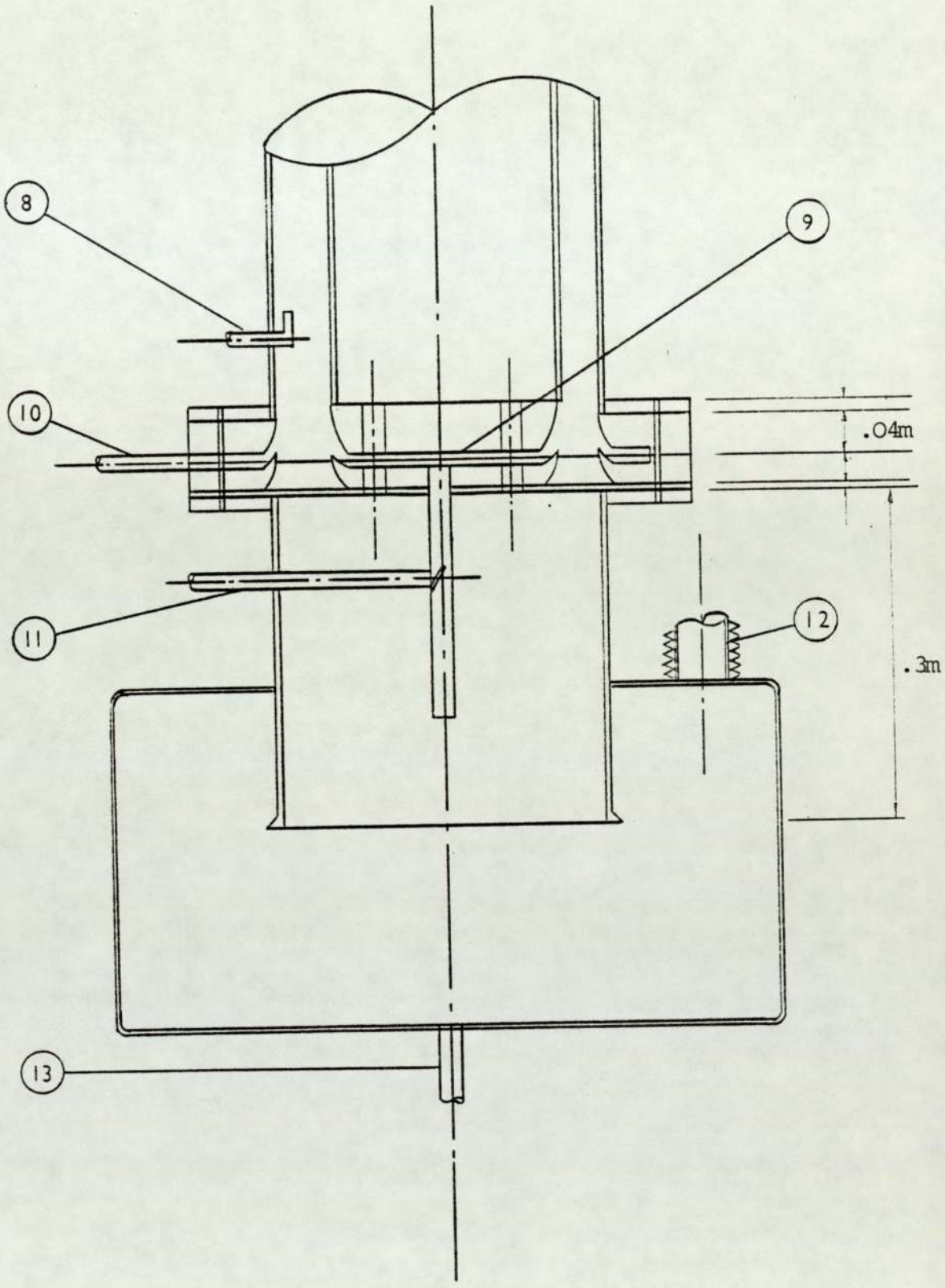

FIG.3.5 LOWER SECTION OF THE COLUMN

Key for Figures 3.4 and 3.5

1. Air Inlet Pipe
2. Ammonia Inlet Pipe
3. Feeding liquid pipe, inner wall
4. Shield, stainless steel
5. Feeding and distribution system, outer pipe
6. Feeding and distribution system, inner pipe
7. Stainless steel pipe
8. Gas sample, collecting point
9. Liquid phase collector, inner pipe
10. Liquid phase collector and sample point, outer point
11. Liquid sample, collecting point, inner pipe
12. Vent, connected to a water tank
13. Drains

The inner pipe inlet and distribution system consisted of a pair of polished stainless steel discs; between which the liquid flows radially outwards through a slot of known width. As before, a shield was installed to protect the development of the falling film. The effect of the width of the slots was analysed experimentally. It was found that a minimum width was necessary to ensure no jetting that could lead to unwanted liquid entrainment at low gas flow rates. It was also observed that when the width of the slot was increased above a critical value, the unprotected liquid film would break up at a critical air flow-rate, well below any theoretical estimation. Therefore, it was decided to use a large width slot (6mm) and protective shields.

The bottom section of the Absorption-Reaction Unit contained the separating, collecting and sampling systems for both falling films. Details can be seen in figures 3.5, 3.8 and 3.9. A recycling unit for the liquid phase, which was used for those experiments in which neither mass transfer nor chemical reaction were involved, was connected to the draining outlet at the bottom of the liquid collector tank, as shown in the schematic diagram of figure 3.1.

3.1.3 The Gas-Phase Flow Unit

This consisted of three different sections. The first provided and measured the volumetric flow of dry air, the second provided and measured the volumetric flow of ammonia

and the third section enabled the two gases to mix and stabilized the flow.

The air section contains an electric fan, a rectangular air duct and a flexible pipe of 4½ inches diameter connecting a centrifugal fan to the top of the column. A centrifugal fan was chosen, because it supplies large volumes of air at atmospheric pressure; and the rectangular perspex duct attached at the inlet of the fan was installed to control and measure the air flowrate. The air flowrate was controlled by changes in the aperture of an iris diaphragm installed in the duct. To obtain an accurate measurement of the flow-rate, a pitot-tube meter was assembled at the entrance of the duct and the pressure difference was determined by an inclined manometer. Further details of this arrangement and calibration of the air flowrate are given in Appendix A.

The ammonia gas was obtained from two cylinders connected to an expansion chamber. The pressure of the gaseous ammonia leaving the cylinders was determined by pressure regulators and an on-off valve was installed at the exit of the expansion chamber. The ammonia was then flowed through a 3.75cm diameter stainless steel pipe to a flow control valve, and then through a 7.5cm diameter stainless steel pipe connected to a glass rotameter, size 35, fitted with a duraluminum float. The ammonia then passed into the mixing chamber.

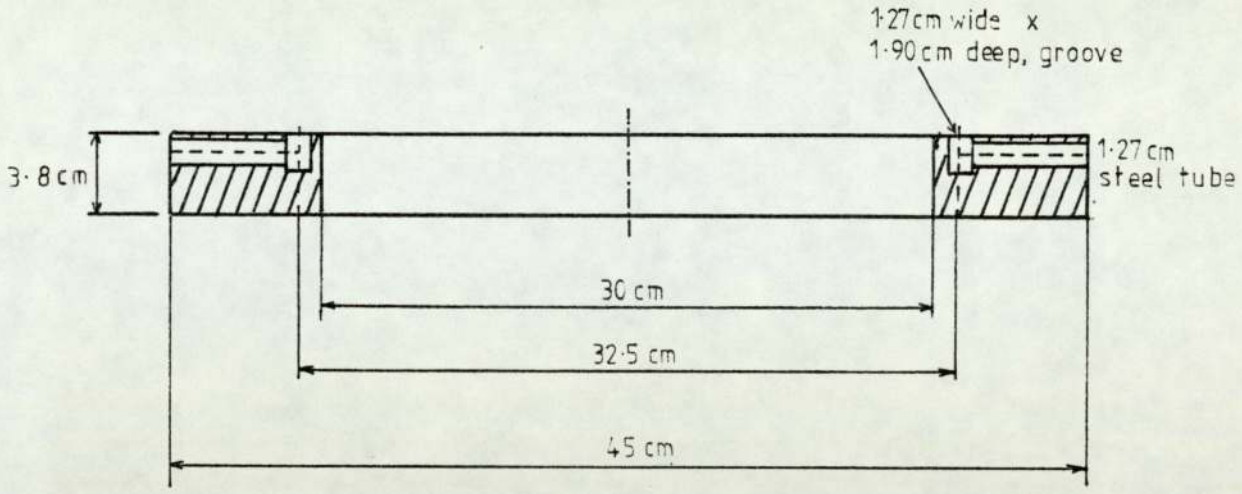

FIG. 3.6.
LIQUID INLET AND DISTRIBUTION SYSTEM, PERSPEX PIPE.

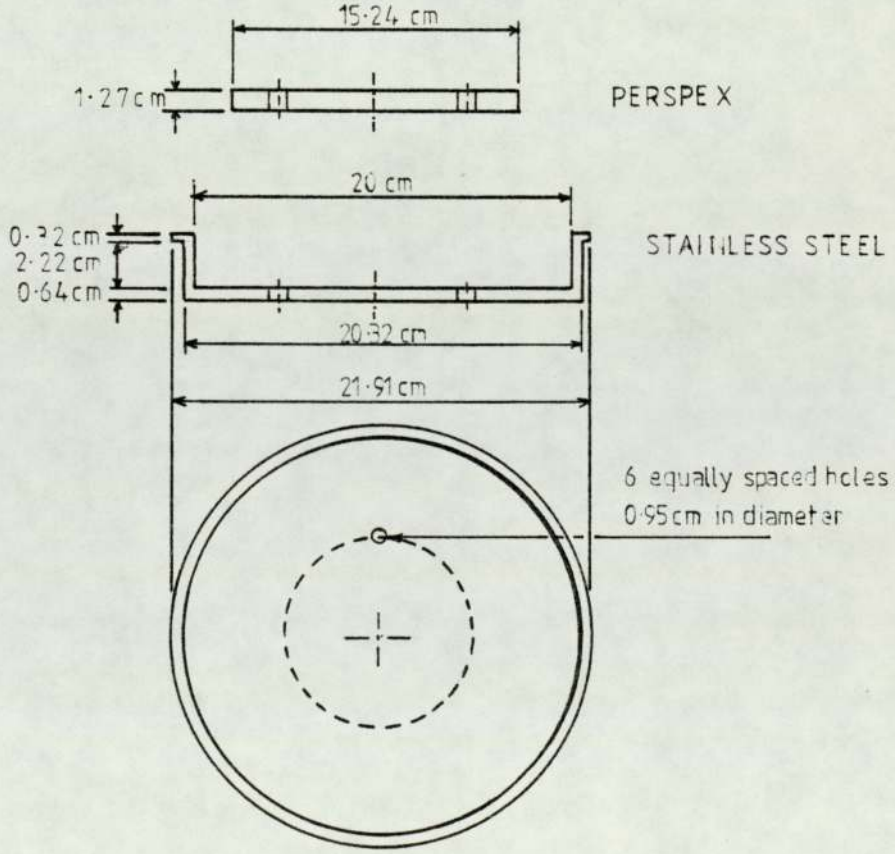

FIG. 3.7.
LIQUID DISTRIBUTION SYSTEM, STAINLESS STEEL PIPE.

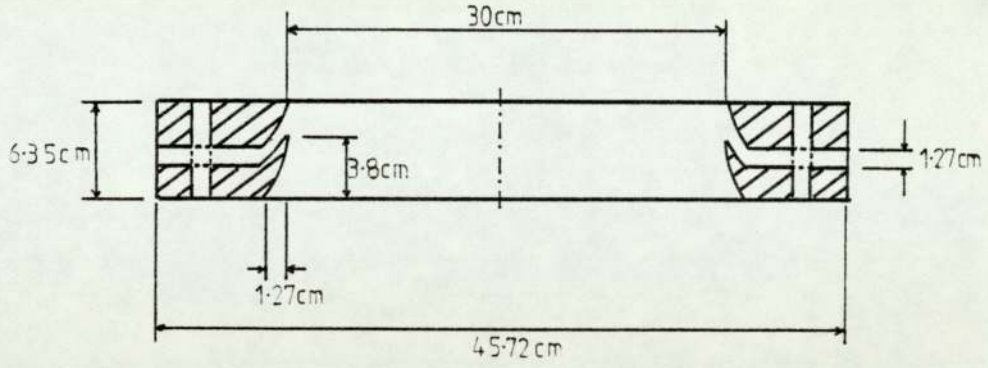

FIG: 3.8.
OUTER PIPE LIQUID COLLECTOR

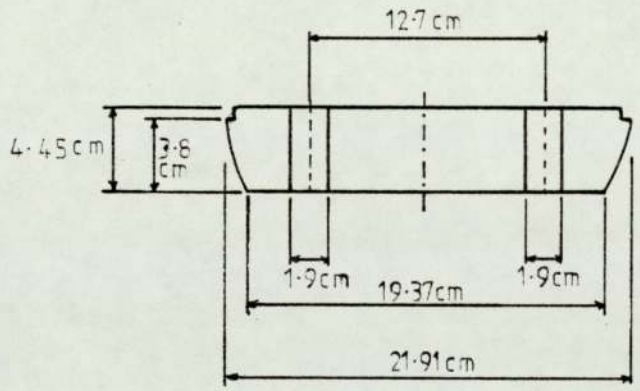

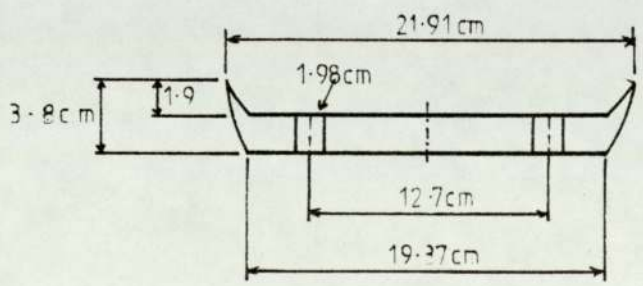

FIG. 3.9.
INNER PIPE LIQUID COLLECTOR.

The mixing chamber consisted of two Q.V.F. glass pipes, of 30cm diameter and 30cm long, situated at the top of the reactor, as shown in figure 3.4. The air entered this chamber from the top and the ammonia was fed into the side, the high turbulence ensured effective and fast mixing. Before contacting with the liquid-phase, the gas was flowed between a pipe of stainless steel of 22 cms diameter and the lower section of glass pipe. This is the "calming" section and enabled the gas flow to become fully developed and stable.

The gas-phase then flowed cocurrently, down the reactor, contacting the falling liquid film. After this, the exit gas flowed into a fresh water tank where any excess ammonia in the air was absorbed. The flow diagram is shown in figure 3.1.

3.2 Vertical Wetted Wall

A bench scale film flow apparatus was designed and built to simulate the conditions at the entrance of the vertical tubular reactor. It consisted of a constant head tank, a centrifugal pump, a storage tank, a film distribution section and a perspex wall. A schematic diagram of the apparatus is presented in figure 3.10.

The liquid was pumped from the storage tank, at ground level, to the constant head tank, placed well above the distributor. The constant head tank maintained a constant flow rate, controlled by a diaphragm valve and measured

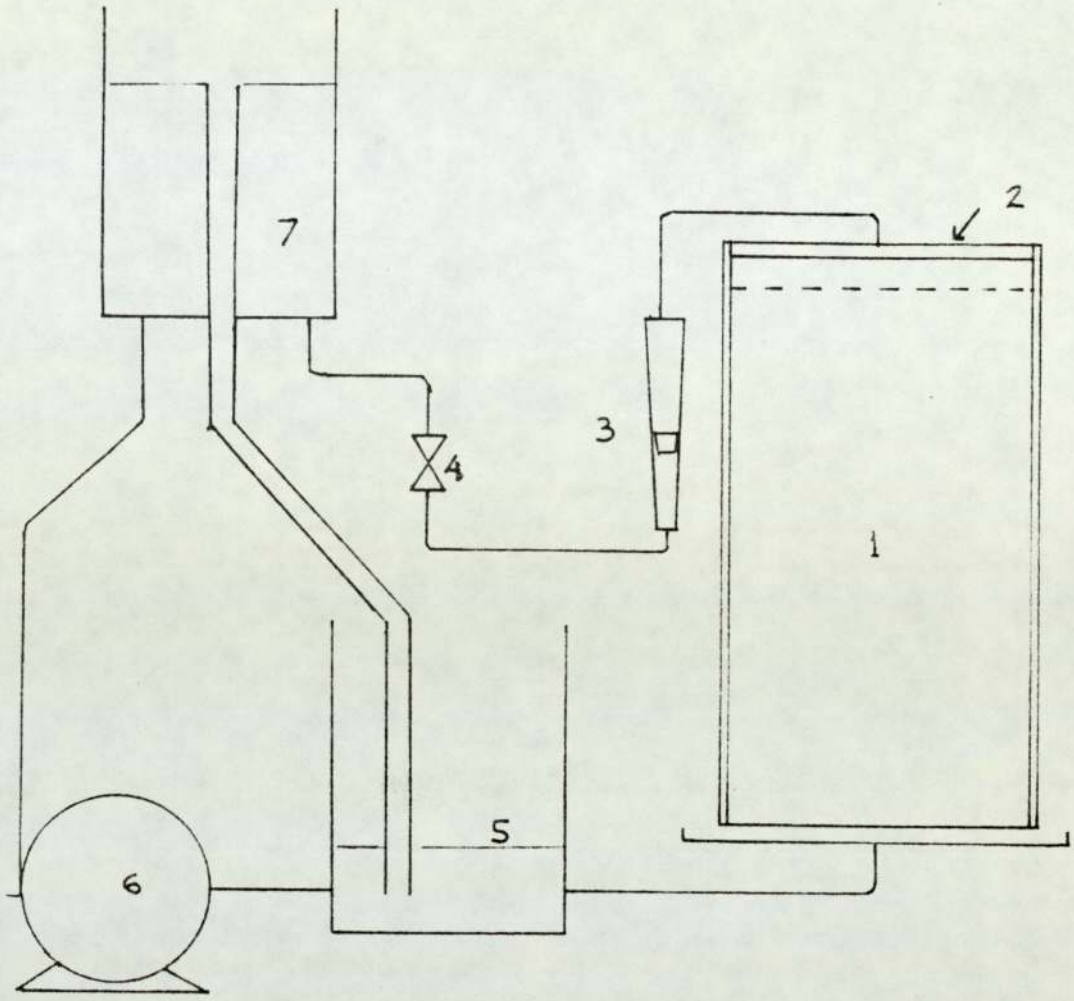

1. Wetted Wall
2. Distributor
3. Rotameter
4. Valve
5. Tank
6. Centrifugal Pump
7. Overhead Tank

Figure 3.10 - Schematic Diagram of Wetted Wall

by a size 18 rotameter, fitted with a stainless steel float.

The film distribution section was a small reservoir, from which the liquid flowed over a weir and down the vertical perspex wall. The height of the weir was designed to match the depth of the channel at the liquid film distributor of the tubular reactor.

The size of the perspex wall was designed so that it would be wide enough (22cm) to minimize the wall effects and long enough (1.1 mt) to avoid any disturbances due to exit effects. The sides of the wall were bordered by 2cms thick sledges. This equipment was used to measure the falling film thickness in the entrance region, for a range of liquids of different viscosities and flow rates. The significance and results of these experiments are discussed in chapter 4 of this study.

3.3 Determination of the Film Thickness

The film thickness is the characteristic parameter of the falling film system. Several methods are found in the literature to measure this, but their applicability and accuracy are suspect. A method was required which offered the following advantages:

1. Accuracy, since the range of film thickness is from .5mm to 1.5mm approximately.

2. No interference with the liquid film. The falling film would be easily disturbed if put in contact

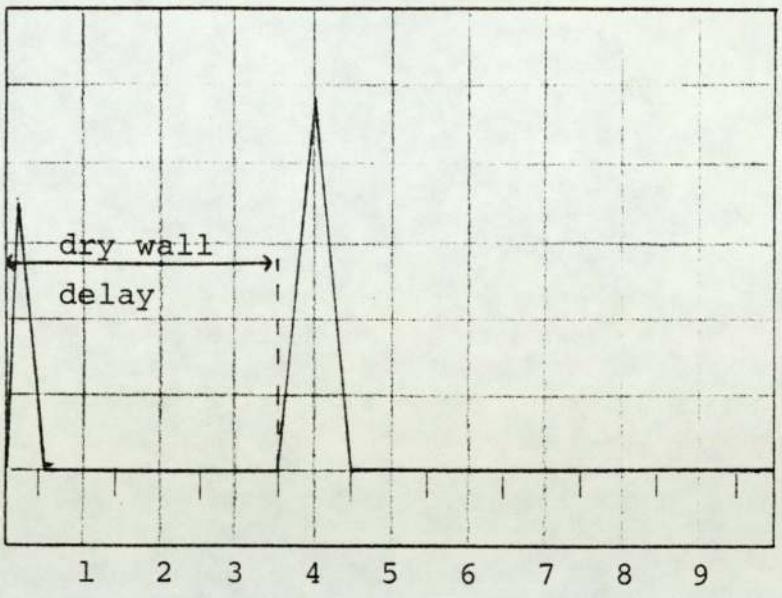

Figure 3.11 - Monitor Screen, Dry Reservoir

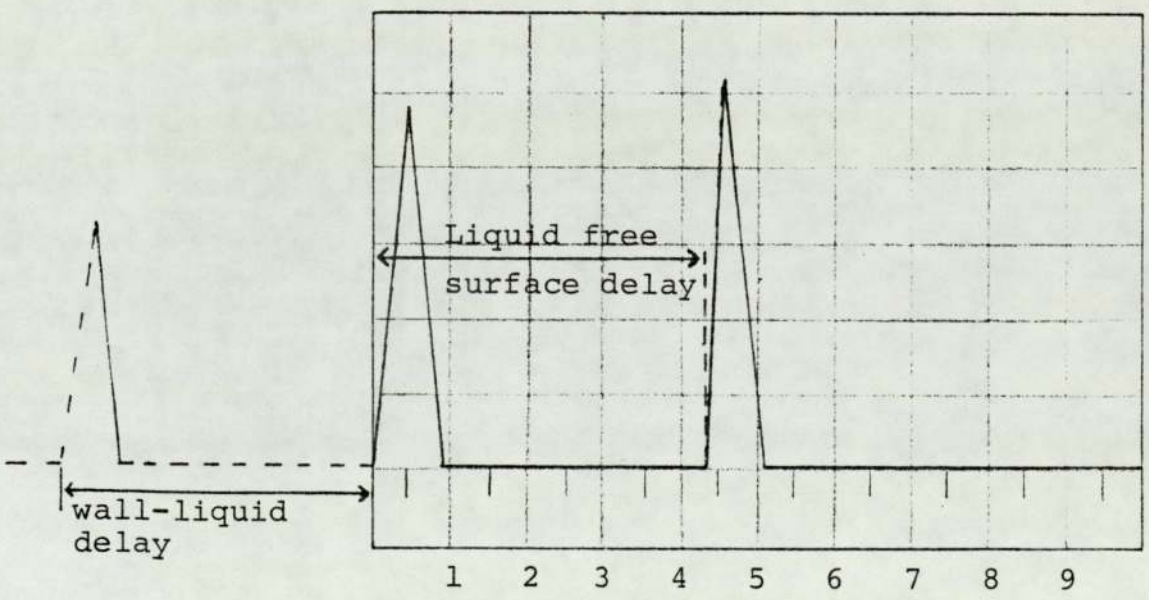

Figure 3.12 - Monitor Screen, Calibration

Figure 3.13 - Electric Circuit

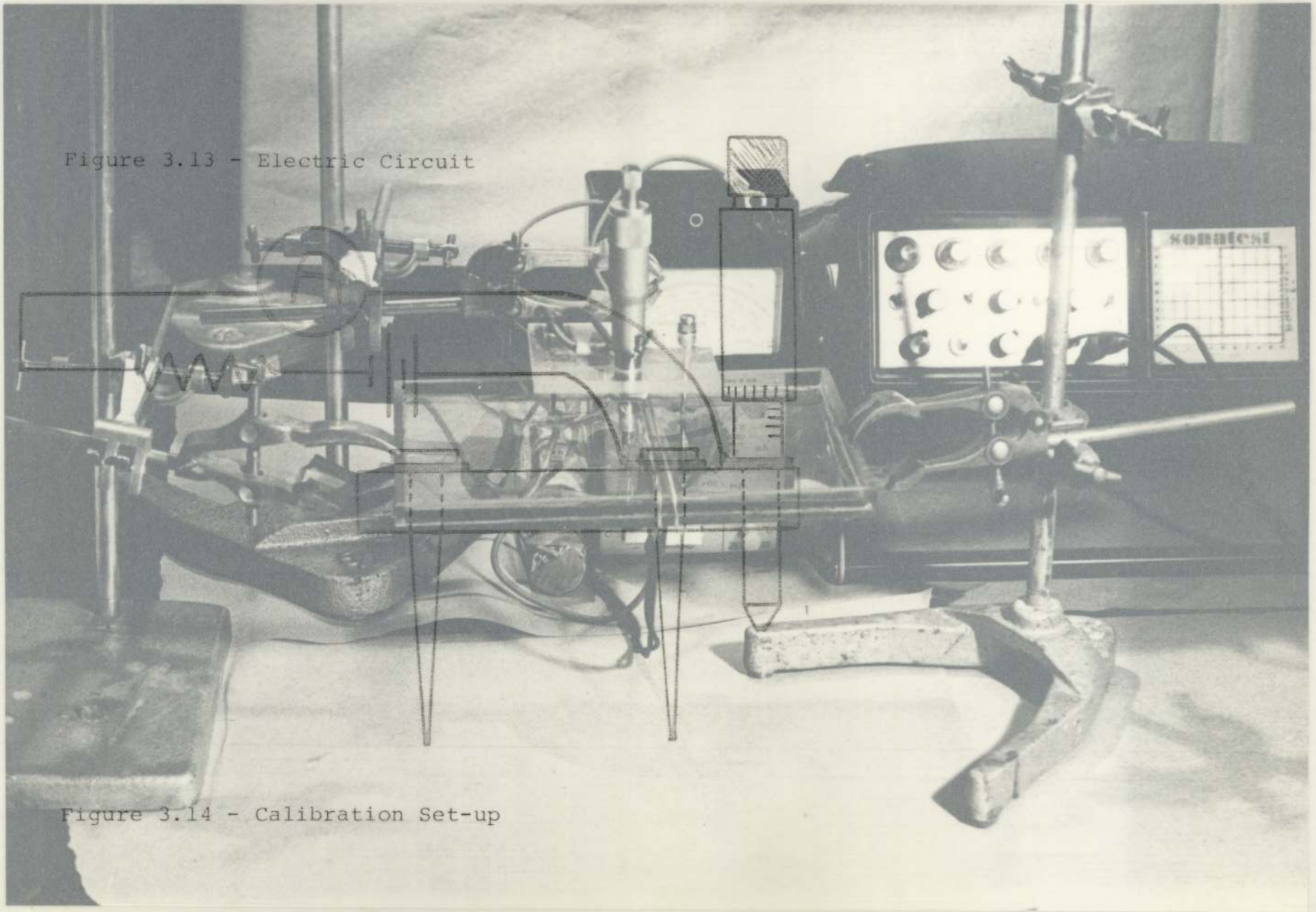

Figure 3.14 - Calibration Set-up

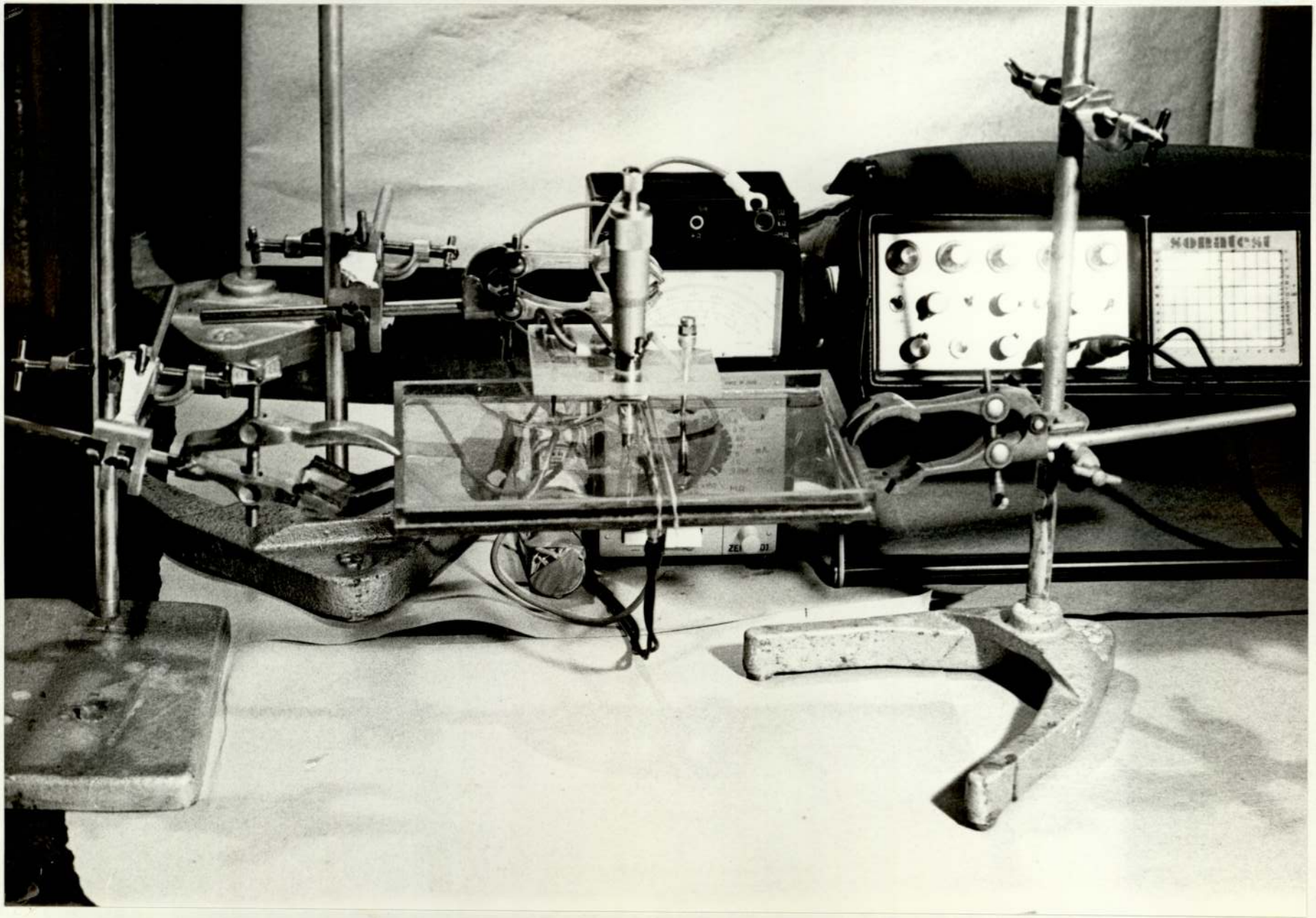

with any foreign device, such as a micrometer.

3. It must allow measurements to be taken along the length of the reactor. Photographic and light refraction methods were considered, but because of the geometry of the reactor, they were found to be inappropriate.

A new method has been successfully tested. It consisted of inserting an ultrasonic probe which emits pulse sound signals and measures the time taken for the signal to return, after bouncing off the free surface of the liquid film. This is illustrated in figures 3.11 and 3.12.

An ultrasonic monitor, model U.F.D. 2M, made by Sonatest, with a double probe, have been used and the photographs in figures 3.2 and 3.13 show the layout of controls of the U.F.D. 2M and the double probe. Appendix B contains the technical specifications of this equipment.

3.3.1 Calibration

The calibration of the ultrasonic method was carried out for every one of the liquids used in the experimental work. A small perspex reservoir and an electric conductance probe, with a vernier depth gauge meter, were used as shown in figures 3.13 and 3.14. First the probe is securely attached to the bottom of the reservoir and to ensure that there was no air trapped in between the perspex surface of the probe and reservoir, the probe surface was wetted with glycerol. Then the controls of the monitor were adjusted as follows:

Time base range select (s): 1

Time base range calibrate (c): 0

Gain control: 70 dB

Reject: 8

Frequency selection: 3-6 MHz band

Probe switch: double

Phase switch: +M

Delay: .25

Once set, two echoes were recorded, as shown in figure 3.11. The first echo corresponded to the probe/perspex interface; the second to the free surface at the dry reservoir. Using the Time Base Delay, the second echo was moved to zero and then the reservoir is filled with liquid and a third echo appeared on the screen. This third echo corresponded to the signal bouncing off the free surface of the liquid (figure 3.12). The film thickness was then measured by means of the electrical conductance method. After withdrawing liquid from the reservoir, a number of successive readings were taken, to obtain a correlation between the film thickness vs time delay.

The electrical conductance procedure is described in figure 3.13. As can be seen, a 1.5 volts battery had one terminal connected to the leg of the measuring device, which was immersed in the liquid. The other terminal was connected to the depth gauge. As soon as the flattened end of the gauge was in touch with the liquid surface, the circuit was completed and a reading shown by the voltimeter, from which the liquid depth can be estimated accurately.

3.3.2 Film Thickness

Falling film flow, however, does not have a constant local thickness. Its surface is wavy and these waves travel at speed. Therefore, the changes on the time delay, during a fixed set of experimental conditions, had to be recorded and later measured individually. Therefore, a video tape recording was made of the signals displayed by the monitor, and the measurements were taken from the video tape monitor, when played back. An average of this reading represents the average local film thickness. Other useful information could be obtained from the readings such as maximum and minimum local thickness.

There was no difficulty in obtaining measurements of the film on the perspex pipe of the tubular reactor, along the whole length of the reactor. This was not the case for the stainless steel inner pipe, therefore, it was necessary to inlay three ultrasonic probes at different heights of the reactor, arranged in the form of a helix and point measurements were taken at these locations.

3.3.3 Other Applications

An additional specification incorporated in U.F.D. 2M was a "window" or "gate" monitor. This "gate" was set up at a start position using the monitor start control. The width of the "gate" could be adjusted from 1mm to 100mm, and the monitor sensitivity controlled the level at which an echo would trigger the monitor.

When a film thickness response triggered the monitor, a signal was recorded by a chart plotter. Peaks in the chart plotter indicated the frequency of waves on the film surface which was of great use to study the effect of increasing the gas-phase linear velocity in the shape of the film surface. An illustration of this application is given in Chapter 7 of this study.

3.4 Measuring and Calibration Techniques

3.4.1 Physical Properties

(a) Specific gravity:- The standard pyknometer technique was employed to determine the specific gravity of all liquids. Measurements were made at 20°C ± .1°C, with a 10ml specific gravity bottle.

(b) Viscosity:- The method of timing the passage of the fluid through a cannon-Fenske capillary U-tube, immersed in a constant temperature bath (20°C ± .1°C) was used.

(c) Interfacial Tension:- The standard Wilhemy Plate method was used on a "Cambridge" Torsion balance.

The table of the results of the physical properties determined is given in Appendix C.

3.4.2 Calibration of Flowrates

(a) Liquid Phase:- Two rotameters of size number 24 with appropriate stainless steel floats were used to measure the flowrate of each feed stream. Calibration was made by measuring volumes over a known time period at $20^{\circ}C \pm 1^{\circ}C$, giving an accuracy of better than 1% of maximum reading. For solutions of sulphuric acid in water, it was assumed that the density and the viscosity variations at the low concentrations used were small enough to allow calibrations for pure water to be used.

(b) Gas Phase:- Measurement and calibration techniques employed for the determination of the air and ammonia flowrates have been described above. Detailed description of the procedures followed are presented in Appendix A.

CHAPTER IV

ENTRANCE REGION

The way in which the film is formed is of great importance in the design of the film absorber/reactor. It affects the velocity distribution and the film thickness of the liquid film as it contacts a cocurrent turbulent gas stream. This section of the reactor is called as the "entrance region" and is characterized by its smooth surface and the motionless appearance of the film. Due to this appearance it is also referred to as the "calming" or "mirror" zone (figure 4.1).

The film is formed by emerging from a flat slit, as shown in figure 4.2, or by flowing freely over the leading edge of a vertical wall, as shown in figure 4.3.

4.1 Theory

Research involving the entrance region flow is relatively unknown and cannot be generalised since it depends upon the feed device used to introduce the liquid.

4.1.1 Flow Emerging from a Closed Channel

Early studies of this type of flow were carried out by Lynn (118) and by Wilkes and Nedderman (119). Lynn proposed a model based on the Navier-Stokes equation (4.1) and the continuity equation (4.2); assuming that the liquid film thickness is constant as given by Nusselt's equation (2.1), after flowing a certain distance. Lynn's predictions compared favourably with his own experimental data, obtained by a photographical method.

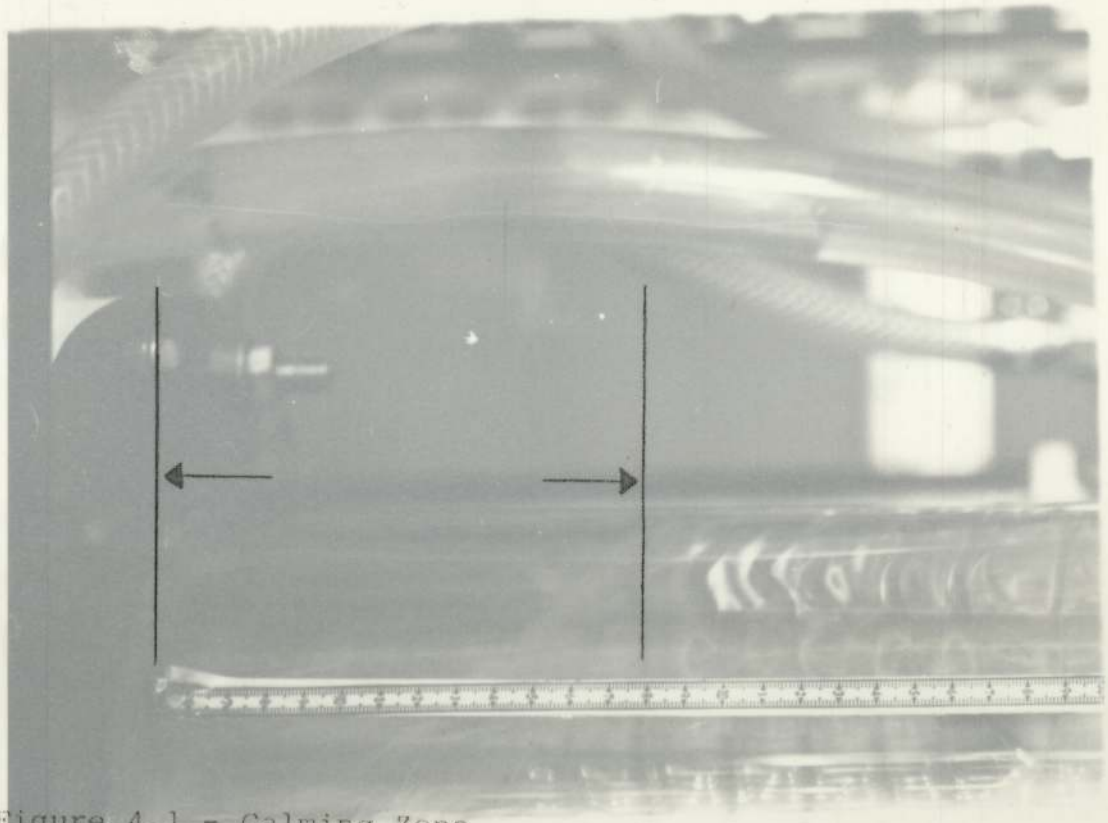

Figure 4.1 - Calming Zone

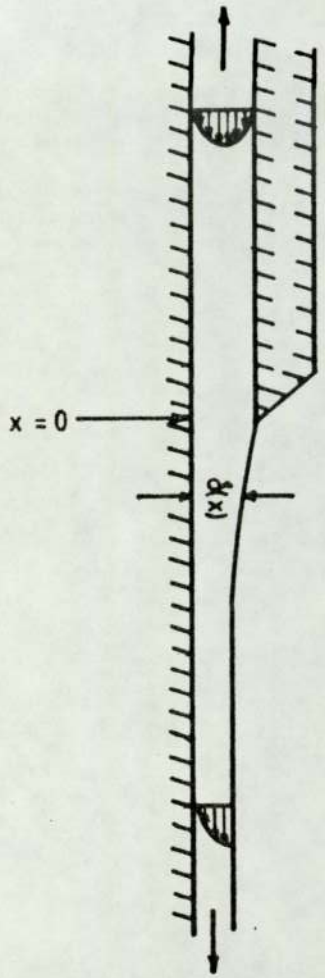

FIG. 4.2
FALLING FILM EMERGING FROM
BETWEEN PARALLEL PLATES

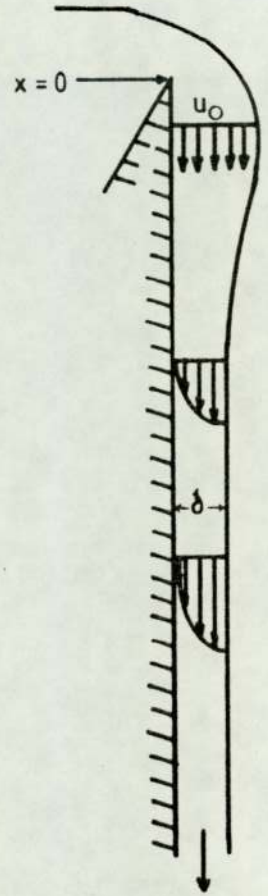

FIG. 4.3
FLOW EMERGING OVER A WEIR

The Navier-Stokes equation for the conditions of the film is:

$$g + \nu \frac{\delta^2 u}{\delta y^2} = u \frac{\delta u}{\delta x} + v \frac{\delta u}{\delta y} \qquad (4.1)$$

and the continuity equation is:

$$\frac{\delta u}{\delta x} + \frac{\delta v}{\delta y} = 0 \qquad (4.2)$$

Wilkes and Nedderman (119) measured the velocity profile after adding a surface active agent to the liquid to supress wave formation. However, due to the very complicated mechanism used to introduce the liquid, this work has little relevance in the present study.

More recent studies include those by Cerro and Whitaker (120,121), Stucheli and Ozisik (122) and Yilmaz and Brauer (123). Cerro and Whitaker (120) solved the governing equations of motion numerically, applying the Von Mises Transformation (124) to the Prandtl boundary layer equations. Two different approaches were considered and compared. The first assumed that the film thickness remains constant, i.e.

$$\delta_o = \delta(x) = \delta_\infty \qquad (4.3)$$

This was found to be incompatible with the boundary layer theory since it either violates the continuity equation or the viscous stress condition at the inter-phase.

The second approach included a variable film depth. The authors neglected the drag at the interface, ignoring the effect of gas-phase shear stress.

Cerro and Whitaker's model in dimensionless form is:

$$\frac{\delta \emptyset}{\delta X} = 4 + \emptyset^{\frac{1}{2}} \left(\frac{\delta^2 \emptyset}{\delta \psi^2}\right) \tag{4.4}$$

where $$\psi = \int_0^Y U dY \tag{4.5}$$

and $$\emptyset = U^2$$

$$X = x/\delta_N Re$$

$$Y = y/\delta_N$$

$$U = 2u/3\bar{u}_\infty$$

$$Re = 3U_\infty \delta_N / 2\nu \tag{4.6}$$

with the following boundary conditions:

$$\text{B.C.1} \quad \emptyset = f(\psi), \quad X = 0 \tag{4.7}$$

$$\text{B.C.2} \quad \emptyset = 0, \quad \psi = 0 \tag{4.8}$$

$$\text{B.C.3} \quad \frac{\delta \emptyset}{\delta \psi} = 0, \quad \psi = 1 \tag{4.9}$$

This model was solved numerically, by an implicit difference technique, and compared with the experimental results of Lynn. Stucheli and Ozisik used an integral method to obtain an expression for the hydrodynamic length

as a function of the Reynolds number and the thickness of the slit. They introduced a sinusoidal velocity profile given by equation 4.10, following the boundary layer approach.

$$u(x,y) = u_s(x) \sin \frac{\pi . y}{2\delta(x)} \qquad (4.10)$$

Their limiting film thickness when $x \to \infty$ was defined as:

$$\delta_\infty = \left(\frac{\nu\pi^2\Gamma}{3}\right)^{1/3} \qquad (4.11)$$

which is 6% less than the values obtained by using Nusselt's equation.

After comparing their results with those of Cerro and Whitaker (129) and Yilmaz and Brauer (123). They concluded that the flow situation at x = 0 is not important.

Yilmaz and Brauer developed empirical equations for the film thickness, mean film velocity and entrance length; as functions of the Reynolds's number and the distance from the origin. Their theoretical results were correlated against the experimental data obtained by Fulford (10) and satisfactory agreement was obtained.

Yilmaz and Brauer's equations are:

$$\delta^*_m = \frac{1}{1.5X^*} + 1 \qquad (4.12)$$

$$U_s = \frac{1.5}{1 + \left(\frac{1.5^2}{6x^*}\right)^{3\,1/6}} \qquad (4.13)$$

Where δ^*_m is the dimensionless film thickness, obtained by dividing the mean film thickness by the terminal film thickness, as predicted by Nusselt's equation. The dimensionless flow distance is defined as:

$$x^* = 4x/\delta_N Re \qquad (4.14)$$

The entry length was found to depend upon the way the liquid was introduced and expressed as the distance at which $\delta(x)$ reaches some fixed percentage deviation from the final value (δ_N).

4.1.2 Flow Emerging Over a Weir

Scriven and Pigford (125) studied this type of flow; they estimated the acceleration of the film surface and its effect on the rate of gas absorption. They assumed that only gravitational forces were acting upon the falling film and therefore they ignored the momentum transfer within the film.

Later theoretical studies were undertaken by a number of authors, among them Bruley (126), Hassan (127), Haugen (128) and Ito and Tomura (129,130). However, Ito and Tomura obtained experimental results by measuring velocity profiles using the hydrogen bubble method.

Both Bruley and Haugen adopted a similar approach, by assuming that the flow could be divided into a boundary layer region of changing thickness and an inviscid and accelerating region, where the only acting force was gravity as illustrated in figure 4.3.

The velocity at the free-falling region is expressed as:

$$\bar{u} = \sqrt{u_o^2 + 2gx} \qquad (4.15)$$

The behaviour of the falling film in the boundary layer was determined by the governing equation of motion (4.1) and the continuity equation (4.2). The film thickness then, was calculated by the following mass balance:

$$\delta(x) = h(x) + \Gamma/\bar{u} \qquad (4.16)$$

where h (x) is the boundary layer thickness.

A flat velocity profile was assumed at x = 0. Bruley assumed the velocity to be continuous between the two regions, and he made use of the Francis weir equation to estimate the initial velocity.

According to the source of Bruley's reference, Perry (13), Francis equation only applies when the liquid has the properties of water and the height of the crest above the weir exceeds .3 feet; which is a consideraly higher value than those used in Bruley.

A common failure of the known equations for full width weirs is the neglecting of the effects of boundary layer development, fluid properties and crest finishing. Recent tests carried out by the Hydraulics Research Station (132), highlights the inaccuracy of these equations and set the limit of applicability at a minimum height of the crest of 2.0cm.

Bruley used a direct numerical integration of the governing equations, with a marching ahead calculation to solve the resulting mathematical model. Haugen left unsolved the problem of determining the initial velocity and made use of an integral method; assuming a second order polynomial to estimate the velocity profile in the boundary layer region. This polynomial provided both for the continuity of velocity and stress between the regions.

Hassan assumed a polynomial of third degree for the velocity profile (4.17) in terms of a dimensionless distance form the wall, η.

$$u = \frac{\Gamma}{\delta(x)} \left(\left(\frac{3\Delta + 12}{5} \right) \eta - \frac{3}{2} \Delta \eta^2 + \left(\frac{4\Delta - 4}{5} \right) \eta^3 \right) \qquad (4.17)$$

$$\eta = y/\delta(x) \qquad (4.18)$$

where Δ is the dimensionless group:

$$\Delta = \frac{1}{3} \frac{\delta^3(x)}{\nu \Gamma} g \qquad (4.19)$$

This polynomial was obtained by assuming zero stress at the inter-phase and a of $\delta(x) \rightarrow \alpha$ as $x \rightarrow 0$.

Cerro and Whitaker compared the three previous studies with their own, finding a better agreement between theirs and Hassan's.

Ito and Tomura [129,130] considered the drag at the interphase and expressed a velocity profile for this region. An attempt to experimentally determine the velocity profile by means of the hydrogen bubble method was made, but due to the very small film thickness, and the fact that the buoyancy forces were not taken into consideration, is not believed to be accurate. They introduced the parameter K, which indicated the shift from Nusselt's analysis and is determined from experimental data. Ito's formula for the film thickness is

$$\delta = \left(\frac{1}{1 - .75K}\right) \delta_N \qquad (4.20)$$

4.2 Experimental Analysis

Two sets of experiments were designed. The first set consisted of a number of experiments, using the tubular reactor, to determine which system of distribution was preferred. The objective of the second set of experiments was to obtain data on the film thickness at small distances from the inlet. A wetted wall was designed and built, as described in chapter 3, in order to perform this experiment.

4.2.1 Entrance Region Experiments, Tubular Reactor

In choosing between the two alternative methods to introduce the liquid film, it was observed that the type of flow consisting of a liquid film flowing freely over a weir gave more satisfactory results. The other choice, liquid flow emerging from a closed channel required a number of special design considerations and a great accuracy wuld have been necessary to determine the width of the slip.

A number of tests were made using different liquids, flow rates and gap widths. The results of these experiments are shown in Table 4.1. It was found that at relatively low Reynolds numbers, for gap widths up to three times larger than the falling film thickness predicted by Nusselt's theory, jetting effect occurred.

Therefore, it was decided to use a gap of 6.0mm at the inlet, which is much larger than the expected film thickness, for the range of Reynolds numbers studied in this investigation. Tests with this width gave excellent results; however, all theories concerning liquid film flowing freely over a weir are not applicable when the liquid has properties different than those of water, as it was previously mentioned.

A protective shield was installed, as shown in figure 3.4 , to allow the liquid to be fully developed and stable before contacting the gas flow. The length of this shield was estimated using the relation given by Pierson and Whitaker (133).

$$x_e \sim \delta_N Re \qquad (4.21)$$

which can be rewritten as

$$x_e \sim (2\nu^2/g)^{1/3} \quad Re^{4/3} \qquad (4.22)$$

Assuming maximum values for the kinematic viscosity and mass flow rates of 1.5 poise and 700 kg/hr respectively, an estimated minimum length (x_e) of 2cm was obtained.

4.2.2 Entrance Region Experiments, Wetted Wall

A number of experiments were carried out with the use of the wetted wall to measure the film thickness at a distance of 2cms from the inlet. The results of these tests are illustrated in Tables 4.2, 4.3, 4.4 and 4.5.

These results are favourably compared with Nusselt's theory predictions of the thickness of stable smooth film flow; as can be seen in figure 4.4.

4.3 Conclusions

From the above discussion, the following conclusions can be made:

1. In order to use an inlet system in which the liquid is fed by flowing freely over the edge of the vertical wall of the reactor, the width of the inlet gap should be at least three times larger than the maximum predicted film thickness, to avoid jetting of the liquid, when the system is operating at high flow rates.

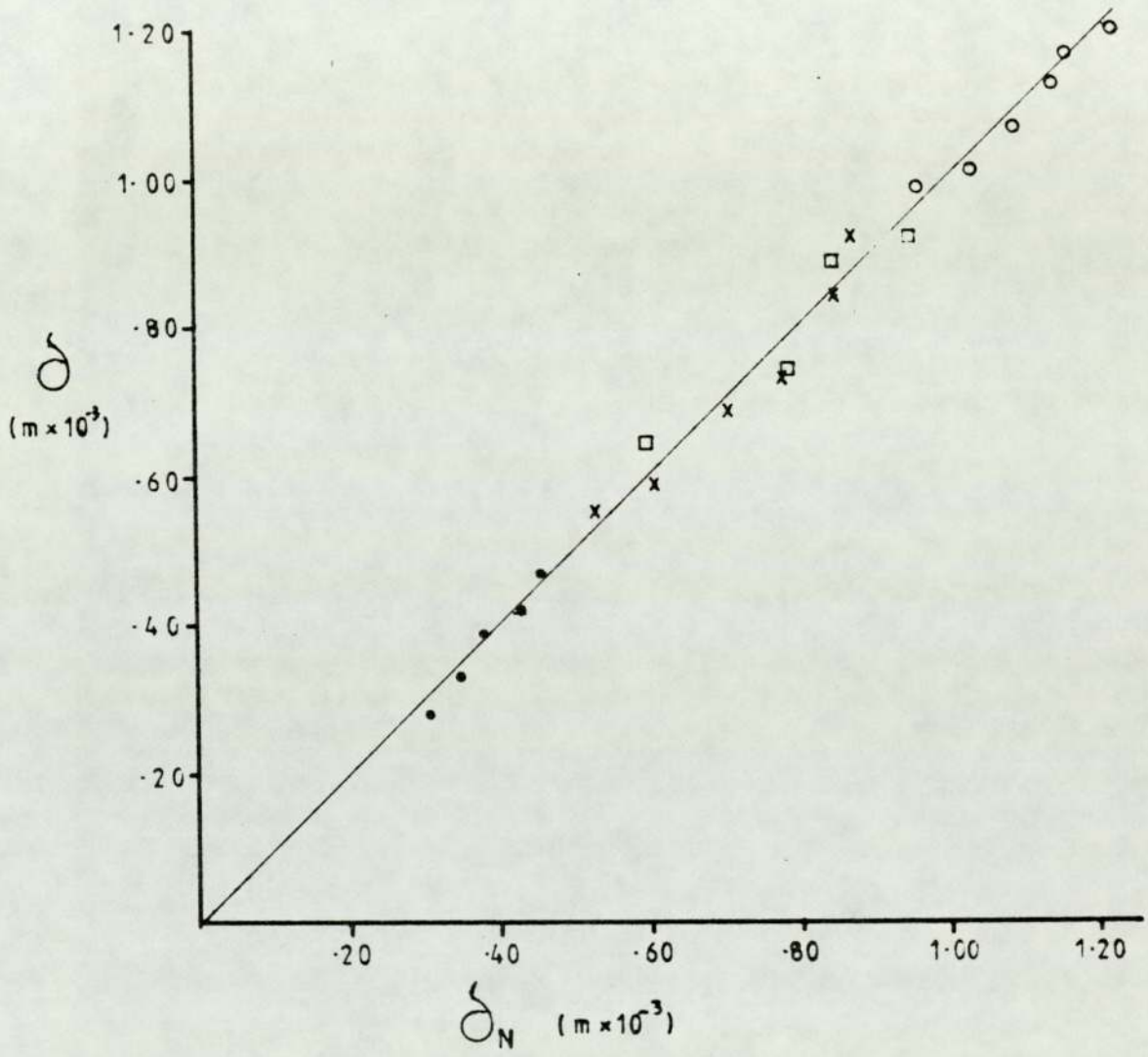

Figure 4.4 - Comparison of Experimental Film Thickness with Theoretical Film Thickness

2. The liquid film should be allowed to develop and become stable before contacting with cocurrent gas stream. A protective shield has been incorporated, with a length exceeding the estimated length of entrance region, as predicted by the surveyed literature.

3. Nusselt's theory for smooth laminar flow can be used to represent the flow of the falling film as it enters the reactor. The assumption made by van Nusselt, that the effects of drag at the free surface can be neglected, is justified only when the liquid is not in contact with a moving gas phase. Experimental observations show the dampening effect of the gas flow, even at relatively low gas flow rates.

Table 4.1 - Minimum Gap Width for Injecting Device

Gap Width (m)	Visual Observations
.001	Jetting at $\Gamma > 1.2 cm^3/cm^2 s$
.003	Jetting at $\Gamma > 2.0 cm^3/cm^2 s$
.006	No jetting observed
.010	No jetting observed

All experiments were carried out with water at $20^{\circ}C$

Table 4.2 - Film Thickness Measurements at the Entrance Region, Water

Physical Characteristics of the Water at 20°C

Specific gravity, ρ = 1.0 gr/cm^3

Viscosity, μ = 1.cP

Kinematic Viscosity, ν = 1.cS

Γ (cm^3/cm s)	Re	δ (mm)	δ_N (mm)
1.00	400	.28	.31
1.39	556	.33	.35
1.83	732	.39	.38
2.5	1000	.42	.43
3.14	1256	.47	.46

Table 4.3 - Film Thickness Measurements at the Entrance Region, Glycerol 65%

Physical Characteristics of Glycerol 65% at 20°C

Specific gravity ρ = 1.17 gr/cm^3

Viscosity, μ = 15cP

Kinematic Viscosity ν = 12.8cS

Γ (cm^3/cms)	Re	δ (mm)	δ_N (mm)
.39	12	.55	.53
.59	18.4	.59	.61
1.21	38.	.73	.78
1.57	49	.84	.85
1.65	52	.92	.87
.9	28	.69	.71

Table 4.4 - Film Thickness Measurement at the Entrance Region, Glycerol 80%

Physical Characteristics of Glycerol 80% at 20°C

Specific gravity ρ = 1.21 gr/cc

Viscosity, μ = 60cP

Kinematic viscosity, ν = 49.59cS

Γ (cm^3/cms)	Re	δ (mm)	δ_N (mm)
.59	4.8	.99	.96
.72	5.8	1.01	1.03
.85	6.9	1.07	1.09
.98	7.8	1.125	1.14
1.01	8.1	1.165	1.16
1.2	10.0	1.20	1.22

Table 4.5 - Film Thickness Measurement at the Entrance Region, Sucrose 65%

Physical characteristics of Sucrose 65% at 20°C

Specific gravity $\rho = 1.265\ gr/cm^3$

Viscosity, $\mu = 35cP$

Kinematic viscosity, $\nu = 27.7cS$

$\Gamma\ (cm^3/cms)$	Re	δ (mm)	δ_N (mm)
.26	4	.64	.60
.59	8.5	.76	.79
.72	10.4	.89	.85
1.03	15.	.92	.95
1.21	17.5	.98	1.01
1.43	21.	1.04	1.07

CHAPTER V

ENTRAINMENT

5.1 Entrainment

If a gas flows parallel to the surface of a liquid film, it will exert a drag on that surface. The effect of the drag changes as the gas flowrate is increased. At relatively low gas velocities, the growth of a liquid velocity induced by the gas flow is negligible, but as the gas velocity is increased the wavy surface of the film undergoes a transformation, from a "cross hatched" appearance to a more uniform flow, with waves having a steeper front, large amplitude and a smooth region between crests. Such waves are called "roll" waves, and have been studied by Hanratty and Hersman (134), Hanratty and Engen (51) and Chung and Murgatroyd (59) among others. At still higher gas velocities, liquid droplets are torn away from the liquid surface and contained by the gas phase.

The process of heat, mass and momentum between the two phases is substantially affected by the inception of entrainment. Entrainment limits the performance and complicates the design of chemical engineering systems, examples are found in the works of Zuber (135), Brodkey (136) and Ishii and Grolmes (137). Therefore, it is of great importance to understand the mechanisms that lead to these conditions and the behaviour of the falling film under such conditions. A considerable amount of theoretical and experimental work has been carried out by several authors, particularly Ishii and Grolmes (137) who in 1975, made a comprehensive review of existing theories and empirical correlations. Previous surveys were made by Wallis (2) and Hewitt

and Hall-Taylor (1).

Published data shows large variability, probably due to the different methods used to detect and measure entrainment. As suggested by Andreussi (138), most detection methods indicate a gas velocity at which entrainment is well above the inception point; for example, pressure drop measurement gives results of critical gas velocities five times greater than results obtained by visual observation. Therefore, because of these conflicting results, given by existing empirical correlations, it is necessary to find the entrainment inception criteria based on a reliable physical model, which would provide a better understanding of the entrainment mechanisms and could be used as a reliable design rule.

It has been substantiated by many authors that droplet entrainment occurs only in the disturbance wave regime. Several mechanisms of droplet entrainment have been described in the literature; Hewitt and Hall-Taylor give good descriptions of the different types, two of which appear to be reasonable physical interpretations of droplet entrainment in a falling film system. The first consists of the shearing off, by the turbulent gas flow, of the top of the rolling wave as shown by Figure 5.1. This has been observed by Hanratty and Hershman (134), and Brodkey (136).

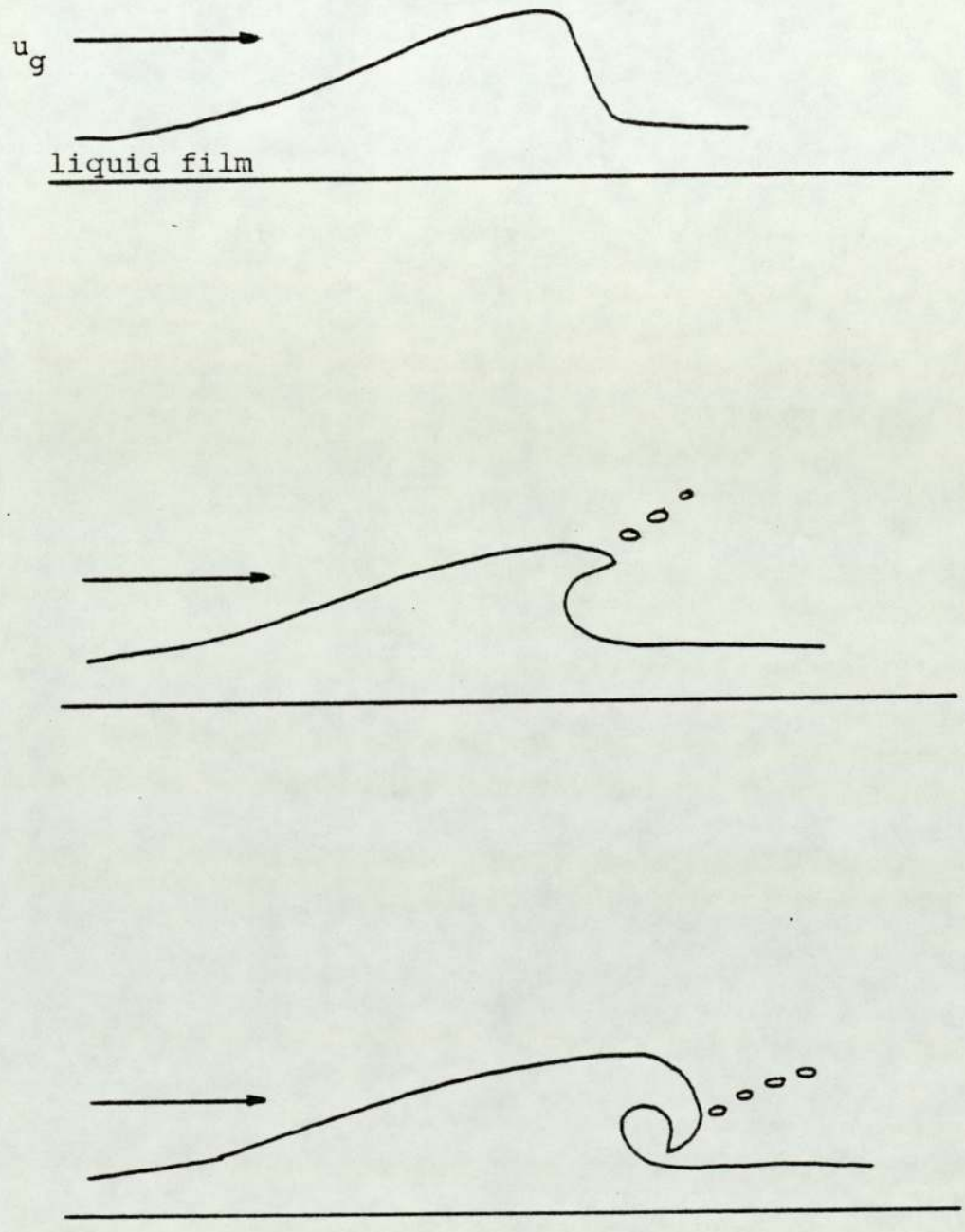

Figure 5.1 - "Shearing off" mechanism

The other type describes droplet entrainment to be caused by the undercutting of the falling film as shown in Figure 5.2. This mechanism resembles the first type, and a strong relation between both types should be expected.

The existing data for the inception of entrainment shows that, at least, three different regimes exist. Experimental data obtained by Van Rossum (139), Zhivaikin (58), and Andreussi (138) indicate that below a certain liquid Reynolds number no entrainment occurs, even at gas velocities exceeding 80 m/s. However, there is a discrepancy in the value of the critical Reynolds number. At very small Reynolds numbers, the liquid film breaks into rivulets, originating from dry patches, because of this abrupt change in the flow pattern. The system is no longer governed by the same equations of motions as falling film flow. In the region of regular wavy flow, the critical gas velocity for the onset of entrainment becomes a function of the liquid Reynolds number. This indicates that liquid flow within the film contributes to the transferring of momentum between phases, as indicated by Hughmark (140). At larger Reynolds number, the critical gas velocity reaches a limiting value, below which entrainment is impossible. This region is located above the liquid Reynolds number for turbulent film flow. Figure 5.3 shows the three regimes as experimentally observed by Andreussi.

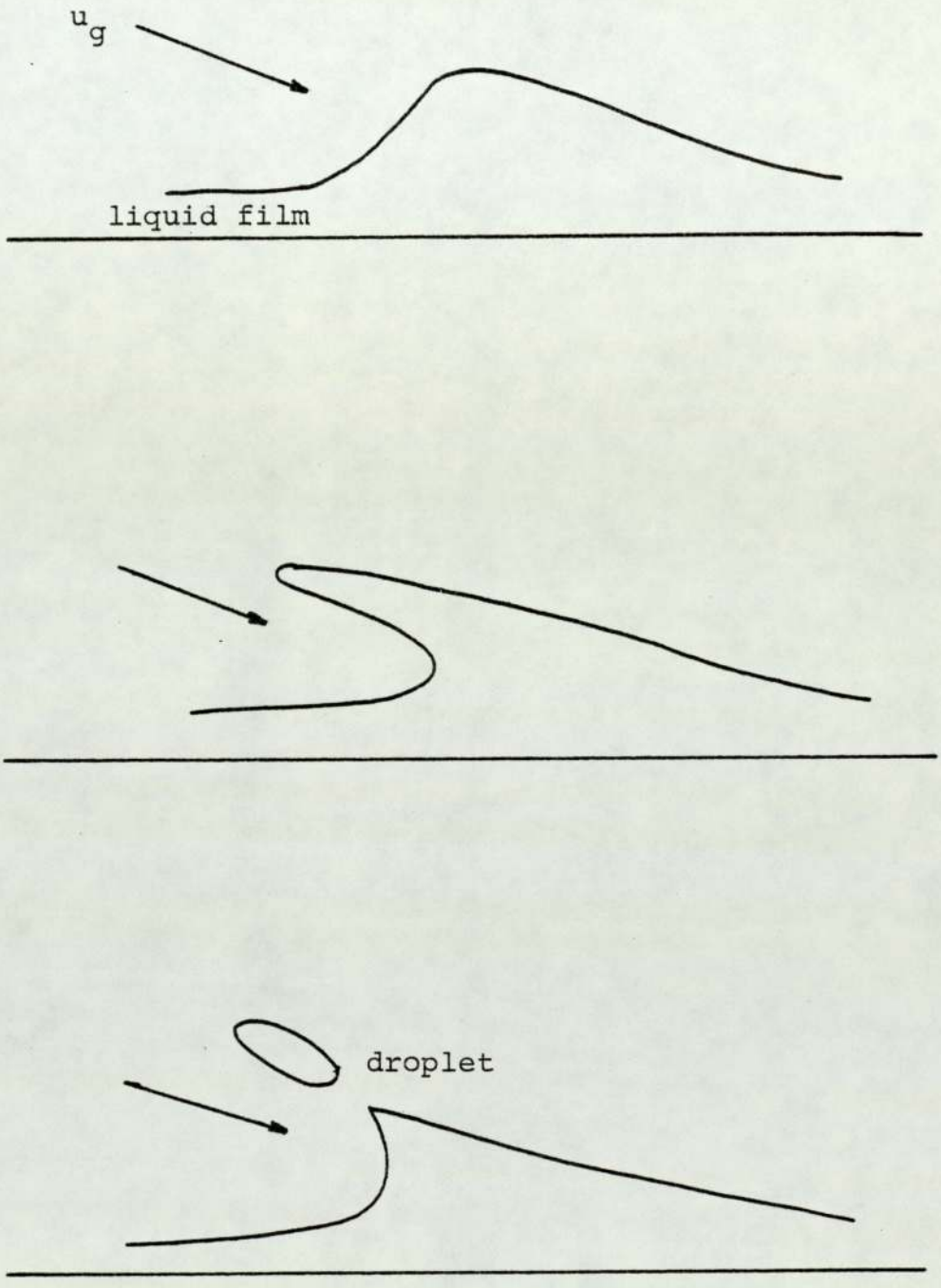

Figure 5.2 - "Undercutting of the wave" mechanism

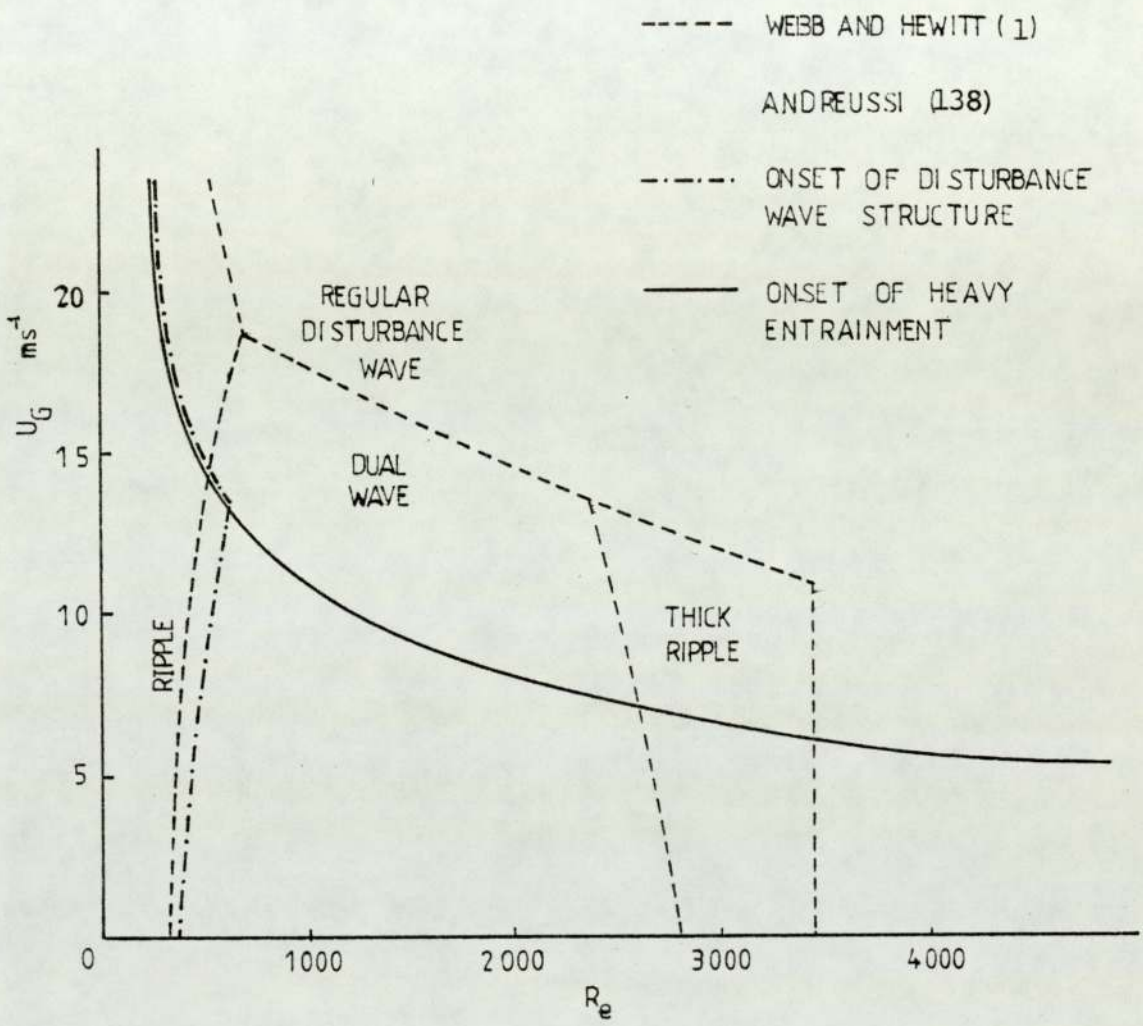

Figure 5.3 - Flow Regimes

5.1.1 Inception Criterium

Ishii and Grolmes developed their inception criterium for the transition regime entrainment, based on the roll wave geometry with the following assumptions:

1. Entrainment is only possible if the drag force (F_d), caused by the shear of the gas flow, becomes greater than the retaining force of the surface tension (F_σ). This criterion was first introduced by Zuber (135) in 1962.

$$F_d > F_\sigma \tag{5.1}$$

2. The interfacial shear force at the top of the wave causes an internal flow of the same order of magnitude as that of the average film velocity. This motion can be described by a shear flow model.

$$\tau_i = Cw\mu\, u_s/a \tag{5.2}$$

where Cw is the surface tension factor in the internal flow and it is a function of the viscosity number $N\mu$

$$N_\mu = \frac{\mu}{(\rho\ \sigma\ (\frac{\sigma}{g(\rho - \rho_g)})^{\frac{1}{2}})^{\frac{1}{2}}} \tag{5.3}$$

The graphical representation of the model used by the authors is shown in Figure 5.4.

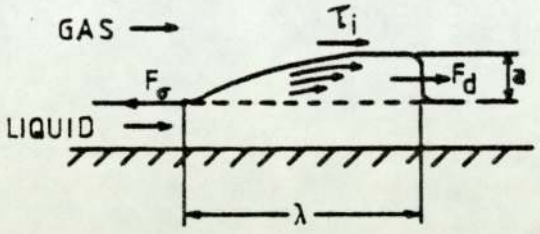

SIDE VIEW

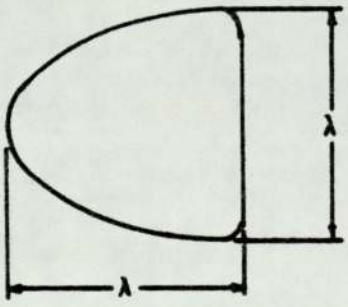

TOP VIEW

FIG. 5.4. MODEL FOR ENTRAINMENT BASED ON ROLL-WAVE BREAKUP.

The drag force, F_d, is defined as

$$F_d = C_d \lambda a \rho_g u_r^2/2 \tag{5.4}$$

Because of the irregular shape of the wave crest, it is reasonable to assume $C_d \simeq 1$; which according to Brodkey (136) is applicable in the Reynolds range from 10 to 50000.

The retaining force, F_σ, is given in terms of C_s, the interfacial shape coefficient.

$$F_\sigma = C_s \lambda \sigma \tag{5.5}$$

But because the base of the wave has a half elliptical form

$$C_s \lesssim .77 \tag{5.6}$$

So the equation 5.1 can be rewritten as:

$$\rho_g \frac{u_r a}{2} > .77\sigma \tag{5.7}$$

The shear force at the interface is represented as:

$$\tau_i = f_{g_i} \rho_g u_r^2/2 \tag{5.8}$$

for the gas friction factor, or

$$\tau_i = f_i \rho_L \bar{u}_L^2/2 \tag{5.9}$$

for the liquid friction factor.

Because the interface is wavy the correlation by Wallis (2) can be applied

$$f_{gi} = .005\ (1 + 3000\ \delta/D) \tag{5.10}$$

and the liquid friction factor is defined by Hughmark (140) as:

$$f_i^{\frac{1}{2}} = K\ Re^m \tag{5.11}$$

Where the constants K and m are functions of the Reynolds number. However, in this region it is a reasonable assumption to state

$$f_i = (1.962\ Re^{-1/3})^2 \tag{5.12}$$

Assuming the film thickness to be much smaller than the hydraulic diameter and the gas velocity to be much larger than the liquid velocity, the inception criteria can be rewritten as

$$\mu_\ell \frac{u_s}{\sigma} \frac{\rho_g}{\rho} > \frac{Re^{1/3}}{3Cw(N\mu)} \tag{5.13}$$

Ishii and Grolmes correlated previous experimental data and defined Cw as,

$$\frac{1}{3Cw} = 11.78\ N_{\mu}^{.8}, \quad \text{for} \quad N_{\mu} < \frac{1}{15} \tag{5.14}$$

or

$$\frac{1}{3Cw} = 1.35 \quad \text{for} \quad N_{\mu} > \frac{1}{15} \tag{5.15}$$

The inception criteria takes the following simplified form:

$$\mu \frac{u_g}{\sigma} \left(\frac{\rho_g}{\rho}\right)^{\frac{1}{2}} > 11.78 N\mu^{.8} Re^{-1/3} \quad \text{for} \quad N_{\mu} < \frac{1}{15} \tag{5.16}$$

or

$$\mu \frac{u_g}{\sigma} \left(\frac{\rho_g}{\rho_\ell}\right)^{\frac{1}{2}} > 1.35\ Re^{-1/3} \quad \text{for} \quad N\mu > \frac{1}{15} \tag{5.17}$$

Ishii and Grolmes work represents a great contribution to the understanding of the mechanisms of droplet entrainment. However, by using Hughmark's correlation for the determination of the friction factor, they limit the applicability of their criteria to upward flow in an apparatus with a "maximum tube diameter of about 4cm and a maximum liquid viscosity of about 5 cP", as stated by Hughmark (140).

5.1.2 Zhivaikin's Model

In 1962, Zhivaikin (58) proposed his criteria for the prediction of the critical gas-phase velocity at which entrainment starts. Three different flow regimes were identified for the falling film. The critical velocity $u_{g,cr}$ is defined as a function of the liquid flow parameters and physical properties.

$$u_{g,cr} = f(\Gamma,\mu,\rho,\sigma) \tag{5.18}$$

For low Reynolds numbers,

$$Re < \frac{.085}{\nu^2}, \tag{5.19}$$

the following empirical correlation was found:

$$u_{g,cr} = \frac{29.2\sigma}{\mu Re^{.75}} ; \tag{5.20}$$

for intermediate Reynolds numbers,

$$\frac{.085}{\nu^2} < Re < \frac{28.8}{\nu} , \tag{5.21}$$

$$u_{g,cr} = \frac{100\sigma}{\rho Re^{.25}} \tag{5.22}$$

and for higher Reynolds numbers,

$$Re > \frac{28.8}{\nu} \tag{5.23}$$

$$u_{g,cr} = 43.2\mu^{.25}\sigma/\rho^{1.25} \tag{5.24}$$

The experimental programme was carried out using two vertical columns, each .83m long with diameters of 13mm and 21mm. The liquids used were glycerol solutions with viscosities in the range of $1cP < \mu < 8cP$. However, Zhivaikin's published work does not provide any information on how the onset of entrainment was determined.

5.2 Minimum Thickness of a Liquid Falling Film

The problem of rupture of the thin liquid film into a series of rivulets is of great importance in the design of a falling film gas-liquid contacting device. The formation of dry patches, as the solid surface is left partially exposed, reduces the contacting surface area, which in turn affects the efficiency in the rates of heat and mass transfer, of the system. The mechanism of this phenomenon is very complex, and several attempts have been made to describe it. However, it has been successfully demonstrated experimentally that a minimum flow rate is necessary to wet or cover the entire solid surface. This minimum wetting rate is related to the properties of the liquid, the contact angle between the liquid and the solid wall, the feed system for the liquid and the shear stress at the gas-liquid interface. This minimum wetting rate also depends on the initial conditions on the solid surface. Hoffman and Potts (141) suggested the three following cases: the first case consists of an initially dry solid surface with the liquid flow increasing from zero, in the second case the surface of the solid had been

previously wetted, and finally the third case, in which the liquid flow is decreased until the appearance of dry patches. The analysis of previous experimental works indicates the following pattern for the minimum flow rate per unit of wetted perimeter (Γ_{min}).

$$\Gamma_{min}(\text{Case 1}) > \Gamma_{min}(\text{Case 2}) > \Gamma_{min}(\text{Case 3})$$

Previous studies of the stability of thin liquid films, based on classical linear theory, Anhus (27) and Krantz (28) amongst others, have failed to provide a description of the mechanisms involved in the break down of the liquid film. This is due to two main factors, firstly, that the linear theory is unable to incorporate disturbances once they have grown enough to cause this rupture and secondly, that it ignores the contact angle between the liquid and solid surface. Hartley and Murgatroyd (142,143) suggested two different approaches to solve this problem, one was based on a force balance made at the upstream point of a dry patch, as shown in Figure 5.5. The second approach, known as the "rivulet model", assumed that a stable film configuration corresponds to a minimum energy or power transmission by the film in the form of kinetic and surface energy.

Hartley and Murgatroyd's "dry patch" model states that for a dry patch to be stable, the surface tension forces acting at the upstream stagnation point must balance the fluid pressure on the surface. The pressure force

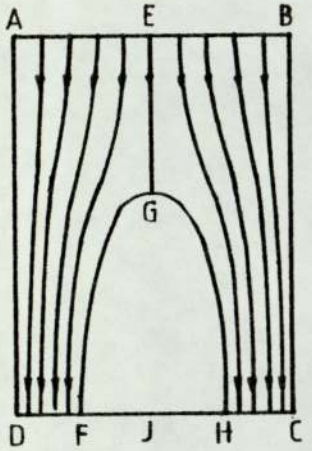

PLAN VIEW

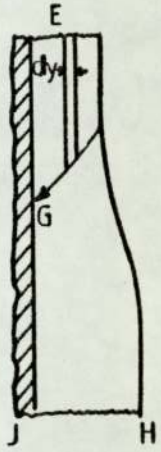

CROSS SECTION
ALONG E G J

Figure 5.5 - "Dry Patch" Model

is due to the transformation of fluid kinetic energy, while the surface tension force is a function of the contact angle. When these two forces are equal, the film thickness and wetting rate are at their minimum values. So the following criterion was formulated.

$$\sigma(1-\cos\phi) = \int_0^{\delta_c} \rho/2\ (u(y))^2\ dy \qquad (5.25)$$

If the laminar liquid film is following under the influence of surface shear, the minimum film thickness (δ_c) according to equation 5.25 is;

$$\delta_c = 1.82\left[\sigma(1-\cos\phi)/\rho\right]^{1/3}\ (\mu/\tau)^{2/3} \qquad (5.26)$$

Hewitt and Lacey (144) compared their experimental results with the above criterion, showing a qualitative agreement between data and the model, but it required unrealistic contact angles for the theory to be satisfied quantitatively. Ruckenstein (145) introduced a dynamic angle $\emptyset_d$ thereby modifying equation 5.25

$$\sigma(\cos\emptyset_d - \cos\emptyset) = f(\emptyset_d) \int_0^{\delta_c} \rho/2\ (u(y))^2 dy \qquad (5.27)$$

Therefore, a stable dry patch would occur for all angles in the range $0 < \emptyset_d < \emptyset$.

Ponter, Davies, Ross and Thornley (146) studied the influence of mass transfer on the break down of a thin liquid film following Hartley and Murgatroyd's "dry patch" model. They demonstrated the validity of the model when

mass transfer was taking place, but since the surface tension changes during absorption, the value of the surface tenstion must be measured under the experimental conditions for a prediction to be correct. Chung and Bankoff (147) and Zuber and Staub (148) extended the analysis to study the effect of non-uniform temperature distribution and evaporation at the surface.

The "rivulet model" as first stated by Hartley and Murgatroyd suggested that a laterally unrestrained liquid film (Figure 5.6) will reach a stable width which corresponds to a minimum in the sum of the kinetic energy flow and the energy flow at the surface. However, their criterion did not take into consideration the effect of the contact angle. Hobler (149,150) accounted for the effect of the contact angle, but did not give any information on the configuration of the rivulet. Hobler's empirical correlation for the minimum wetting rate had a poor fit when compared to his experimental data.

Bankoff (151) extended Hartley and Murgatroyd's "rivulet model", proposing that the continuous falling-film would break up into rivulets in the shape of an arc. The criterion was based on the assumption that no loss of mass or energy occurred in the transition from film flow to rivulet. Mikielewicz and Moszynski (152) based their analysis on the two previous works mentioned above, allowing for a dry space between rivulets. A variable β was defined as the ratio of the rivulet base to the corresponding undisturbed film width, as in

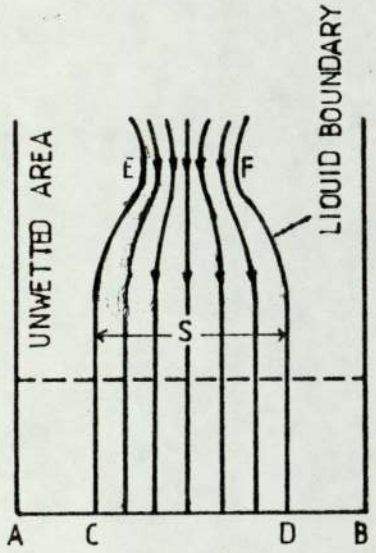

PLAN VIEW

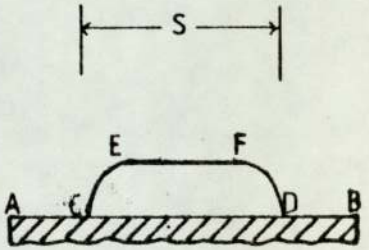

CROSS SECTION

Figure 5.6 - "Rivulet" Model

Hobler and Czajka's work (149,150) and Bankoff's assumption of no energy or mass loss was made. The energy of the rivulet configuration was required to have a minimum for $\beta < 1$, for the configuration to be stable.

The mechanical energy of the undisturbed film (e_f) per wetted perimeter consisted of the sum of the kinetic energy of the liquid film and the surface tensions at the free interface and at the solid wall, e.q. 5.21.

$$e_f = \int_o^{\delta} \rho/2 \; u^2(y)\,dy + \sigma_{sf} + \sigma_{fg} \qquad (5.28)$$

The mass flow per wetted perimeter of the rivulet is defined, assuming a velocity profile as in an undisturbed film of the same thickness, so the following expression is obtained

$$\dot{m}_{riv} = 2 \int_o^{R\sin} \int_o^{\delta(z)} \rho u(y,z)\,dz\,dy \qquad (5.29)$$

Making an energy balance at the point of contact of the three phases, where an equilibrium of the surface tensions must exist for the rivulet to be stable.

$$\sigma_{sg} = \sigma_{fs} + \sigma_{fg} \cos \phi \qquad (5.30)$$

So the total energy of the rivulet is expressed as;

$$e_{riv} = \frac{\rho}{\lambda} \int_o^{R\sin\phi} \int_o^{\delta(z)} u^2(z,y)\,dz\,dy + \left(\frac{2R\phi}{\lambda} + \cos \phi - \right.$$

$$\left. \frac{R\sin\phi}{\lambda}\right) \sigma_{fg} + \sigma_{fs} \qquad (5.31)$$

Therefore, the ratio of wetted surfaces, β, is

$$\beta = \frac{2R\sin\emptyset}{\lambda} \tag{5.32}$$

Also, e_{riv} could be rewritten as a function of β. Then, for the rivulet flow to be stable the following conditions must be fulfilled

$$\frac{\delta e_{riv}}{\delta \beta} = 0 \tag{5.33}$$

and

$$e_f = e_{riv} \tag{5.34}$$

while

$$\beta < 1 \tag{5.35}$$

Mikielewicz and Moszynski's criteria has been successfully tested for laminar falling film. For falling film under the effect of shear and form drag due to a cocurrent gas stream, it is necessary to determine the friction factor and velocity profile of the film, before being applied.

In 1977, Ponter and Awald (153) tested the validity of the above theory, by comparing the predicted values of minimum film thickness with experimental data collected by themselves and with data obtained by Norman and McIntyre (153), Munakata, Watanabe and Miyashita (155), Iijiima and Kuzuoka (156) and Ponter and Boyers (157). Mikielewicz and Moszynski's equations proved to be

superior to that of previous studies by Hobler, Hartley and Murgatroyd, and Bankoff. However, it showed deviations for systems where water films were experimenting changes in temperature.

CHAPTER VI

MATHEMATICAL MODEL OF THE HYDRODYNAMICS OF A FALLING FILM

In this chapter the hydrodynamics of the system will be analysed. The system consists of a turbulent gas and a semi-laminar liquid film flowing downwards, cocurrently in a vertical annular column. The falling liquid film is fully developed and flows uniformly and steadily, undisturbed by either formation of dry patches or droplet entrainment, under the influence of gravitational forces and interfacial shear stress. The gas stream is fully turbulent and flows in between either one wetted and one dry wall, or two wetted walls. A model proposed is based on a microscopic description of the flow, following a phenomenological approach. The system is illustrated in Figure 6.1.

6.1 Mathematical Model

The following assumptions have been made:

1. Because of the geometry of the system, the radius of curvature is much greater than the expected thickness of the falling film. Therefore, the system can be represented as a very wide flat wall, so that the effect of the sides on the flow are negligible and the film is two-dimensional. The system coordinates are x and y, where x is the distance from the point at which both phases come into contact with each other; y is the distance perpendicular to the wall, adjacent to the liquid film.

2. There is no change in temperature along or across the reactor. The viscosity and density of the liquid film are constant.

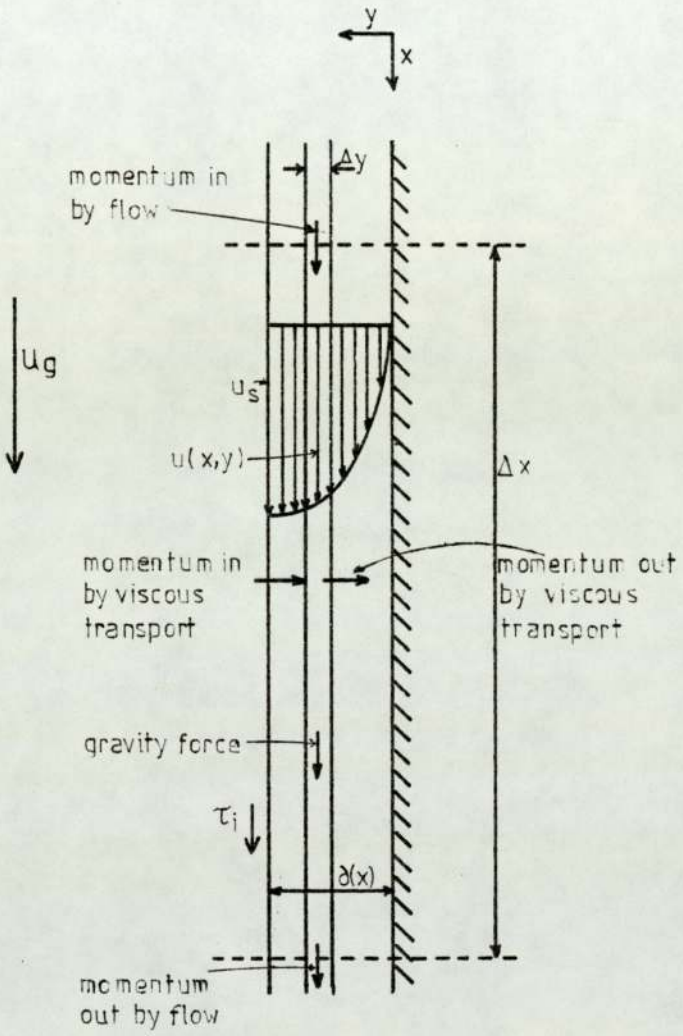

Figure 6.1 - Graphical representation for the Mathematical Model of the Hydrodynamics of the Liquid Film

The governing equations for the flow of a newtonian falling film on a vertical plane can be expressed as

$$u \frac{\delta u}{\delta x} + v \frac{\delta u}{\delta y} = g - \frac{1}{\rho} \frac{dP}{dx} + \nu\left(\frac{\delta^2 u}{\delta x^2} + \frac{\delta^2 u}{\delta y^2}\right) \tag{6.1}$$

$$u \frac{\delta v}{\delta x} + v \frac{\delta v}{\delta y} = \frac{1}{\rho} \frac{dP}{dx} + \nu\left(\frac{\delta^2 v}{\delta x^2} + \frac{\delta^2 v}{\delta y^2}\right) \tag{6.2}$$

which are the Navier-Stokes equations of motion, in the x and y direction respectively; and the continuity equation for incompressible two-dimensional flow which takes the form

$$\frac{\delta u}{\delta x} + \frac{\delta v}{\delta y} = 0 \tag{6.3}$$

However, the equation of motions can be simplified by making the following assumptions, based on the boundary layer theory:-

1. The flow motion in the x direction is much greater than in the y direction, so $u >> v$. Therefore, the term v can be neglected.

2. Following the same argument as above, $\delta^2 u/\delta x^2 << \delta^2 u/\delta y^2$ so $\delta^2 u/\delta x^2$ can be neglected.

Then the equation of motion can be rewritten as

$$u \frac{\delta u}{\delta x} = g - \frac{1}{\rho} \frac{dP}{dx} + \nu \frac{\delta^2 u}{\delta y^2} \tag{6.4}$$

For a constant axial pressure gradient, equation 6.4 becomes

$$u \frac{\delta u}{\delta x} = G + \nu \frac{\delta^2 u}{\delta y^2} \qquad (6.5)$$

where G is constant equal to the term $g - \frac{1}{\rho}\delta P/\delta x$.

The boundary conditions for equation 6.5 are

B.C.1 $u(x,y) = u_o(y)$; at $x = 0$, when $0 < y < \delta_o$

B.C.2 $u(x,y) = 0$; at $y = 0$, for all x

B.C.3 $u(x,y) = u_s(x)$; at $y = \delta(x)$, when $0 < x < L$

The boundary conditions at $x = 0$, is based on the assumption that the film is laminar before coming into contact with the turbulent gas stream. The inlet film thickness δ_o and the velocity profile $u_o(y)$ are given by Nusselt's equations, as described in Chapter 4. The secondary boundary condition satisfies the condition of no slip at the wall. The third indicates that the velocity of the film at the interface u_s along the length of the reactor, is affected by the gas-phase drag. In order to satisfy the continuity equation and the second and third boundary conditions, the film thickness cannot remain constant, as it has been assumed in previous models proposed in the literature.

The problem of solving the non-linear equation is simplified by using the von Mises transformation [124], which consists of introducing the stream function ψ, defined as

$$u = \frac{\delta\psi}{\delta y} \tag{6.6}$$

and

$$v = -\frac{\delta\psi}{\delta x} \tag{6.7}$$

Equations 6.6 and 6.7 satisfy the continuity equation. Rearranging equation 6.6 and integrating it between the limits y = o and δ_o, the film thickness at x = O,

$$\psi_o = \int_o^{\delta_o} u\,dy = \bar{u}_o \delta_o \tag{6.8}$$

where $\bar{u}_o$ is the initial average velocity. However, the product of $\bar{u}_o$ and δ_o is equal to the volumetric flow per wetted perimeter Γ, which is constant along the length of the reactor. So now, the region

$$O < y < \delta(x)$$
$$x < O \tag{6.9}$$

is mapped into the region

$$O < \psi < \Gamma$$
$$x < O \tag{6.10}$$

Setting up the new set of coordinates $\psi - \zeta$, where ζ is the length coordinate. Then

$$\frac{\delta u}{\delta x} = \frac{\delta u}{\delta \zeta} \cdot \frac{\delta \zeta}{\delta x} + \frac{\delta u}{\delta \psi} \cdot \frac{\delta \psi}{\delta x} \tag{6.11}$$

$$\frac{\delta u}{\delta y} = \frac{\delta u}{\delta \zeta} \cdot \frac{\delta \zeta}{\delta y} + \frac{\delta u}{\delta \psi} \cdot \frac{\delta \psi}{\delta y} \qquad (6.12)$$

But from the definition of variables and the known equations, the following pertains:

$$\frac{\delta \zeta}{\delta x} = 1 \quad \text{and} \quad \frac{\delta \psi}{\delta x} = -v \qquad (6.13)$$

$$\frac{\delta \zeta}{\delta y} = 0 \quad \text{and} \quad \frac{\delta \psi}{\delta y} = u \qquad (6.14)$$

After substituting in equations 6.11 and 6.12 they are rewritten as

$$\frac{\delta u}{\delta x} = \frac{\delta u}{\delta \zeta} - v \frac{\delta u}{\delta \psi} \qquad (6.15)$$

and

$$\frac{\delta u}{\delta y} = u \frac{\delta u}{\delta \psi} \qquad (6.16)$$

substituting equations 6.15 and 6.16 into equation 6.5 it becomes

$$u\left(\frac{\delta u}{\delta \zeta} - v \frac{\delta u}{\delta \psi}\right) + vu \frac{\delta u}{\delta \psi} = G + \nu \left(u \frac{\delta^2 u}{\delta \psi^2} + \frac{\delta u}{\delta y} \frac{\delta u}{\delta \psi}\right) \qquad (6.17)$$

which is transformed to

$$u \frac{\delta u}{\delta \zeta} = G + \nu u \frac{\delta (u \delta u / \delta \psi)}{\delta \psi} \qquad (6.18)$$

Introducing a new variable $\chi = u^2$, so

$$\frac{\delta \chi}{\delta \zeta} = 2u \frac{\delta u}{\delta \zeta} \tag{6.19}$$

and

$$\frac{\delta \chi}{\delta \psi} = 2u \frac{\delta u}{\delta \psi} \tag{6.20}$$

Equation 6.18 can be rearranged as

$$\frac{\delta \chi}{\delta \zeta} = 2G + \nu \chi^{\frac{1}{2}} \frac{\delta^2 \chi}{\delta \psi^2} \tag{6.21}$$

Therefore, by means of the von Mises transformation, the unpleasant task of locating the free surface, which arises because of the changing film thickness, has been solved, by going from the irregular x-y region to the rectangular region ζ-ψ. However, the use of this method gives rise to a singularity in $\frac{\delta^2 \chi}{\delta \psi^2}$ at =0, since if equation 6.21 is inspected it is found that

$$\frac{\delta^2 \chi}{\delta \psi^2} \to \infty \quad \text{as} \quad \psi \to 0$$

This singularity was discussed by Ames (158) and it was shown by Mitchell and Thomson (159) that it could be neglected for the case of an accelerating flow.

After replacing ζ by its equivalent coordinate x, the mathematical model for the hydrodynamics of the falling film and its new boundary conditions are:

$$\frac{\delta \chi}{\delta x} = 2G + \chi^{\frac{1}{2}} \frac{\delta^2 \chi}{\delta \psi^2} \tag{6.22}$$

B.C.1 $\chi(0,\psi)$ given by Nusselt's equation

B.C.2 $\chi(x,0) = 0$ for all values of x

B.C.3 $\chi(x,\Gamma) = u_s^2$ when $0 < x < L$

6.1.1 Pressure Gradient

The pressure gradient ($\delta P/\delta x$) is given by the difference between the static pressure of the gas stream at the top and at the bottom of the column, divided by its height, L. The total pressure drop in the case of a turbulent gas stream is defined as

$$\Delta P = (\Delta P)_f - \rho_g \, g \, L \tag{6.23}$$

The frictional pressure drop, $(\Delta P)_f$, is expressed by Wallis (2) as

$$(\Delta P)_{f/L} = \tfrac{1}{2} \, f_g \rho_g \, \bar{u}_g \, \frac{1}{R_h} \tag{6.24}$$

where f_g is the friction factor for the gas flow and R_h is the hydraulic radius, which is defined as the ratio of the cross sectional area of the column to its total perimeter; in the case of an annular column:

$$R_h = \frac{(\pi r_o^2 - \pi r_i^2)}{2\pi r_i + 2\pi r_o} = \tfrac{1}{2} (r_o - r_i) \tag{6.25}$$

The friction factor as suggested by Wallis is

$$f_g = 0.005 \left(1 + 360 \, \delta/R_h \right) \tag{6.26}$$

But since $R_h >> \delta$, its value can be assumed correctly as 0.005. Equation 6.23 takes the final form:

$$\frac{\delta P}{\delta x} = \frac{\Delta P}{L} = .005\ \rho_g\ \bar{u}_g\ \frac{1}{(r_o - r_1)} - \rho_g\ g \qquad (6.27)$$

6.1.2 The Surface Velocity

The shear force at the interface can be expressed as a function of the interfacial velocity u_s,

$$\tau_i = f_i\ \frac{\rho u_s^2}{2} \qquad (6.28)$$

where f_i is the liquid friction factor; however, it can also be written as a function of the gas friction factor as

$$\tau_i = f_g\ \rho_g\ \frac{u_r^2}{2} \qquad (6.29)$$

where u_r is the relative velocity of the gas flow with respect to the liquid velocity at the interface.

Dividing equation 6.28 by equation 2.69, and rearranging it, an expression for the surface velocity is obtained

$$u_s = u_r\ (f_g/f_i)^{\frac{1}{2}}\ (\rho_g/\rho)^{\frac{1}{2}} \qquad (6.30)$$

but since $u_r = \bar{u}_g - u_s$, then equation 6.30 becomes

$$u_s = \frac{1}{(1 + (f_g/f_i)^{\frac{1}{2}} (\rho_g/\rho)^{\frac{1}{2}})} \bar{u}_g (f_g/f_i)^{\frac{1}{2}} (\rho_g/\rho)^{\frac{1}{2}} \quad (6.31)$$

The liquid factor fi, remains to be defined. Previous work by Hughmark in counter-current flow indicates its dependence in the liquid phase Reynolds number, it was also suggested by Fulford (10) that it was affected by the liquid viscosity; and, since the film thickness changes along the length of the reactior it is correct to assume a corresponding change in the friction factor. It is then required to find an empirical correlation which should take into account all the factors mentioned above.

6.2 Numerical Solution

Equation 6.22 can be solved numerically by following either an explicit or an implicit procedure. The explicit or "marching forward" method is very unstable (Ames (158)), so an explicit method developed by Crank and Nicholson (160) was preferred.

First, the equation of the model must be written in finite differences form. The derivative $\delta\chi/\delta x$ is approximated by a forward difference:

$$\frac{\delta\chi}{\delta x} = \frac{\chi_{i+1,j} - \chi_{i,j}}{\Delta x} \quad (6.32)$$

The term $\delta\chi^2/\delta\psi^2$ is approximated by an average of approximations in the j and j+1 rows, see in Figure 6.2. the notation for the rectangular mesh and the graphical representation of equations 6.32 and 6.33,

$$\frac{\delta^2\chi}{\delta\psi^2} = \frac{1}{2}\frac{1}{\Delta\psi^2}\left[\left(\chi_{i+1,j-1}-2\cdot\chi_{i+1,j}+\chi_{i+1,j+1}\right) + \left(\chi_{i,j-1}-2\cdot\chi_{i,j}+\chi_{i,j+1}\right)\right] \qquad (6.33)$$

By combining equations 6.22, 6.23 and 6.33 the following expression is obtained

$$\frac{\chi_{i+1,j}-\chi_{i,j}}{\Delta x} = 2G + \left(\chi_{i,j}\right)^{\frac{1}{2}}\frac{\nu}{2\Delta\psi^2}\left(\left(\chi_{i+1,j-1}-2\cdot\chi_{i+1,i}+\chi_{i+1,j+1}\right) + \left(\chi_{i,j-i}-2\,\chi_{i,j}+\chi_{i,j+1}\right)\right) \qquad (6.34)$$

so by knowing the value of χ in the i row, a n-1 number of equations can be written, where n is the number of steps in the ψ direction.

For the first set of equations the values of χ, as defined by the first boundary conditions are used to calculate the coefficients. Because of boundaries conditions 2 and 3, the values of χ at j=1 and j=n+1 are:

$$\chi_{i,1} = 0 \quad \text{and} \quad \chi_{i,n+1} = u_s^2$$

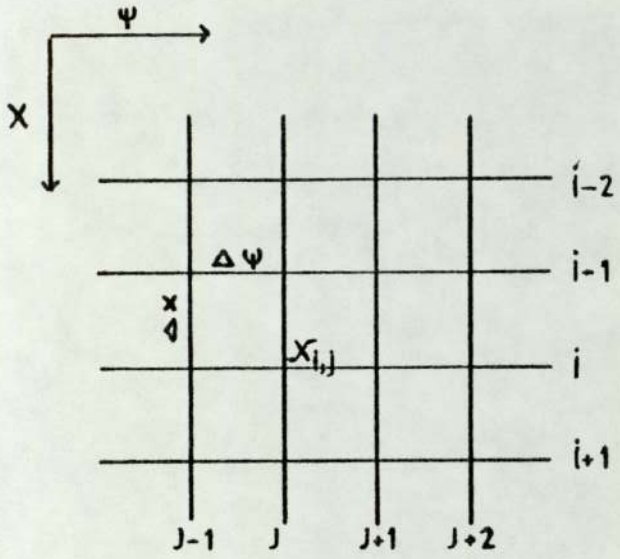

NOTATION FOR THE RECTANGULAR MESH

$$\left.\frac{\partial X}{\partial x}\right| = \frac{1}{\Delta X}\left\{ \begin{matrix} -1 \\ \\ +1 \end{matrix} \right.\quad \left.\begin{matrix} i,j \\ \\ i+1,j \end{matrix}\right\}$$

$$\left.\frac{\partial^2 X}{\partial \psi^2}\right| = \frac{1}{\Delta \psi^2}\left\{ \begin{matrix} -1 & +2 & -1 \\ +1 & -2 & +1 \end{matrix} \right.\quad \left.\begin{matrix} i,j-1 & i,j & i,j+1 \\ i+1,j-1 & i+1,j & i+1,j+1 \end{matrix}\right\}$$

COMPUTATIONAL MOLECULES FOR THE PARTIAL DERIVATIVES

Figure 6.2 - Notation and Computational Molecules for the Partial Derivatives

The resulting equations have a "tridiagonal" form. They are solved using the Gauss-Jordan iteration. The listing of the computer program is presented in Appendix F.

6.3 Velocity Profile

A knowledge of the velocity distribution within falling films is important in the calculation of the rates of convective heat and mass transfer processes. Because of the thinness of the film, experimental determination of the velocity profile becomes very difficult. A possible procedure, first suggested by Kapitza (19), consists of assuming a parabolic distribution, normalised by the local average velocity $\bar{u}(x)$.

$$\frac{u}{\bar{u}(x)} = \frac{y}{\delta(x)} - \frac{1}{2}\left(\frac{y}{\delta(x)}\right)^2 \qquad (6.35)$$

This approach does not account for the effect of drag at the interface. Ito and Tomura (130) corrected the above equation by introducing a parameter K, which defines the shift from the parabolic distribution; it was rewritten as

$$\frac{u}{\bar{u}} = \left[\left(1 - \frac{1}{2}K\right)\left(\frac{y}{\delta}\right) - \frac{1}{2}\left(\frac{y}{\delta}\right)^2\right]\left(\frac{4}{3} - K\right)^{-2/3} \qquad (6.36)$$

and a value for K was obtained experimentally to be 0.134.

The ratio of the surface velocity u_s to the average velocity was 1.39, which is smaller than that predicted by a parabolic distribution, viz 3/2. Ito and Tomura's work included only the drag at the interface caused by a stagnant gas phase. However, it is significant since it demonstrated the unsuitability of a parabolic distribution to be a correct description of an accelerating film.

Berbente and Ruckenstein (77) suggested the use of a power series in y, to describe the velocity profile in a wavy film with no drag at the interface. A similar approach is followed in this study. The velocity distribution will be described by a third order polynomial

$$\frac{u}{u_s} = a_1 \left(\frac{y}{\delta}\right) + a_2 \left(\frac{y}{\delta}\right)^2 + a_3 \left(\frac{y}{\delta}\right)^3 \qquad (6.37)$$

where u, δ and u_s are functions of distance, and the flow parameters. Equation 6.37 must satisfy the boundary conditions mentioned above.

Since $u = u_s$, when $y = \delta$, equation 6.37 assumes the following form at the interface

$$1 = a_1 + a_2 + a_3 \qquad (6.38)$$

A second equation is obtained by deriving equation with respect to y

$$\frac{1}{u_s}\frac{du}{dy} = a_1/\delta + 2a_2\left(\frac{y}{\delta^2}\right) + 3a_3\left(\frac{y^2}{\delta^3}\right) \tag{6.39}$$

but since

$$\left.\frac{du}{dy}\right|_{\delta} = 0 \tag{6.40}$$

at the interface, equation 6.37 is rewritten as

$$0 = a_1 + 2a_2 + 3a_3 \tag{6.41}$$

The third equation is obtained by multiplying both sides of equation 6.37 by dy and integrating within the limits

$$\int_0^{\delta} \frac{u}{u_s}\,dy = \int_0^{\delta} \left(a_1\left(\frac{y}{\delta}\right) + a_2\left(\frac{y}{\delta}\right)^2 + a_3\left(\frac{y}{\delta}\right)^3\right) dy \tag{6.42}$$

but the left-hand side of equation 6.42 can be written as

$$\frac{1}{u_s}\int_0^{\delta} u\delta y = \frac{\Gamma}{u_s} \tag{6.43}$$

Substituting back into equation 6.43 and integrating the right-hand side,

$$\frac{\Gamma}{u_s} = \left(\frac{a_1}{2}\frac{y^2}{\delta} + \frac{a_2}{3}\frac{y^3}{\delta^2} + \frac{a_3}{4}\frac{y^4}{\delta^3}\right)\Bigg|_0^{\delta} \tag{6.44}$$

substituting into equation 6.44 and dividing both sides of the equation by the film thickness, δ.

$$\frac{\Gamma}{\delta u_s} = \frac{a_1}{2} + \frac{a_2}{3} + \frac{a_3}{4} \tag{6.45}$$

But the volumetric flow per wetted perimeter is

$$\Gamma = \bar{u}\ \delta \tag{6.46}$$

where the average velocity $\bar{u}$ and δ are function of x. Equation 6.45 is transformed into

$$\frac{\bar{u}}{u_s} = \frac{a_1}{2} + \frac{a_2}{3} + \frac{a_3}{4} \tag{6.47}$$

Equations 6.38, 6.41 and 6.47 were solved simultaneously to obtain the parameter in the equation 6.37. The following relationships were found

$$a_1 = 12\left(\frac{\bar{u}}{u_s} - \frac{2}{3}\right) + 2 \tag{6.48}$$

$$a_2 = 24\left(\frac{\bar{u}}{u_s} - \frac{2}{3}\right) - 1 \tag{6.49}$$

$$a_3 = 12\left(\frac{\bar{u}}{u_s} - \frac{2}{3}\right) \tag{6.50}$$

So equation 6.37 is expressed as

$$\frac{u}{u_s} = 12\left(\frac{\bar{u}}{u_s} - \frac{2}{3}\right)\left(\left(\frac{Y}{\delta}\right) - 2\left(\frac{Y}{\delta}\right)^2 + \left(\frac{Y}{\delta}\right)^3\right) +$$

$$\left(2\left(\frac{Y}{\delta}\right) - \left(\frac{Y}{\delta}\right)^2\right) \tag{6.51}$$

Equation 6.51 describes a non-parabolic velocity profile. The effect of the drag at the interface is taken into account by the ratio of the average velocity to the velocity at the surface. In the case of no drag at interface, the assumption of a ratio of 2/3, results in a parabolic velocity profile.

Following the same procedure as above the following velocity distribution, normalised by the average velocity, was found

$$\frac{u}{\bar{u}} = 12\left(1 - \frac{2}{3}\frac{u_s}{\bar{u}}\right)\left(\left(\frac{Y}{\delta}\right) - 2\left(\frac{Y}{\delta}\right)^2 + \left(\frac{Y}{\delta}\right)^3\right) + \frac{u_s}{\bar{u}}\left(2\left(\frac{Y}{\delta}\right) - \left(\frac{Y}{\delta}\right)^2\right) \qquad (6.52)$$

CHAPTER VII

PRESENTATION AND ANALYSIS OF RESULTS, HYDRODYNAMICS

An experimental programme has been carried out to investigate the hydrodynamic characteristics of a liquid film flowing downwards under the effect of interfacial shear caused by a cocurrent turbulent gas stream. Results from the film thickness experiments, the minimum wetting rate experiments and the inception of droplet entrainment are reported and presented graphically of where appropriate, a correlation has been proposed.

Five different liquids of varying viscosities, from 10^{-3} Ns/m^2 to 6 x 10^{-2} Ns/m^2 have been studied in the experimental programme. The liquids used were filtered mains water and four glycerol solutions, which were prepared by mixing known volumes of glycerol and water. The densities were measured and they agreed with the values given by the C.R.C. handbook (161) for the measured concentrations of glycerol. The absolute viscosities were determined by a U-tube Cannon-Fleske viscometer, which had been previously calibrated. The gas used was air at 1 bar pressure and 20^{o}C temperature. The properties of air were obtained from the corresponding tables in the C.R.C. handbook. The physical properties of the liquid and gas phases are presented in Appendix C.

Further, measurements of the film thickness were analysed, using the mathematical model described in Chapter 6. Based on this analysis, relationships for the surface velocity of the film have been proposed in terms of the friction factor at the interface, as functions of the gas and liquid phase flow parameters and physical

constants, and the distance along the length of the reactor. Comparison of the results has been made with previous models. The criteria for the minimum wetting rate and the critical velocity for the onset of droplet entrainment have been analysed and reformulated in accordance with the experimental findings of this work.

7.1 Film Thickness

7.1.1 Experimental Programme

The average film thickness was measured using an ultrasonic probe device, as described in Chapter 3. A receiver-transmiter ultrasonic probe generates a pulsating sound wave which is reflected from the interface between the two phases. The thickness is measured in terms of the time required for the signal to return to the receiver. The accuracy of the measurements was $\pm 10^{-5}$m.

The mass flow rate of the liquid was in the range from .05 kgs^{-1} to .3 kgs^{-1}. It was measured by a rotameter, which had been calibrated for each liquid mixture. The falling film was laminar, with low Reynolds numbers up to 1200. The air flowrate vaired from .195 kgs^{-1} to a maximum of .6 kgs^{-1} corresponding to Reynolds numbers in the range $25000 < Re_g < 80000$, the air flow was characterised by turbulence conditions.

The experimental procedure followed was:

1. The surface of the vertical tube was cleaned thoroughly before every group of experiments. "Teepol" and tap water were used for the washing. The whole system was flushed with water for at least half an hour, before draining in order to avoid any contamination of the liquid mixture by the surfactant "Teepol"

2. The column was flushed with the liquid being investigated. After this, samples of the liquid were taken and its physical properties measured, i.e. viscosity and density, to ensure that the solution had not been contaminated. The rotameter was then calibrated.

3. The liquid flow was maintained at the desired rate for a minimum of 3 minutes for the falling film to become stable.

4. The air fan was switched on, the diagphram been previously set in order to restrict the air flow to the required volumetric rate. A reading from the inclined manometer was then taken.

5. The film thickness was measured at known distances along the length of the reactor. The technique for the measurements was described in Chapter 3.

By following the above procedure, there was no problem in obtaining an even and continuous liquid film, without any "dry patches" or "rivulets" at flow rates above the minimum wetting rate. These procedures were based on recommendations outlined by Portalski (34) in 1963.

Measurements were taken for each set of values of the volumetric flow per wetted perimeter Γ, and the linear gas velocity u_g, at distances of 0.5m, 1.04m and 2.04m (bottom of the column) from the first contact point between the two phases at the top of the column.

7.1.2 Presentation of Results

The measurements of the average film thickness are presented in Tables 7.1 to 7.5. The values for average gas flow velocity were calculated by dividing the total volumetric air flowrate by the cross-sectional area of the column which was assumed to remain constant along the whole length of the reactor.

7.1.3 Analysis

Inspection of the results indicate a dependence of the film thickness on the flow parameters. As the gas velocity is increased, the film thickness decreased. This effect increased as measurements were made further down the reactor's length. In order to satisfy the law of conservation of mass, since no mass transfer takes place, the increase of the falling film velocity, due to the gravitational force and the drag at the interface, reduces the film thickness. However, previous models failed to incorporate the effects of either one of these two separate forces. Existing correlations such as Zhivaikin's (58), Kulov's (39), and others (49,47) do not specify the distance from the origin at which the measure-

ments were taken. Salazar (44), Portalski (45) and others reported a reduction of the average film thickness as distance from the top of the reactor increased; however, their experiments were made in the absence of interfacial drag.

The dependence of the mean film thickness on the liquid flow rate is taken into account with sufficient accuracy by the parameter $\Gamma^{1/3}$, as has been previously reported. Figure 7.1 indicates such a relationship. Similarly, the effect of the kinematic viscosity of the liquid is in agreement with previous findings, i.e proportional to the parameter $\nu^{1/3}$. The film thickness is therefore linearly proportional to the product $(\Gamma\nu)^{1/3}$ as stated by Nusselt.

The change in the film thickness along the length of the reactor, is increased as the gas velocity is increased. This is illustrated in Figure 7.2. However, examination of results at the same location, Figure 7.3, indicates a linear dependence of the decrease of the film thickness on the gas velocity, as suggested by Zhivaikin (58). Consequently, the following correlation is proposed

$$\delta = (1-a(u_g-b))\delta_N \qquad (7.1)$$

Defining a new term δ^*, which is the ratio of the film thickness δ to the value predicted by Nusselt's theory, δ_N.

$$\delta^* = \delta/\delta_N \qquad (7.2)$$

TABLE 7.1 - Measurements of the Film Thickness, Water

Liquid Properties: 1) Viscosity = 1. x 10^{-3} NsM^{-2} 2) Density = 1.0 x 10^{-3} KgM^{-3}							
Run	Γ (10^{+4} M^2/s)	Re	u_g (m/s)	Re_g	δ (10^2 M)		
					sta.1	sta.2	sta.3
1	3.45	1380	3.58	26733	.048	.045	.040
2	3.45	1380	6.10	45592	.043	.040	.035
3	3.45	1380	7.58	56654	.042	.039	.034
4	3.45	1380	8.80	65773	.041	.037	.032
5	2.87	1148	3.58	26733	.044	.043	.038
6	2.87	1148	6.10	45592	.041	.044	.036
7	2.87	1148	7.58	56654	.040	.036	.032
8	2.87	1148	8.80	65773	.039	.035	.030
9	2.34	936	3.58	26733	.042	.043	.037
10	2.34	936	6.10	45592	.037	.034	.033
11	2.34	936	7.58	56654	.038	.034	.030
12	2.34	936	8.80	65773	.036	.033	.028
13	1.46	584	3.58	26733	.035	.033	.032
14	1.46	584	6.10	45592	.033	.030	.029
15	1.46	584	7.58	56654	.032	.030	.026
16	1.46	584	8.80	65773	.031	.030	.024

Table 7.2 - Measurements of the Film Thickness, Glycerol 63%

Liquid properties: 1) viscosity 13.1×10^{-3} NsM^{-2} 2) density 1.17×10^{-3} KgM^{-3}							
Run	Γ (10^{4} m^2/s)	Re	u_g (m/s)	Re_g	δ (10^2 M)		
					sta.1	sta.2	sta.3
17	2.57	92	3.81	28477	.094	.089	.084
18	2.57	92	5.71	42678	.092	.080	.074
19	2.57	92	7.20	53814	.087	.082	.071
20	2.57	92	9.18	68613	.082	.074	.065
21	1.98	71	3.81	28477	.086	.079	.077
22	1.98	71	5.71	42678	.038	.076	.073
23	1.98	71	7.20	53814	.077	.076	.065
24	1.98	71	9.18	68133	.076	.067	.061
25	1.60	57	3.81	28477	.080	.077	.070
26	1.60	57	5.71	42678	.077	.069	.063
27	1.60	57	7.20	53814	.076	.068	.063
28	1.60	57	9.18	68613	.066	.064	.053
29	1.13	40	3.81	28477	.069	.068	.063
30	1.13	40	5.71	42678	.066	.064	.058
31	1.13	40	7.20	53814	.067	.060	.054
32	1.13	40	9.18	68613	.063	.057	.048
33	0.72	26	3.81	28678	.062	.061	.056
34	0.72	26	5.71	42678	.061	.0 53	.0 52
35	0.72	26	7.20	53814	.057	.053	.048
36	0.72	26	9.o8	68613	.0 54	.0 50	.042

Table 7.3 - Measurements of the Film Thickness, Glycerol 70%

Liquid properties: 1) viscosity = 23.7×10^{-3} NsM^{-2} 2) density = 1.18×10^{-3} KgM^{-3}							
Run	Γ (10^4 m^2/s)	Re	u_g (m/s)	Reg	δ (10^2M)		
					sta.1	sta.2	sta.3
37	2.15	43	3.60	26907	.106	.102	.097
38	2.15	43	5.95	44471	.101	.094	.088
39	2.15	43	7.20	53814	.096	.094	.081
40	2.15	43	9.66	72200	.090	.088	.074
41	1.73	34	3.60	26907	.097	.095	.088
42	1.73	34	5.95	44471	.094	.089	.080
43	1.73	34	7.20	53814	.091	.084	.077
44	1.73	34	9.66	72200	.086	.077	.070
45	1.23	25	3.60	26907	.089	.083	.081
46	1.23	25	5.95	44471	.085	.079	.072
47	1.23	25	7.20	53814	.082	.073	.076
48	1.23	25	9.66	72200	.078	.072	.061
49	0.96	19	3.60	26907	.082	.078	.075
50	0.96	19	5.95	44471	.075	.070	.067
51	0.96	19	7.20	53814	.079	.070	.065
52	0.96	19	9.66	72200	.075	.065	.058
53	0.71	14	3.60	26907	.074	.071	.066
54	0.71	14	5.95	44471	.071	.066	.061
55	0.71	14	7.20	53814	.072	.065	.056
56	0.71	14	5.95	72200	.067	.060	.051

TABLE 7.4 - Measurements of the Film Thickness, Glycerol 75%

Liquid Properties: Viscosity = 34.5×10^{-3} NsM^{-2} Density = 1.2×10^{-3} kgM^{-3}							
Run	Γ (10^{+4} M^2/s)	Re	u_g (m/s)	Re_g	δ (10^2 M)		
					sta.1	sta.2	sta.3
57	1.94	27	3.52	26309	.117	.108	.107
58	1.94	27	5.91	44173	.114	.101	.096
59	1.94	27	7.24	54113	.108	.098	.083
60	1.94	27	8.70	65025	.104	.087	.079
61	1.94	27	10.20	76236	.098	.081	.079
62	1.65	23	3.52	26309	.111	.107	.101
63	1.65	23	5.91	44173	.105	.100	.087
64	1.65	23	7.24	53113	.096	.089	.079
65	1.65	23	8.70	65025	.096	.084	.077
66	1.65	23	10.20	76236	.091	.079	.076
67	1.42	20	3.52	26309	.105	.104	.100
68	1.42	20	5.91	44173	.101	.096	.085
69	1.42	20	7.24	54113	.100	.095	.082
70	1.42	20	8.70	65025	.092	.081	.074
71	1.42	20	10.20	76236	.086	.078	.070
72	1.19	16.5	3.52	26309	.098	.096	.091
73	1.19	16.5	5.91	44173	.096	.092	.083
74	1.19	16.5	7.24	54113	.094	.081	.077
75	1.19	16.5	8.70	65025	.088	.080	.070
76	1.19	16.5	10.20	76236	.082	.076	.068
77	0.97	13.4	3.52	26309	.093	.090	.088
78	0.97	13.4	5.91	44172	.091	.084	.081
79	0.97	13.4	7.24	54113	.087	.079	.073
80	0.97	13.4	8.70	65025	.084	.077	.069
81	0.97	13.4	10.20	76236	.078	.075	.062

TABLE 7.5 - Measurements of Film Thickness, Glycerol 80%

Liquid Properties: Viscosity = 59.40 10^{-3} NsM^{-2} Density = 1.217 10^{-3} KgM^{-3}							
Run	Γ (10^{+4} M^2/s)	Re	u_g (m/s)	Re_g	δ (10^2 M)		
					sta.1	sta.2	sta.3
82	1.26	10.25	3.52	26284	.115	.110	.100
83	1.26	10.25	6.55	48956	.110	.099	.090
84	1.26	10.25	10.50	78363	.098	.092	.079
85	0.81	6.65	3.52	26284	.105	.100	.092
86	0.81	6.65	6.52	48956	.097	.094	.086
87	0.81	6.65	10.50	78363	.094	.087	.070
88	0.44	3.61	3.52	26284	.087	.084	.074
89	0.44	3.61	6.52	48956	.083	.079	.069
90	0.44	3.61	10.50	78363	.078	.073	.062

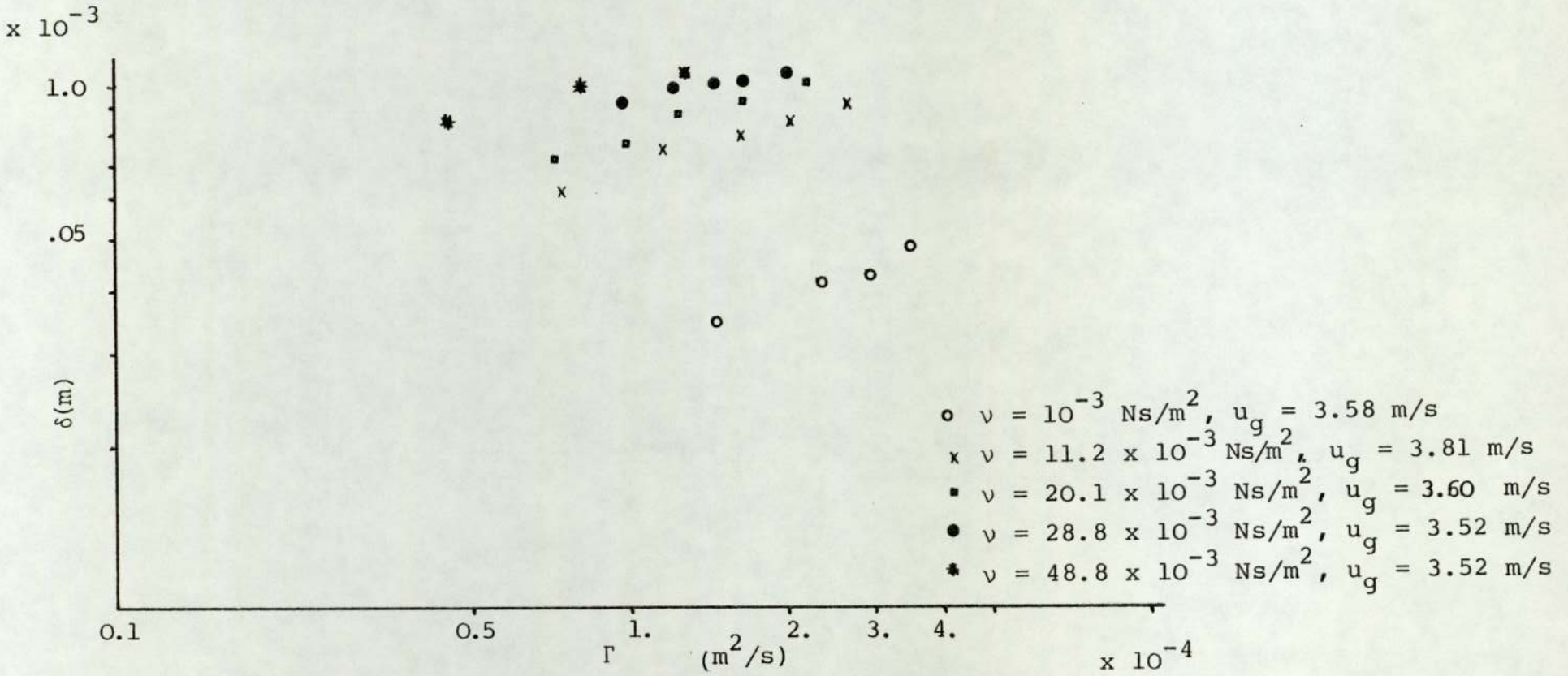

Figure 7.1 - Film Thickness Dependence on Liquid Flowrate

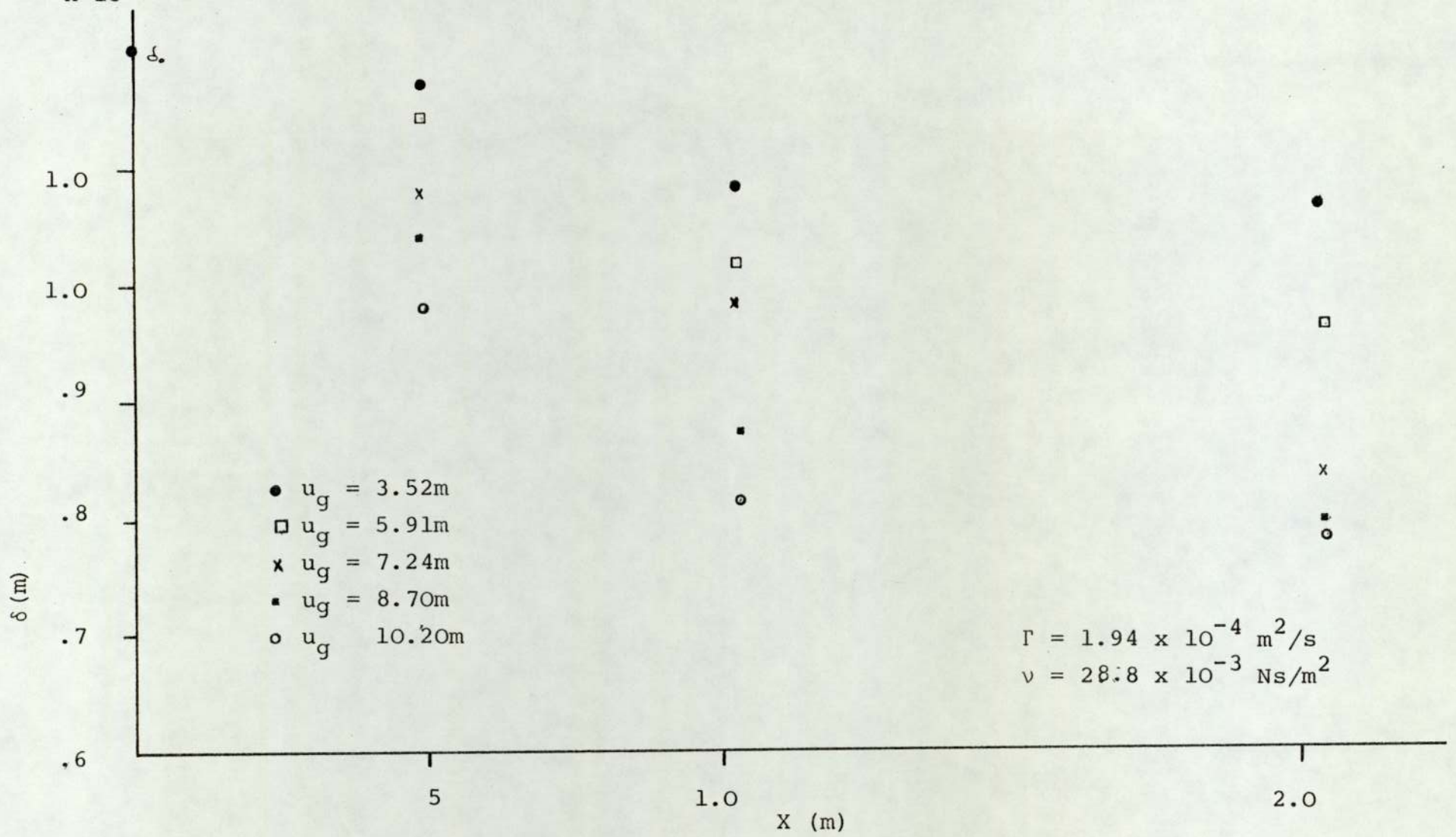

Figure 7.2 - Dependence of the Film Thickness on Gas Velocity and Distance

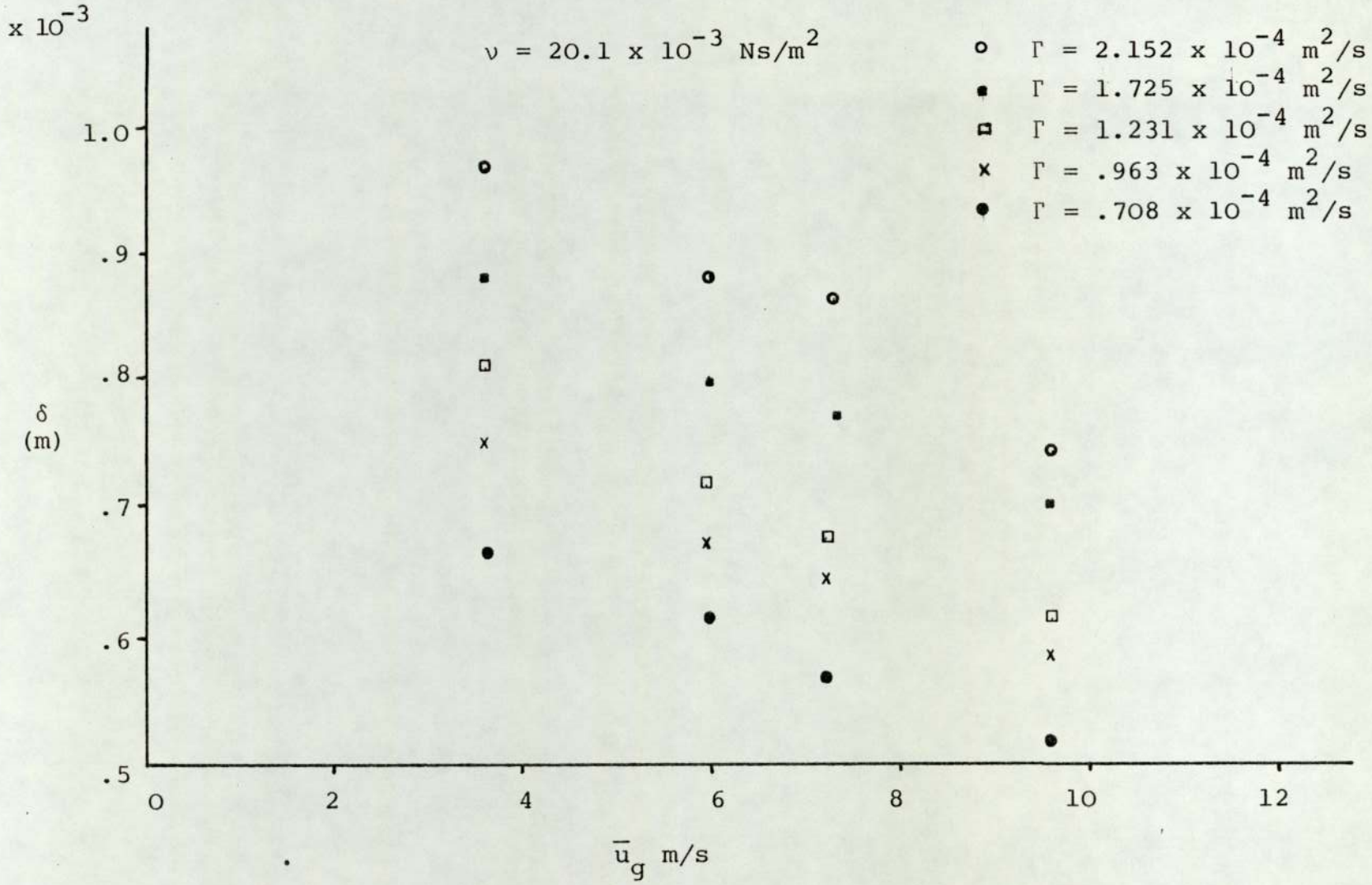

Figure 7.3 - Dependence of the Film Thickness on Gas Velocity, at x = 2.04m

and substituting into equation 7.1 gives

$$\delta^* = (1-a(u_g-b)) \tag{7.3}$$

then, introducing the relative deviation α, defined as

$$\alpha = \frac{\delta_N - \delta}{\delta_N} = a\ (u_g-b) \tag{7.4}$$

so that $\delta^* = (1-\alpha)$.

The least square method was applied for the above correlation, using a Fortran IV computer program in the University ICI 1904 S computer. The listing of the program is given in Appendix F. The following values for the parameters a and b. The following relationships were found for equation 7.3.

$$\alpha = .02162\ (\bar{u}_g - 2.749) \tag{7.5}$$

at x = .5m, with a regression coefficient, r, of .9043.

For the second station, located at 1.04m from the top

$$\alpha = .02797\ (\bar{u}_g - 1.3) \tag{7.6}$$

with

$$r = .892$$

and finally at the bottom of the reactor

$$\alpha = .03448\ (\bar{u}_g + .02) \tag{7.7}$$

with

$$r = .952$$

The values obtained for the correlation coefficients suggest a very good linear relationship between the average gas velocity, measured in metres per second, and the relative deviation α. Following Zhivaikin's interpretation of its empirical correlation, equation 2.26, the minimum air velocity necessary to affect the film thickness in a significant way, changes along the length of the reactor. This indicates a dependence of the film thickness on the relative velocity between the average velocity of the accelerating liquid film and the average velocity of the air stream. For example, the minimum air velocity reported by Zhivaikin as 4 ms^{-1} would cause a decrease of no more than 7% in the film thickness, if the total length of the reactor was .83m corresponding to the one used in this work.

Further, inspection of the values obtained for a and b, indicate a linear relationship between each and the distance along the reactor. A linear regression analysis gave the following results.

$$a = .0081\ x + .\ 0183 \qquad (7.8)$$

with a regression coefficient of .98, which indicated that the assumption of a linear dependence was correct.

$$b = -1.74\ x + 3.42 \qquad (7.9)$$

A similar regression coefficient to that above was applied to equation 7.3, rewritten as

$$\delta^* = (1-(.0183 + 0.0081\ x)\ (u_g-(3.42 - 1.74\ x)) \quad (7.10)$$

Assuming that the dependence on length is inversely proportional to the hydraulic diameter of the reactor, and that the existing dependence on the gas velocity can be expressed in terms of the Reynolds number of the gas stream; equation 7.10 is reformulated as

$$\delta^* = (1-(2500-8.7x^*)\ (Re_g-(2550-1040x^*))x10^{-8}) \quad (7.11)$$

A similar relationship between the "effect on the shape of the falling film", and the distance along the reactor, was observed by Wallis (2) and Kulov (50), when studying the inception of droplet entrainment. However, as was mentioned above, no attempt was made to correlate the combined effect of these two parameters with either the friction at the interface nor the film thickness.

The degree of fit between the experimental and correlated film thickness (±5%) are shown in the graph plotter printout in figure 7.4. It is considered to be good.

7.2 Simulation of the Falling Film Hydrodynamics

The mathematical model described in Chapter 6 was solved, using the measured values of the film thickness. Given a fixed set of flow parameters, Γ and u_g, and physical characteristics of the two phases, equation

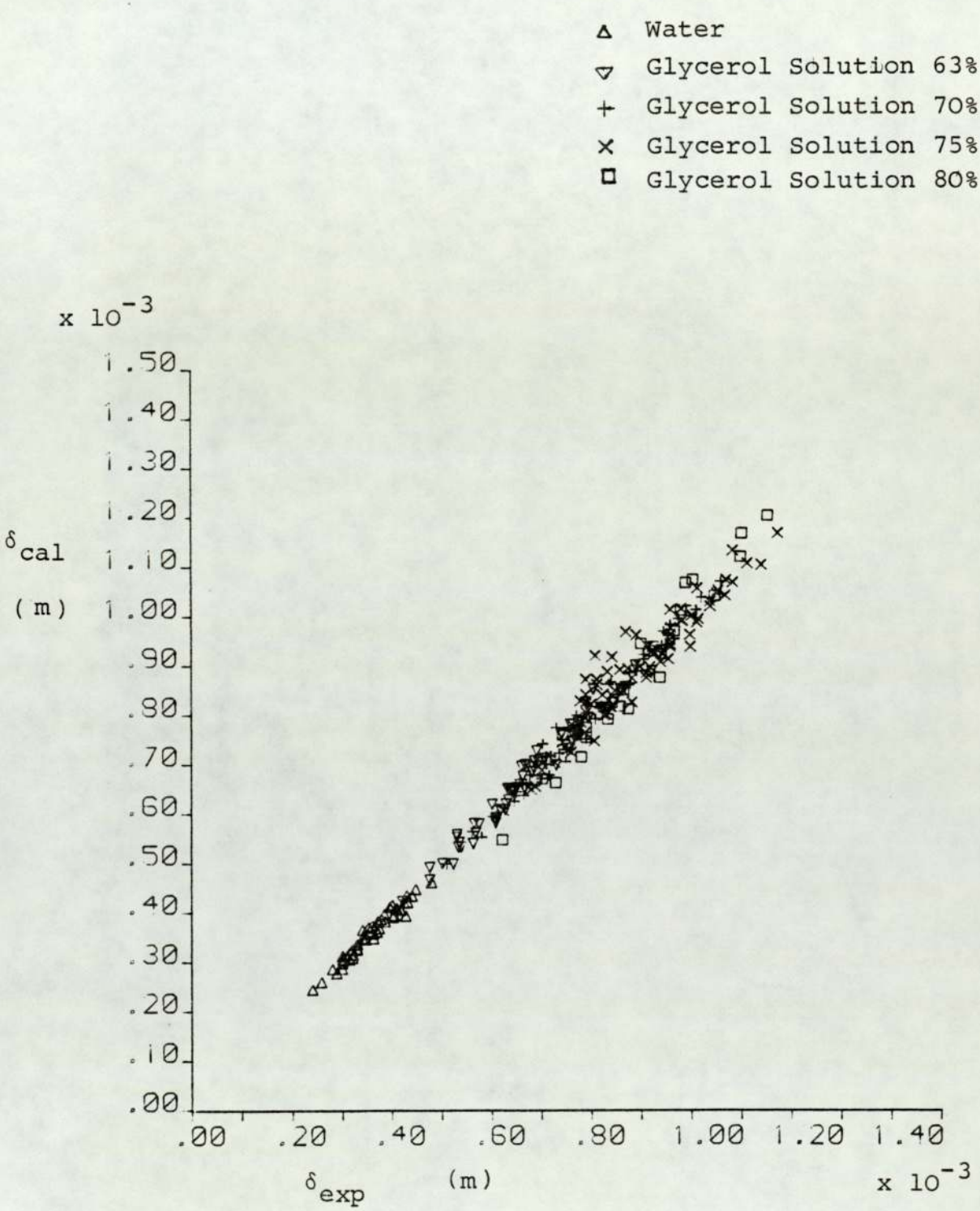

Figure 7.4 - Experimental vs Predicted Film Thickness

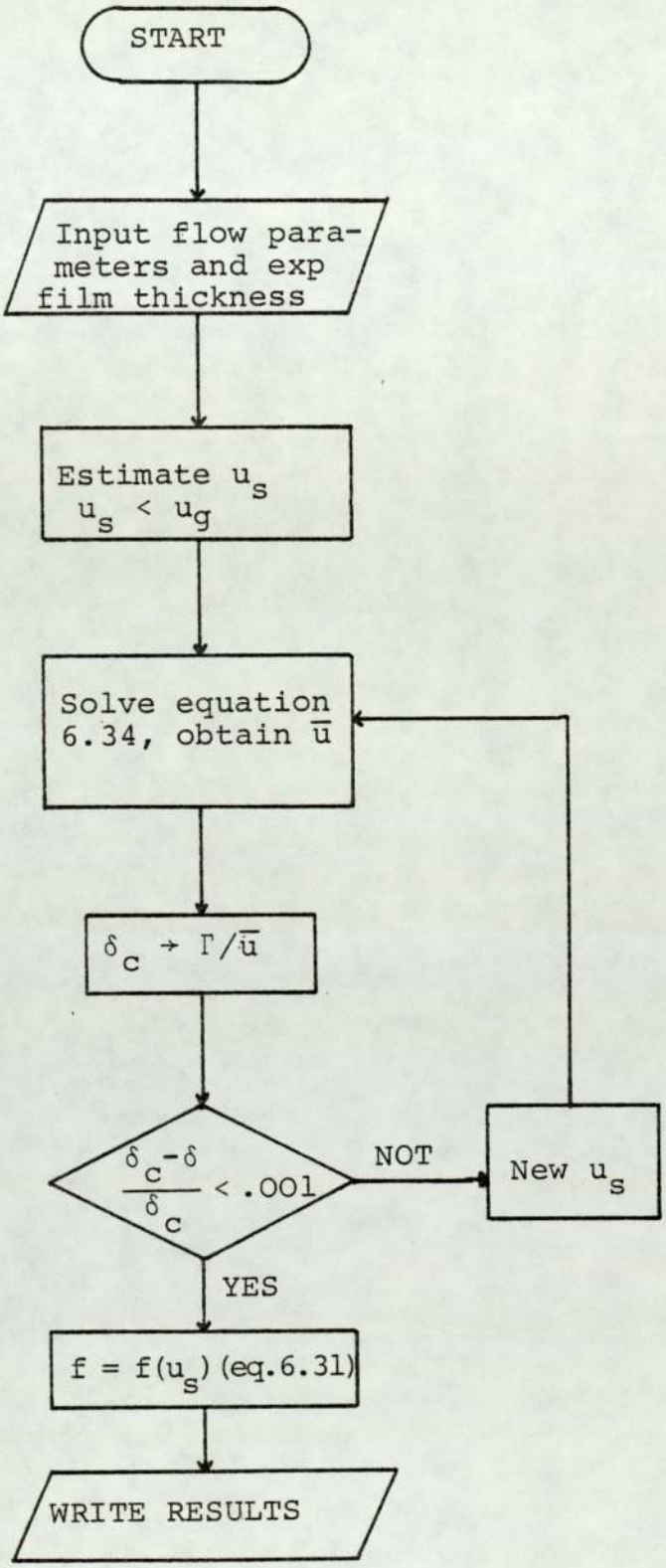

Figure 7.5 - Logic Diagram of the Simulation of the Hydrodynamics Mathematical Model

6.21 has a unique solution for a given value of the film thickness. Since the values for the friction factor were unavailable, an original estimate of the surface velocity, u_s, was made. Equation 6.3 was solved for the given value of u_s, and an average velocity $\bar{u}$ was obtained from the resulting velocity profile. Then, a value of the film thickness was found, from the following relationship

$$\Gamma = \delta\bar{u} \tag{7.12}$$

The calculated film thickness was compared with the experimental film thickness. If the relative deviation, Δ, was greater than 1% a new estimate of the surface velocity was made and the iteration repeated.

$$\Delta = \frac{\text{predicted - experimental}}{\text{predicted}} \times 100 \tag{7.13}$$

Once a satisfactory value of the film thickness was obtained, equation 6.31 was used to predict the friction factor at the interface. The logic diagram of this iteration is shown in Figure 7.5 at a listing of the Fortran III program is given in Appendix F.

The results obtained from the computer are given in Tables 7.6 to 7.10.

TABLE 7.6 - Simulation Results, Water

Run no.	Friction Factor $f_i \times 10^3$			Average Velocity $\bar{u}$ $(m.s^{-1}) \times 10^2$			Surface Velocity u_s $(m.s^{-1}) \times 10^2$		
	sta.1	sta.2	sta.3	sta. 1	sta.2	sta.3	sta. 1	sta.2	sta.3
1	.05	.04	.04	72.08	77.48	87.84	153.12	163.93	184.64
2	.11	.09	.07	80.97	87.07	99.26	170.91	183.10	207.50
3	.16	.14	.11	82.02	90.43	100.94	173.01	189.83	210.86
4	.20	.17	.13	85.34	93.07	109.87	179.65	195.14	228.71
5	.06	.06	.04	64.59	65.87	76.14	135.41	137.98	158.51
6	.15	.14	.12	69.73	71.36	79.50	145.70	148.95	165.22
7	.22	.18	.14	70.70	79.51	89.44	147.62	165.25	185.10
8	.27	.22	.17	74.87	82.92	96.35	155.96	172.07	198.91
9	.08	.08	.06	56.40	54.40	63.05	117.06	114.11	130.34
10	.19	.16	.15	62.57	68.61	71.19	129.38	141.44	146.60
11	.30	.24	.20	62.03	69.00	77.01	128.31	142.11	158.22
12	.38	.31	.23	63.81	70.77	83.29	131.86	145.76	170.78
13	.15	.13	.13	41.93	44.68	45.68	85.72	91.20	93.04
14	.39	.32	.29	44.28	49.04	50.95	90.42	99.92	103.72
15	.57	.50	.36	45.53	48.63	51.32	92.90	99.10	116.44
16	.74	.65	.43	46.31	49.27	61.13	94.46	100.38	124.03

TABLE 7.7 - Simulation Results , Glycerol 63%

Run no.	Friction Factor $f_i \times 10^3$			Average Velocity $\bar{u}$ $(m.s^{-1}) \times 10^2$			Surface Velocity u_s $(m.s^{-1}) \times 10^2$		
	sta 1	sta 2	sta. 3	sta. 1	sta. 2	sta 3	sta. 1	sta. 2	sta. 3
17	.29	.27	.24	27.48	28.66	30.43	66.18	62.53	66.05
18	.63	.5	.42	28.04	31.89	34.78	61.3	68.96	74.31
19	.92	.82	.62	29.40	31.26	36.28	63.95	67.70	77.7
20	1.32	1.10	.86	31.42	34.71	39.63	68.03	74.57	84.39
21	.46	.39	.36	22.40	24.56	25.49	48.05	52.35	54.20
22	.95	.81	.76	23.41	25.40	26.39	50.06	54.00	55.98
23	1.31	1.31	.96	25.26	25.26	29.76	53.79	53.74	62.68
24	2.09	1.62	1.38	25.44	29.21	31.72	54.10	61.58	66.57
25	.58	.53	.45	20.04	21.00	22.91	42.55	44.43	48.22
26	1.23	1.01	.83	20.69	22.97	25.50	43.83	48.34	53.34
27	1.88	1.55	1.33	21.20	23.48	25.44	44.83	49.35	53.23
28	2.34	2.2	1.55	24.40	25.24	30.31	51.14	52.82	62.90
29	.89	.86	.77	16.35	16.69	17.69	34.36	35.01	37.00
30	1.88	1.77	1.43	16.96	17.48	19.57	35.55	36.57	40.67
31	2.95	2.47	1.98	17.06	18.74	21.08	35.75	39.04	43.65
32	4.3	3.55	2.57	18.07	20.01	23.68	37.72	41.55	48.79
33	1.73	1.69	1.48	11.64	11.82	12.70	24.67	25.00	26.70
34	3.72	2.84	2.84	11.94	13.84	13.85	25.24	28.91	28.91
35	5.33	4.72	3.85	12.65	13.51	15.07	26.60	28.27	31.28
36	7.81	6.73	4.9	13.38	14.49	17.14	28.01	30.17	35.35

TABLE 7.8 - Simulation Results, Glycerol 70%

Run no.	Friction Factor $f_i \times 10^3$			Average Velocity $\bar{u}$ (m.s^{-1}) $\times 10^2$			Surface Velocity u_s (m.s^{-1}) $\times 10^2$		
	sta1	sta2	sta.3	sta. 1	sta. 2	sta 3	sta. 1	sta. 2	sta. 3
37	.47	.44	.40	20.37	20.97	22.16	44.69	45.87	48.22
38	1.20	1.05	.90	21.11	22.70	24.28	46.15	49.29	52.43
39	1.60	1.50	1.20	22.44	23.09	26.35	48.77	50.06	56.52
40	2.50	2.40	1.70	23.84	24.73	29.20	51.55	53.32	62.18
41	.6	.6	.50	18.08	18.70	20.22	39.13	40.33	43.34
42	1.66	1.49	1.20	18.18	19.26	21.68	39.19	41.30	46.10
43	2.10	1.80	1.50	19.65	21.30	23.28	42.20	45.50	49.40
44	3.80	2.80	2.30	19.52	23.14	25.39	41.95	49.10	53.57
45	1.06	.94	.91	13.82	14.79	15.11	29.61	31.49	32.11
46	2.70	2.30	2.00	14.30	15.70	17.08	30.54	33.25	35.95
47	3.60	2.96	2.56	15.16	16.86	18.21	32.20	35.52	38.18
48	5.90	5.20	3.80	15.98	17.14	20.12	33.82	36.07	41.95
49	1.48	1.37	1.25	11.74	12.23	12.89	25.15	26.10	27.38
50	3.48	3.10	2.77	12.73	13.58	14.42	27.05	28.69	30.33
51	5.60	4.50	3.80	12.13	13.69	14.90	25.90	28.92	31.26
52	9.10	6.90	5.70	12.81	14.92	16.55	27.21	31.30	34.48
53	2.20	2.00	1.80	9.45	9.96	10.65	20.49	21.47	22.76
54	5.50	4.80	4.20	9.93	10.71	11.58	21.48	22.87	24.53
55	8.13	7.00	5.30	9.96	10.85	12.61	21.50	23.13	26.51
56	10.30	10.70	7.90	10.63	11.83	13.96	22.71	25.00	29.13

TABLE 7.9 - Simulation Results, Glycerol 75%

Run No.	Friction Factor $f_i \times 10^3$			Average Velocity $(m.s^{-1})$ $\bar{u} \times 10^2$			Surface Velocity $(m.s^{-1})$ $u_s \times 10^2$		
	sta.1	sta.2	sta.3	sta.1	sta.2	sta.3	sta.1	sta.2	sta.3
57	.56	.57	.56	16.67	17.88	18.20	36.81	39.18	39.77
58	1.75	1.41	1.28	17.10	19.30	20.30	37.60	41.84	43.96
59	2.38	2.02	1.48	18.06	19.75	23.42	39.53	42.83	50.08
60	3.16	2.20	1.95	18.29	22.57	24.60	41.21	48.03	52.44
61	3.92	2.84	2.64	20.00	23.83	25.00	43.33	50.93	52.82
62	.82	.79	.76	14.97	15.60	16.51	32.73	33.93	35.74
63	2.12	1.93	1.50	15.71	16.55	19.00	34.18	35.78	40.60
64	2.89	2.68	1.99	16.58	17.25	20.30	35.86	37.19	43.16
65	3.87	3.03	3.28	17.27	19.73	21.36	37.22	42.06	45.29
66	4.83	3.68	3.58	18.20	21.10	21.60	39.05	44.77	45.72
67	1.01	1.01	.93	13.59	13.60	14.22	29.51	29.51	30.74
68	2.66	2.40	1.92	14.11	14.93	16.87	30.52	32.14	35.91
69	3.68	3.25	2.60	14.76	15.80	17.87	31.78	33.79	37.80
70	4.88	3.88	3.35	15.45	17.52	18.96	33.13	37.19	40.03
71	5.99	4.87	4.01	16.45	18.40	20.34	35.07	38.90	42.73
72	1.28	1.22	1.11	12.11	12.43	13.07	26.23	26.84	28.08
73	3.45	3.19	2.65	12.40	13.00	14.36	26.78	27.87	30.60
74	4.98	3.86	3.55	12.70	14.58	15.27	27.31	31.01	32.35
75	6.39	5.43	4.26	13.53	14.80	16.90	28.97	31.41	35.49
76	7.66	6.79	5.45	14.60	15.60	17.55	31.00	32.94	36.79
77	1.68	1.59	1.55	10.52	10.85	11.01	22.84	23.46	23.78
78	4.69	4.09	3.75	10.60	11.45	12.02	22.97	24.61	25.70
79	6.39	5.43	4.68	11.20	12.25	13.30	24.11	26.14	28.17
80	8.77	7.48	6 10	11.52	12.60	14.07	24.75	26.80	29.65
81	10.56	9.83	6.89	12.40	12.90	15.63	26.42	27.40	32.70

TABLE 7.10 - Simulation Results, Glycerol 80%

Run No	Friction Factor f_i x10^3			Average Velocity u (m.s^{-1}) x 10^2			Surface Velocity u_s (m.s^{-1}) x 10^2		
	sta.1	sta.2	sta.3	sta.1	sta.2	sta.3	sta. 1	sta. 2	sta.3
82	1.50	1.39	1.17	10.91	11.40	12.55	24.05	24.99	27.19
83	4.79	3.98	3.36	11.42	12.70	13.96	25.03	27.48	29.92
84	10.03	9.03	6.79	12.82	13.60	15.90	27.70	29.20	33.67
85	2.82	2.62	2.29	7.77	8.13	8.83	17.54	18.20	19.47
86	8.46	8.19	7.01	8.50	8.66	9.49	18.85	19.15	20.70
87	20.88	18.40	12.86	8.69	9.36	11.48	19.20	20.45	24.46
88	5.40	5.22	4.40	5.20	5.30	5.97	12.10	12.90	14.03
89	17.97	16.74	13.71	5.30	5.60	6.45	12.93	13.40	14.80
90	41.95	38.29	30.27	5.68	6.06	7.10	13.54	14.17	15.91

7.2.1 Analysis

The evaluation of the main hydrodynamic characteristics has been carried out, as described above. Comments on the effect of the following parameters on the hydrodynamics of the falling film are made below.

1. Physical properties of the liquid.

2. Liquid flowrate.

3. Gas velocity.

In addition, comments have been made on the prediction of the velocity distribution in the film, the surface velocity and the friction factor at the interface, from the calculated values and the theoretical considerations discussed above. Graphical representation of the results, including predicted values of previous theories have been presented.

7.2.1.1 Physical Properties

The effect of the absolute viscosity on the behaviour of the falling film, was as expected. The surface and average velocity decreased with increasing viscosity. However, the ratio of the surface velcoity to the average increased as viscosity increased.

7.2.1.2 Liquid Flowrate

The variation of surface velocity and average velocity as the liquid flowrate varied, follows the same pattern as the changes in the absolute viscosity. The effect of the flowrate on the friction factor was as expected. That is, the friction factor decreased as the flow rate was increased, this is explained by the decrease in relative velocity at the interface.

7.2.1.3 Gas Velocity

The surface velocity increased with increasing gas velocity (figure 7.6). The friction factor at the interface increased equally with the gas velocity, but it decreased along the length of the column. This is to be expected by considering the acceleration of the falling film, due to the gravity force and the shear at the interface, and the smoothening of the film surface.

7.2.2 Velocity Profile

From the above behaviour of the falling film it is reasonable to assume that the value of the surface velocity for a fully developed liquid flow under interfacial shear stress can be estimated to be twice the average velocity of the film to within 8%. That is

$$\frac{u_s}{\bar{u}} = 2 \qquad (7.14)$$

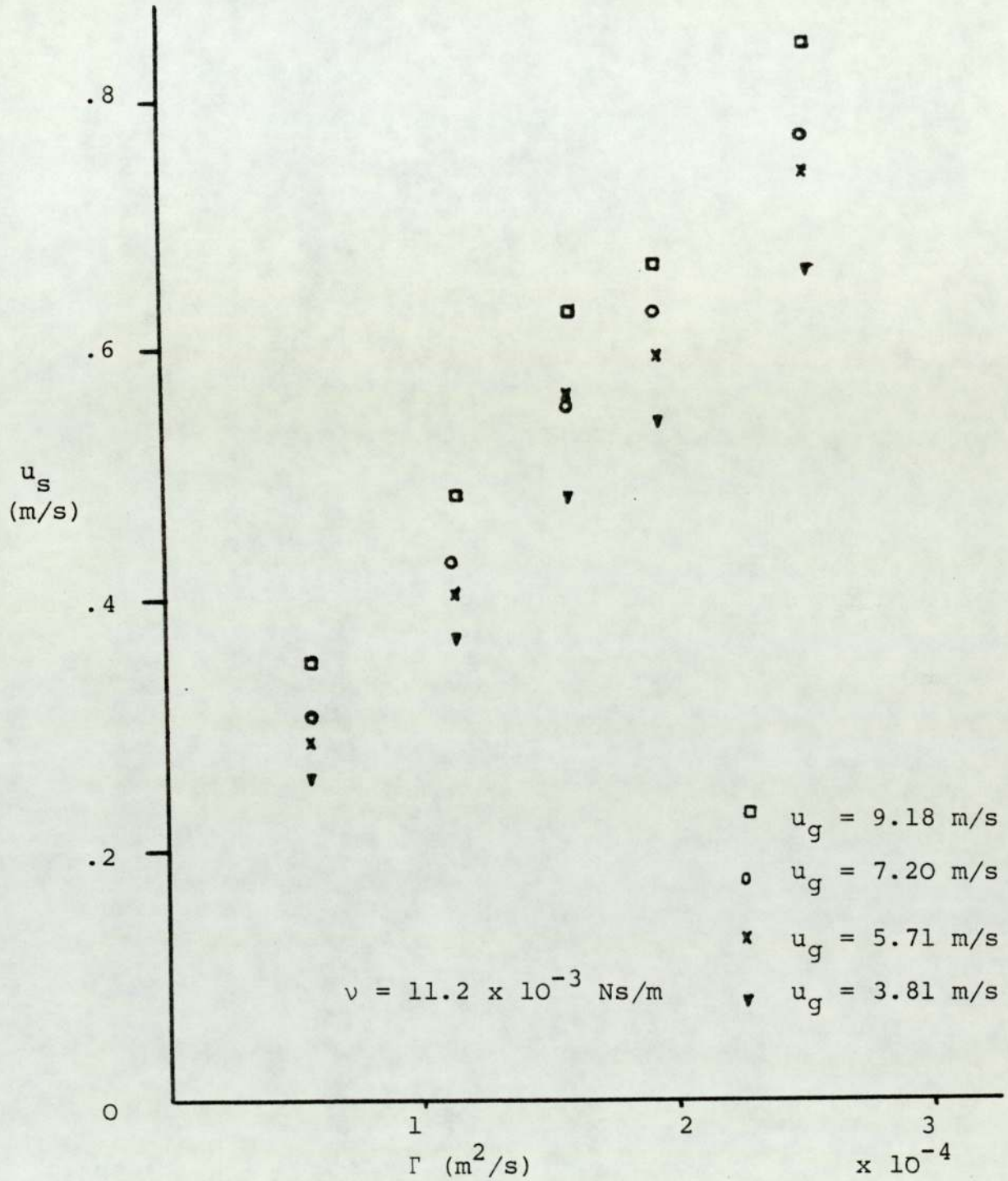

Figure 7.6 - Surface Velocity of the Liquid Film vs Liquid Flow Rate, at x = 2.04m

But the average velocity can be predicted from the known value of the volumetric flow per wetted perimeter, Γ, and the film thickness, as estimated by equation 7.11.

$$\bar{u} = \frac{\Gamma}{\delta(x)} \tag{7.15}$$

so equation 6.52 can be written as

$$\frac{u}{\bar{u}} = 6(y/\delta)^2 - 4(\bar{y}/\delta)^3 \tag{7.16}$$

or

$$u = (1 - \frac{2}{3}\, y/\delta)\, \frac{6y^2\Gamma}{\delta^3} \tag{7.17}$$

where δ, the film thickness is a function of the liquid physical properties and flowrate, location along the length of the column and the average velocity of the gas stream. The velocity profile as predicted by equation 7.16 is shown in Figure 7.7.

The surface velocity can be predicted from equation 7.7 as

$$u_s = 2\, \frac{\Gamma}{\delta} \tag{7.18}$$

Substituting into equation 7.18, the surface velocity to be expressed as a function of the flowrate parameters, liquid phase properties and distance from the origin. Thus

$$u_s = 2\, \frac{\Gamma^{2/3}}{\delta^*}\, (\frac{g}{3\nu})^{1/3} \tag{7.19}$$

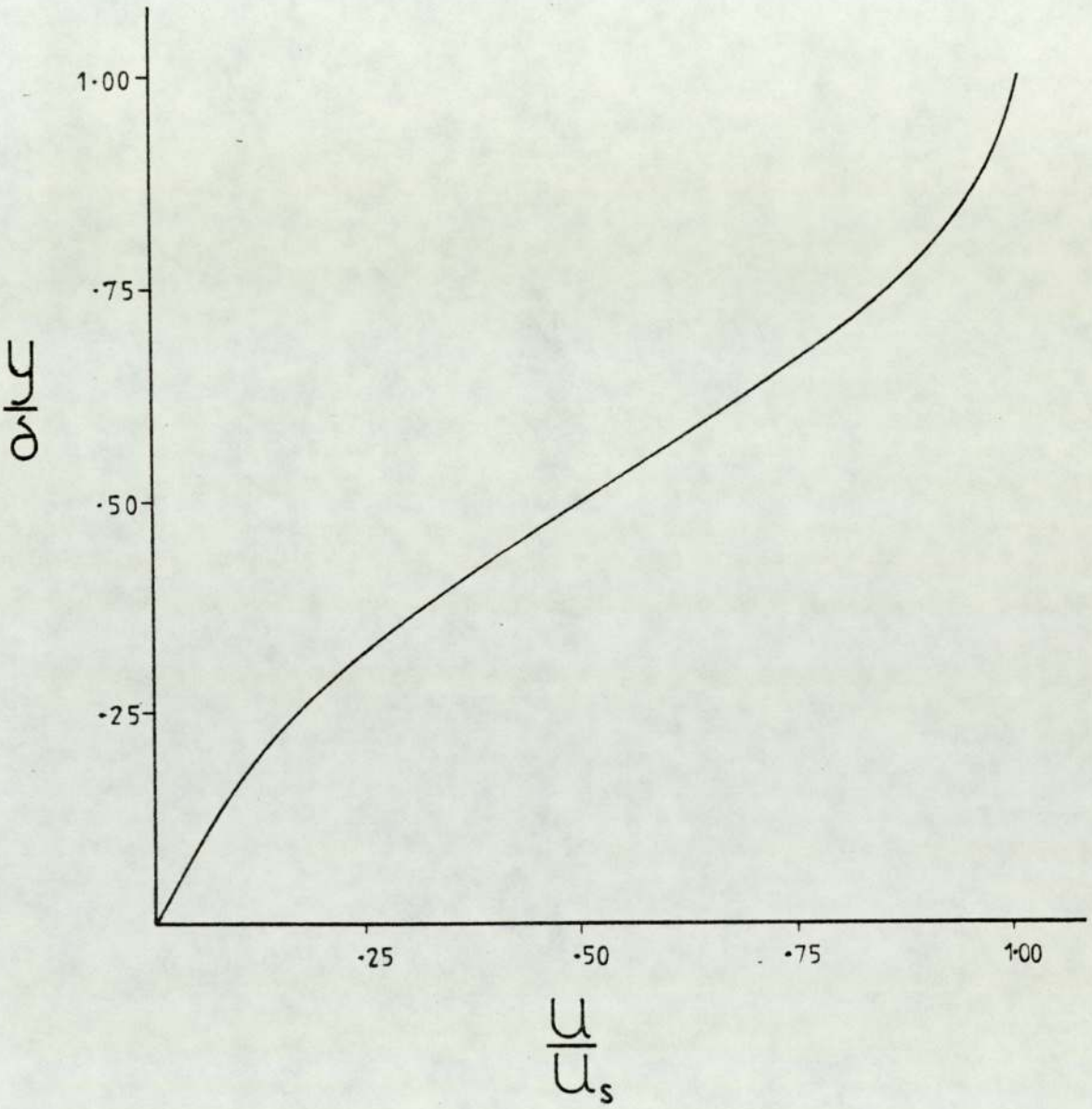

Figure 7.7 - Velocity Profile

where δ^* is defined by equation 7.11, as a function of the ration x/R_h and the Reynolds number of the gas phase. A comparison of the results obtained from the simulation of the mathematical models and those obtained by equation 7.19 is presented in Figure 7.8.

7.2.3 Friction Factor at the Interface

The liquid friction factor f_i, can be obtained from equation 6.30, as follows.

$$f_i = f_g \left(\frac{u_r}{u_s}\right)^2 (\rho_g/\rho) \qquad (7.20)$$

where u_r is the relative velocity, between the two phases at the interface.

$$u_r = u_g - u_s \qquad (7.21)$$

The gas phase friction factor has been previously defined, equation 6.26, using an expression first suggested by Wallis.

$$f_g = .005\ (1+360\delta/R_h) \qquad (6.26)$$

Since the surface velocity has been defined previously, equation 7.20 can now be solved. Figure 7.9 shows the calculated friction factor compared with values obtained from the analysis of the film thickness.

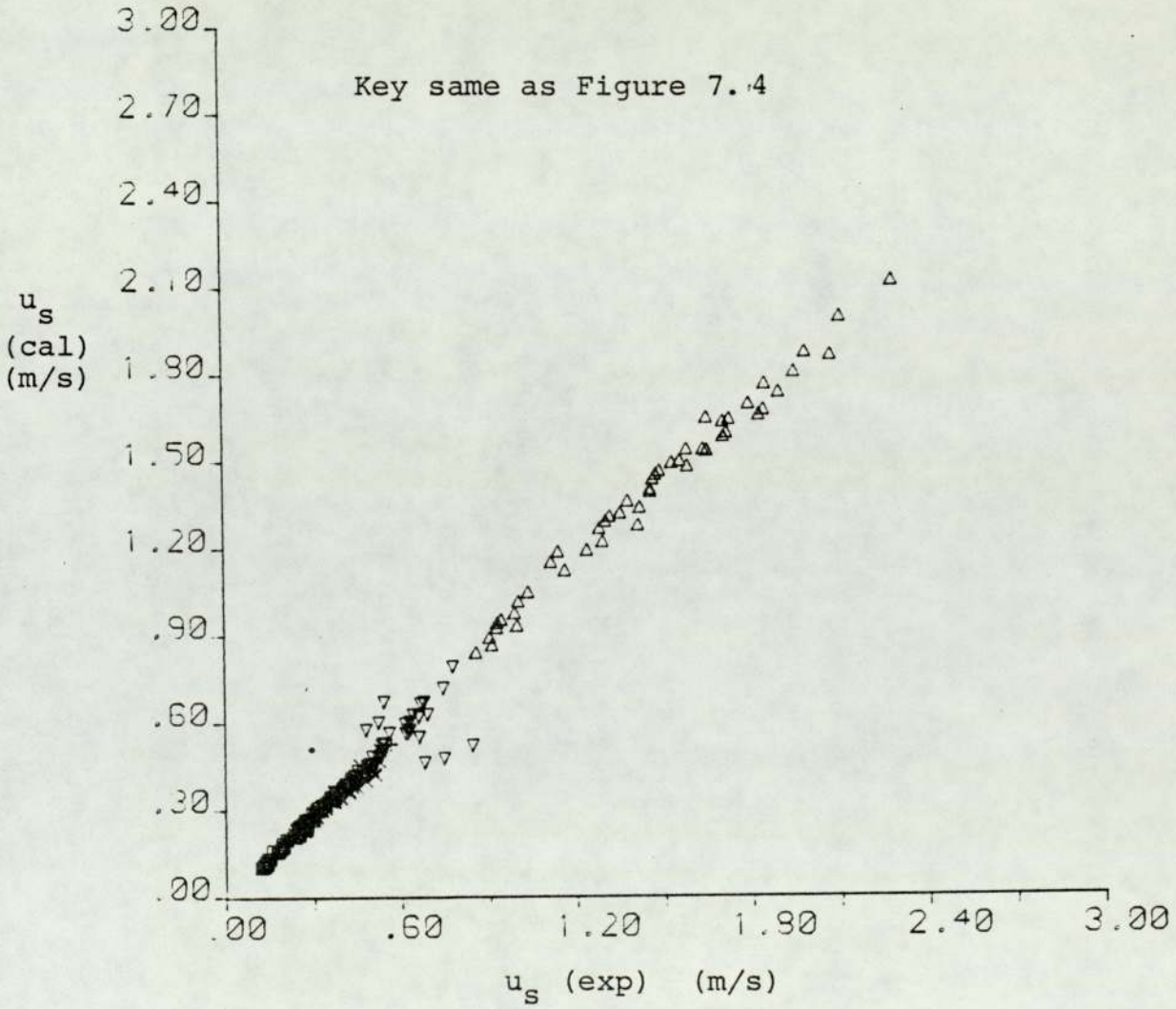

Figure 7.8 - Experimental vs Theoretical Surface Velocity

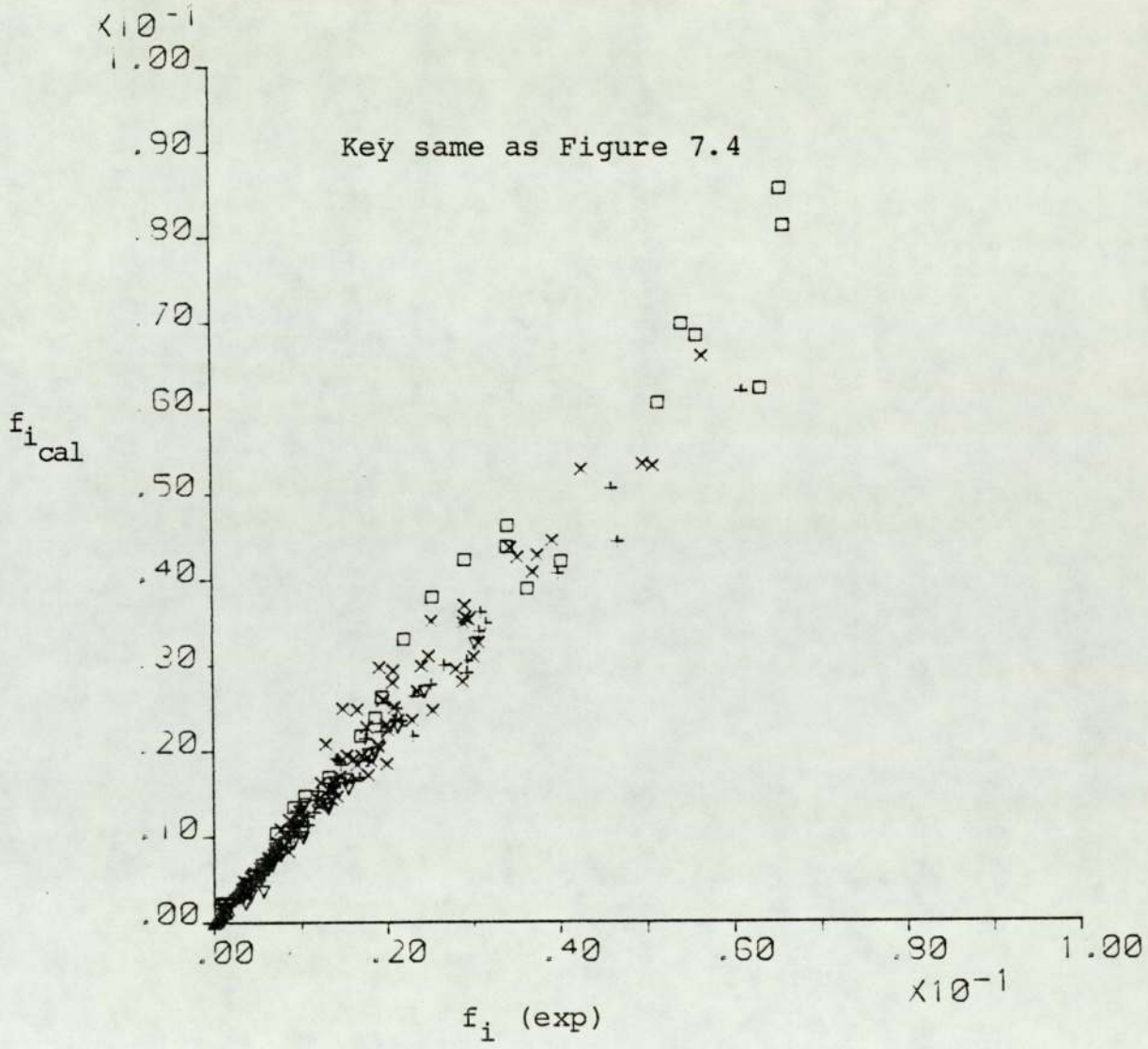

Figure 7.9 - Experimental vs Predicted Friction Factor at the Interface

7.3 Inception of Droplet Entrainment

7.3.1 Experimental Programme

A number of experiments were designed to define the limits of the transition regime. Firstly it was necessary to establish under what conditions "roll waves" are initiated, and then to determine the gas velocity at which entrainment becomes apparent. As previously reported by Wallis it is necessary to provide protection for the falling film at the inlet from the cocurrent gas stream. Since the gas contacts the liquid at an angle of approximately 90°, entrainment was detected at gas velocities much lower than expected, i.e. for liquid Reynolds numbers $300 < Re < 1000$, entrainment was observed at a gas velocity of 1.5 m/s. This result corresponds with a water-air system. Similar results were obtained for liquids with viscosities in the range $10^{-3} Ns/m^2 < \mu < 6 \times 10^{-2} Ns/m^2$. Therefore, only measurements taken after a protective shield had been installed were considered relevant. The liquids used in the experimental programme were the same as those employed in the film thickness experiments.

7.3.2 Determination of the Critical Gas Velocity for the Onset of "Roll" Waves

The technique used to determine the point at which the falling film undergoes a change in its flow pattern from cross-hatched wavy flow to a regular "roll" waves, consisted of recording the frequency of the waves,

using an ultrasonic probe and the "UFD 2M" monitor described in section 3.3 of Chapter 3. Visual observations on the change in the film surface are also reported.

7.3.2.1 Presentation and Analysis of Results

An example of the change in the frequency of the rolling wave and its final regular pattern is shown in Figure 7.10. The wave peaks were recorded for increasing gas velocities; a definite change in the structure of the liquid film was noted as the gas velocity increased above a certain value. The film surface observed was similar to that reported by Chung and Murgatroyd (59).

> "Eventually the film between the waves will be depleted to such an extent that it will not produce surface waves"

Figure 7.11 shows the shape and flow pattern of the roll wave as suggested by Chung and Murgatroyd. Where s is the length between crests, B, the length of the roll wave at its base, and the ratio δ/h is equal to .248.

A change in the structure of the flow pattern was observed at u_g = 3.5 ms^{-1} for all the different liquids used at all liquid flowrates. However, it is possible that for longer columns, an even smaller gas velocity would have a similar effect on the shape of the wave. This result confirms previously reported values for the gas velocity, as 4.m s^{-1} by Zhivaikin (58) and Portalski (45).

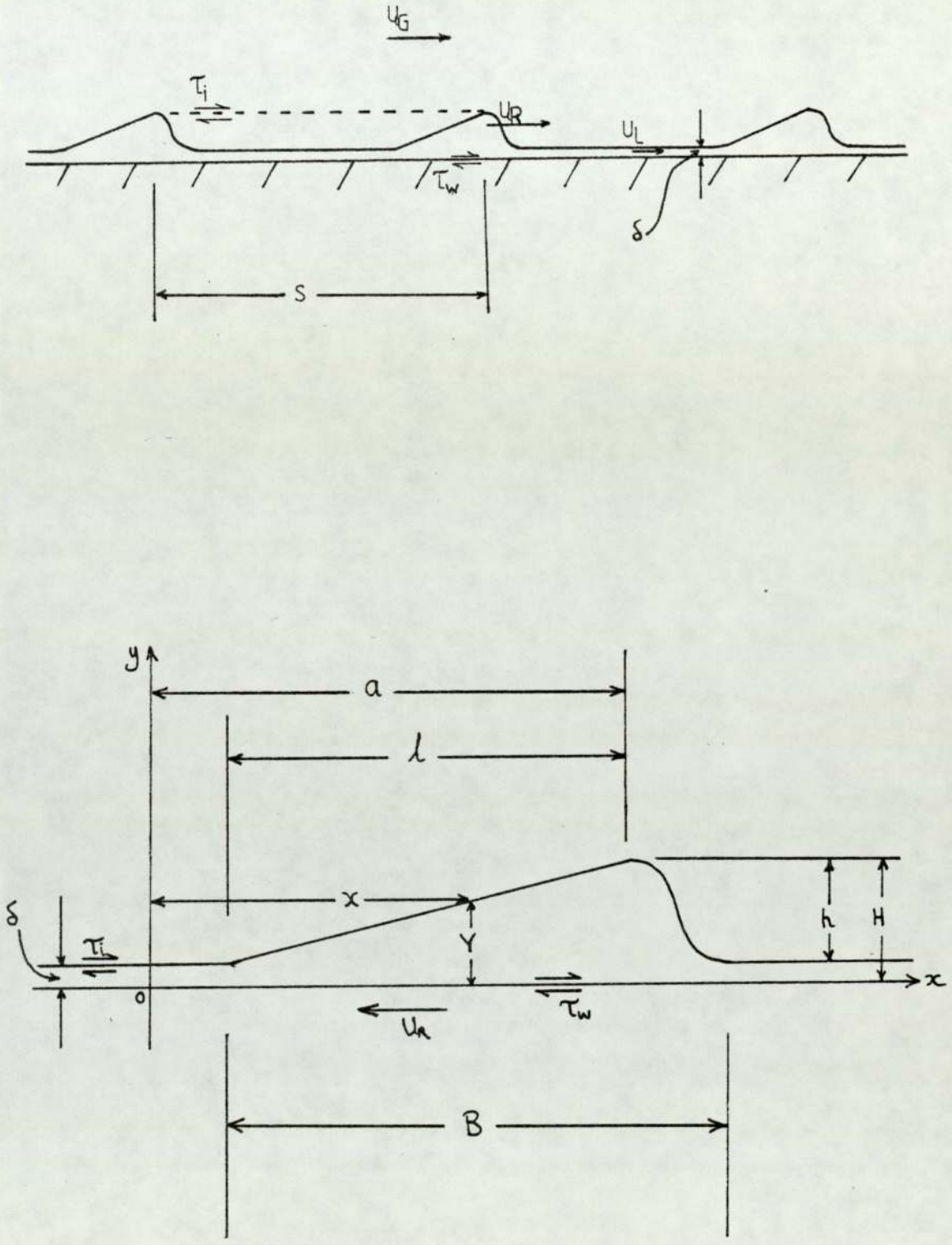

Figure 7.11 - Chung and Murgatroyd "Roll Wave" Model

7.3.3 Determination of the Critical Gas Velocity for the Onset of Entrainment

The onset of entrainment was defined as the first detectable sign of droplet entrainment. Observations were made visually. This method was preferred to the other detection methods, based on the work of Andreussi (138), who researched into the adequacy of several methods in order to explain the disagreement among the many existing correlations. Measurements of the critical gas velocity determined by pressure drop were up to five times higher than the critical velocity visually observed. The results are presented in Table 7.11.

7.3.3.1 Analysis of Results

The effect of the liquid flowrate was as expected, that is the critical gas velocity decreased as the liquid flowrate increased, until reaching a limit value above which entrainment would happen independently of the liquid flow rate. This is shown in Figure 7.12.

Figure 7.13 indicates that the viscosity of the liquid phase has a small effect on the critical gas velocity, contrary to what Zhivaikin suggested, but more in accord with Andreussi's findings. Because of the small variation in the surface tension, no conclusion on its effect on the inception point has been drawn.

Visual observations indicated that the wave structure in the transition regime is controlled by the interaction

Table 7.11 - Measurements of Entrainment Critical Air Velocity

ν Ns/m^2	Γ $(m^2/s) \times 10^4$	Re	u_g (m/s)	Re_g
.001	0.70	280	11.75	87823
.001	0.98	392	11.25	84086
.001	1.48	600	10.90	81470
.001	2.03	815	11.10	82965
.001	2.63	1050	11.00	82217
.001	3.40	1360	10.80	80722
.011	0.60	22	12.50	93430
.011	0.97	35	12.50	93430
.011	1.23	45	12.20	91186
.011	1.70	62	11.40	85207
.011	2.14	78	11.00	82217
.020	.48	9.3	13.00	97166
.020	.90	18	12.80	95670
.020	1.13	23	12.65	94550
.020	1.64	33	12.20	91186
.020	2.15	43	12.20	91186
.048	.46	4	13.8	103145
.048	.87	7.2	13.2	98660
.048	1.2	10	13.	97160
.048	2.0	17	12.6	94175

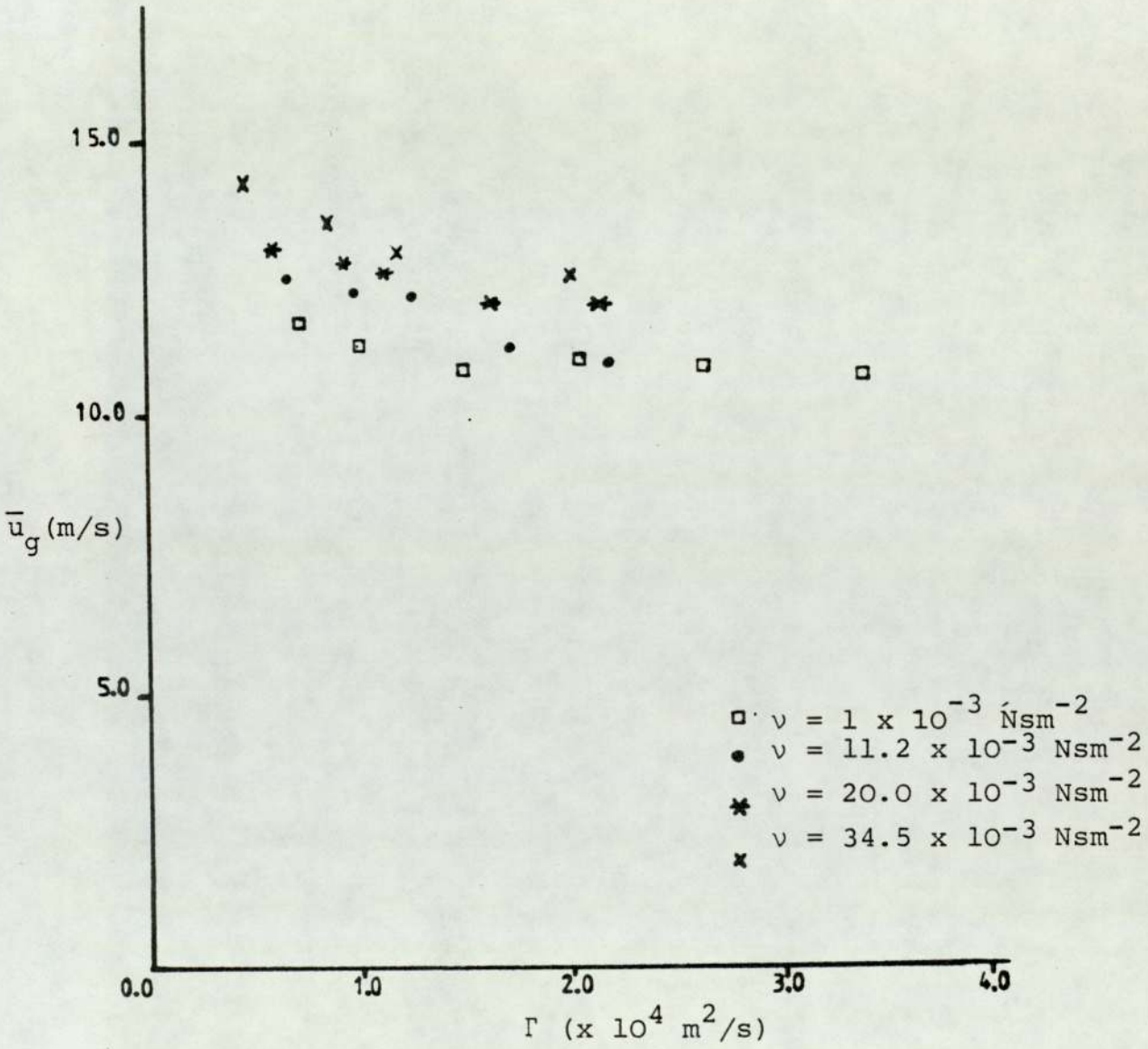

Figure 7.12 - Inception of Droplet Entrainment, Critical Gas Velocity

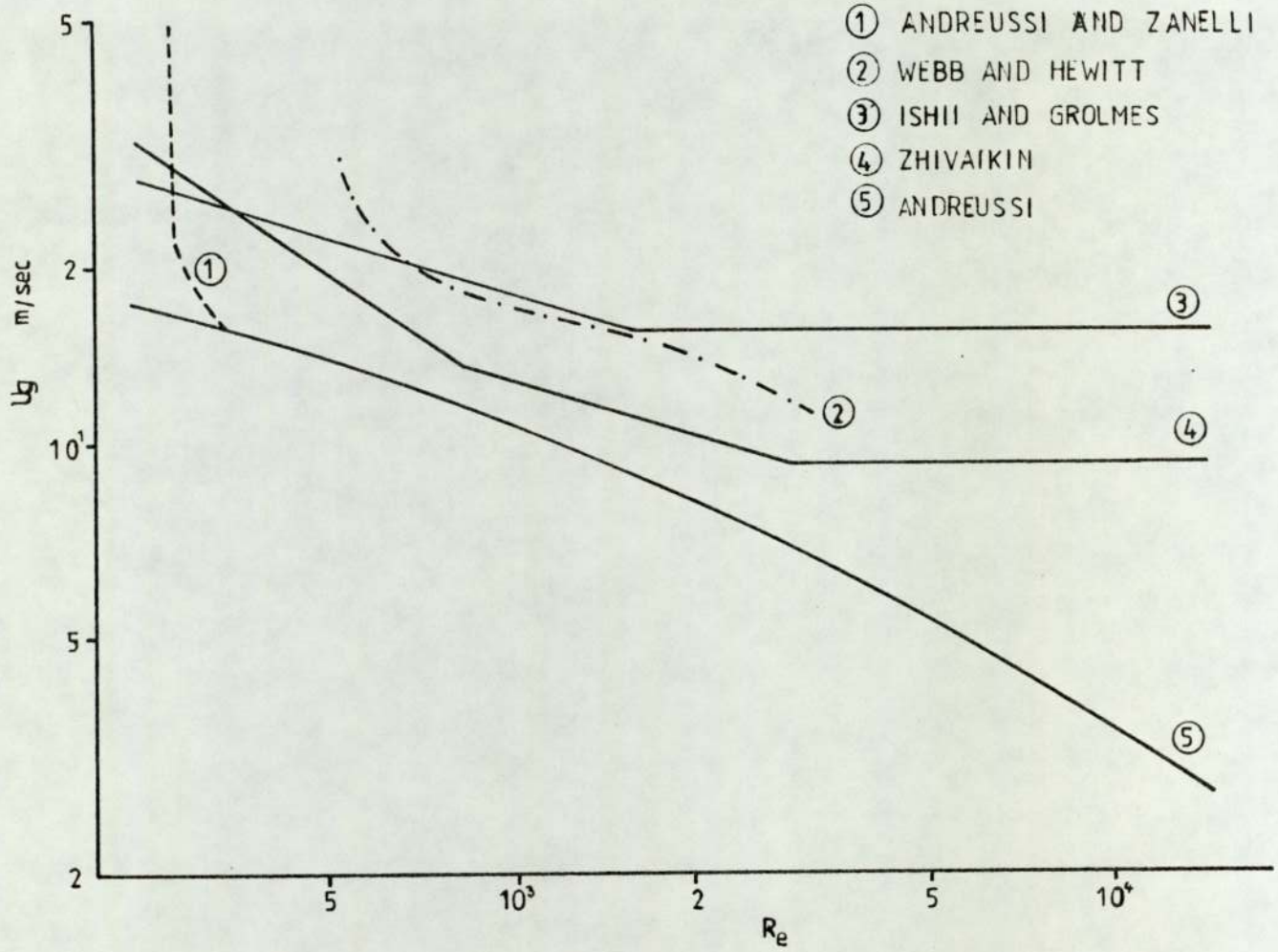

Figure 7.13 - Comparison of Various Criteria for the Inception of Droplet Entrainment

at the interface. Therefore, the same mechanism which causes the "roll wave" structure, determines the onset of entrainment.

7.3.3.2 Inception Criterion

Assuming the shape of the wave as postulated by Chung and Murgatroyd, Ishii and Grolmes (137) criterion, equation 5.7, is rewritten as

$$a\rho_g u_r^2 > .77 \tag{7.22}$$

Solving equation 7.22 for some typical experimental results in a value of $a \approx \delta_{exp}$ which suggests that entrainment occurs as described by the roll wave mechanism, shown in Figure 5.2.

A criterion has been proposed, based on the assumption that the inception point for droplet entrainment is caused by an imbalance between the drag force acting at the interface and the containment force due to surface tension. A similar approach was followed by Andreussi (138) and the criterion was represented by

$$\omega_e^* > \omega_{e_c} \tag{7.23}$$

The Weber number was defined as

$$\omega_e = \rho_g u_g^2 \delta/\sigma \tag{7.24}$$

The rate of growth of the wave wad described in terms of the friction velocity u* as

$$\omega_e^* = \rho_g \dot{u}^{*2} \delta/\sigma \qquad (7.25)$$

The criterion can be reformulated in the following form,

$$\rho_g \frac{u^{*2}\delta}{\sigma} > \omega_{e_c} \qquad (7.26)$$

Where the friction velocity is defined as suggested by Tatterson (166,167), to take into consideration the velocity profile in the gas phase as

$$u^* = u_g (f_i/2)^{\frac{1}{2}} \qquad (7.27)$$

The film thickness δ can be estimated from equation 7.11. The friction factor at the interface is defined by equation 7.20.

The value for the critical Weber number found by Andreussi was $\omega_c \simeq 5.5 \times 10^{-3}$. This value correlates fairly well with the experimental results as shown by Figure 7.12.

7.4 Minimum Wetting Rate

It has been demonstrated experimentally that a minimum liquid flowrate is necessary to wet the whole surface of the column. This minimum wetting rate was determined visually by observing the appearance of dry patches in the column. The procedure followed was similar the the one described above for the film thickness experiments. The same gas-liquid systems were used.

The entire surface was wetted first, then the liquid flowrate would be decreased until the appearance of dry patches was observed.

7.4.1 Presentation and Analysis of Results

The results are presented in Table 7.12. As expected, the minimum wetting rate decreased as the viscosity of the liquid film was increased. The gas stream was found to have a stabilizing effect on the film, allowing for lower values for the minimum wetting rate than those predicted, in the absence of shear stress at the interface.

Since it was not possible to measure the contact angle between the liquid film and the solid wall, no conclusions can be drawn on the adequacy of the existing criteria for the prediction of the minumum wetting rate.

Table 7.12 - Minimum Flow Rate

Water:	$\Gamma_{min} < 1.3 \times 10^{-4}$ m^2/s,	Re = 520
Glycerol 63%:	$\Gamma_{min} < 0.68\ 10^{-4}$ m^2/s,	Re = 25
Glycerol 70%:	$\Gamma_{min} < 0.65 \times 10^{-4}$ m^2/s,	Re = 13
Glycerol 75%:	$\Gamma_{min} < 0.65 \times 10^{-4}$ m^2/s,	Re = 9
Glycerol 80%:	$\Gamma_{min} < 0.400 \times 10^{-4}$m^2/s,	Re = 3

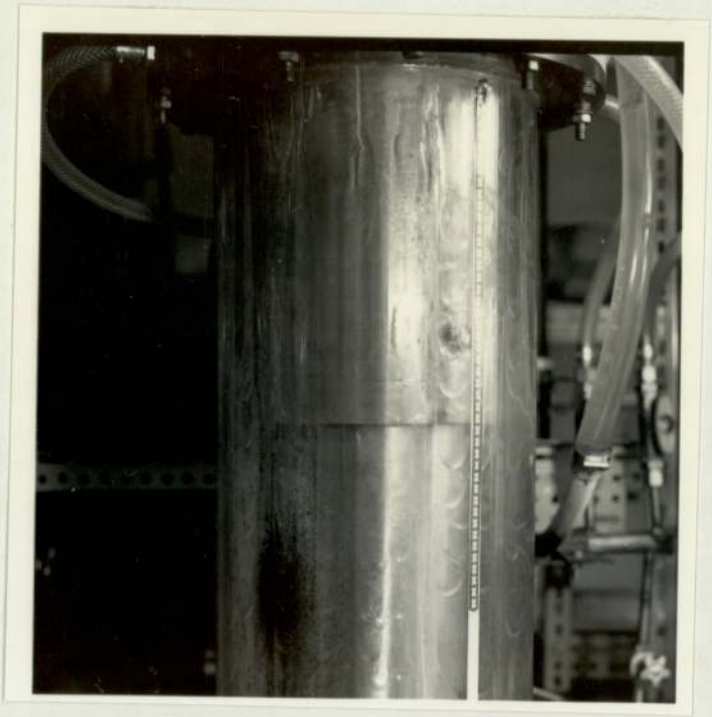

Figure 7.14 - Rupture of Liquid Film

CHAPTER VIII

MASS TRANSFER, PRESENTATION AND ANALYSIS OF RESULTS

An experimental programme has been designed to investigate the effects of gas and liquid flow rates on gas-phase mass transfer from a turbulent gas stream into a falling liquid film, in a vertical annular absorber/ reactor. Two sets of experiments were carried out on the absorption of a low concentration gas into water and into a diluted solution of acid. The mass transfer coefficients were calculated from the experimental data using the classical two film theory.

8.1 Experimental Procedure

8.1.1 Physical Absorption

Ammonia was absorbed from a low concentration ammonia-air mixture, into distilled water at 20^{o}C. The Reynolds numbers for the turbulent gas stream ranged from 65000 to 94000. For the liquid film the Reynolds number varied from 700 to 1200. The air and ammonia volumetric flows were measured separately by the methods described in Appendix A. The gas streams were introduced at the top of the column, above the calming section. The turbulence of the air stream ensured an even mixing of the two gases. The system was operated at atmospheric pressure.

Samples of the liquid phase were collected at the bottom of the vertical column. Known volumes of the samples and .5M hydrochloric acid solution were immediately mixed in order to avoid any evaporation of the ammonia from the liquid, which would affect the results. The amount of ammonia absorbed was determined by titrating

the excess hydrochloric acid with a sodium hydroxide solution, using methyl-red as an indicator. The procedure followed in the chemical analysis is described in Appendix G. The diffusivity of ammonia in air, D_g, at 20°C was estimated to be .203 x 10^{-4} m^2/s.

The start-up procedure was similar to that followed for the hydrodynamic experiments (Chapter 7). The liquid-phase flowed down the inner wall of the perspex tube forming an evenly distributed film. The experiments were carried out under such conditions that neither droplet entrainment nor rupture of the film would take place. The physical properties of the two phases are given in Appendix C.

8.1.2 Chemical Absorption

Experiments on the absorption of ammonia from an air-ammonia mixture into an aqueous sulphuric acid solution were also carried out. The apparatus and procedure were the same as described above for the physical absorption experiments. A dilute acidic solution was prepared using sulphuric acid and distilled water, without any surface active agent. The molarity of the sulphuric solution was determined by titration with sodium hydroxide, using methyl-red as indicator. Samples of the liquid phase were collected at the bottom of the reactor. The amount of ammonia absorbed was determined by measuring the amount of unreacted sulphuric acid in the samples. The essential reaction is:

$$2\ NH_3 + 2\ H_2O + H_2SO_4 \rightarrow (NH_4)_2SO_4 + 2H_2O$$

The concentration of non-absorbed ammonia in the gas stream was calculated from a mass balance of the two phases. For each mole of reacted sulphuric acid, two moles of ammonia were absorbed. Knowing the concentration of sulphuric acid in the inlet, $M_{o,s}$ (g-moles/litre), and at the outlet, $M1_{,s}$, the number of absorbed moles of ammonia per liter of solution is given by the expression

$$M_{NH_3} = 2(M_{o,s} - M_{1,s}) \text{ (g-moles/litre)} \qquad (8.1)$$

Since the concentration of ammonia is very small in the gas stream and the acid solution is very dilute, the molar velocity in the two phases can be assumed to remain constant along the length of the reactor. A mass balance between top and bottom of the column was obtained as:

$$G_M\ (Y_o - Y_1) = L_M\ (M_{NH_3}/M_{H_2O}) \qquad (8.2)$$

the total number of moles in one litre of distilled water is:

$$M_{H_2O} = \frac{1000 \text{ g/litre}}{18 \text{ g/g-moles}} = (\frac{.1}{.018}) \text{ g-moles/litre}$$

Therefore, combining the above equations, Y_1 was expressed as

$$Y_1 = Y_o - .036\ \frac{L_M}{G_M}\ (M_{o,s} - M_{1,s}) \qquad (8.3)$$

The liquid and gas flowrates used were in the same range as in the physical absorption method. The physical properties of the two phases are given in Appendix C.

The flow rates and hydrodynamic parameters of the two sets of experiments are listed in Table 8.1. The initial concentration of ammonia in air was 3% in volume. The experimental results are presented in Table 8.2.

8.2 Determination of the Mass Transfer Coefficient

The rate at which absorption takes place is proportional to the mass transfer coefficient, the surface area and the driving force promoting it, as represented in Figure 8.1. The rate of absorption per unit volume, r_A, is expressed as:

$$r_A = k_g \, a_v \, P(Y-Y_i) \qquad (8.4)$$

Where k_g is the mass film coefficient and a_v is the interfacial area per unit of volume. The driving force across the film has been defined as the difference in the concentration of the soluble gas in the gas bulk flow, Y, and at the gas-liquid interface, Y_i. However, since conditions at the interface are usually difficult to determine, it is preferred to express the driving force in terms of the difference between the concentration Y and the equilibrium concentration Y*, corresponding to the concentration of the soluble gas in the liquid phase, X. Equation 8.4 is then rewritten as:

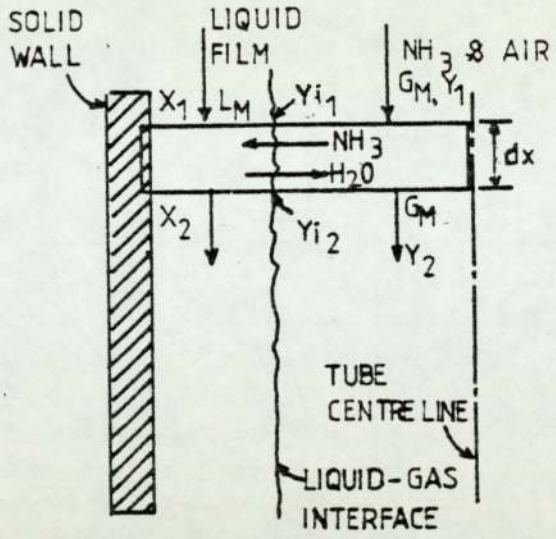

Figure 8.1 - Mass Balance Across the Interface

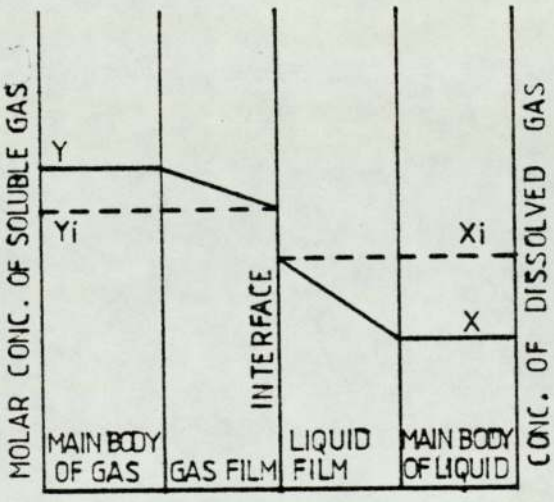

Figure 8.2 - Film Model for Mass Transfer at the Interface

$$r_A = K_g a_v P(Y-Y^*) \qquad (8.5)$$

Where K_g is the overall mass transfer coefficient on gas-phase basis. For dilute ammonia-air mixture it is possible to assume that the equilibrium curve is linear over the range in which it is used.

$$Y^* = m X \qquad (8.6)$$

For a 3% concentration in volume of ammonia in air the equilibrium constant, m, is 1.03 at 20°C, 1 atm. If a mass balance is taken between top and bottom, see Figure 8.3 (to avoid confusion, the total length of the column L, has been called Z)

$$r_a Z = G_M (Y_o-Y_1) = L_M (X_1-X_o) \qquad (8.7)$$

Therefore, equation 8.5 can be rewritten as;

$$G_M (Y_o-Y_1) = K_g a_v ZP (Y-Y^*)_{ave} \qquad (8.8)$$

Also, the "operating" line can be obtained from equation 8.7, substituting $x_o = 0$.

$$Y = Y_o - \frac{L_M}{G_M} X \qquad (8.9)$$

The absorption process is represented graphically in figure 8.4. As can be seen a cocurrent absorption system never reaches equilibrium, since an infinite contact time would be necessary.

The driving force term $(Y-Y^*)_{ave}$ has been derived from equations 8.9 and 8.6; since both equations are

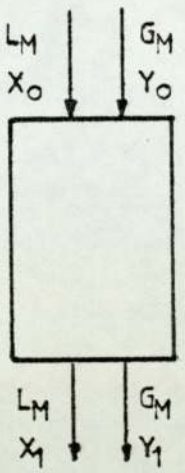

Figure 8.3 Diagrammatic Sketch of Cocurrent Absorber-Reactor

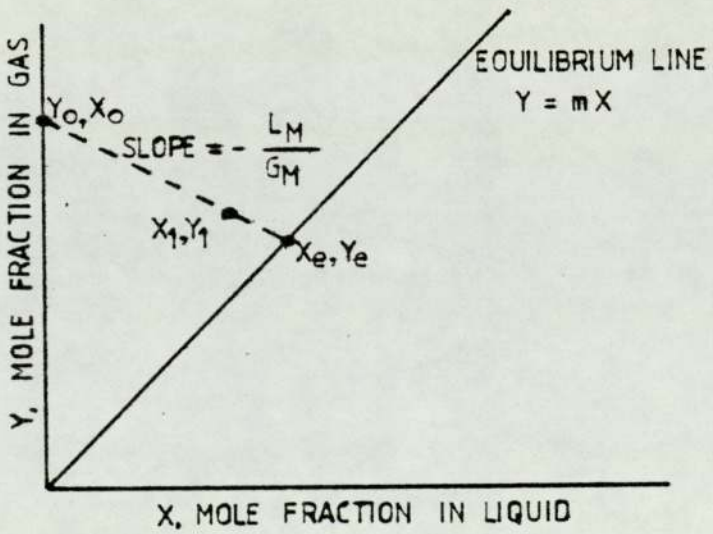

Figure 8.4 - Design Diagram of Cocurrent Absorption

linear, it follows that (Y-Y*) is linear in Y, so

$$\frac{d(Y-Y^*)}{dY} = \frac{(Y-Y^*)_o-(Y-Y^*)_1}{Y_o-Y_1} \qquad (8.10)$$

whence

$$(Y-Y^*)av = \frac{(Y-Y^*)_o-(Y-Y^*)_1}{\ln((Y_o-Y_o^*)/(Y_1-Y^*))} \qquad (8.11)$$

But $Y_o^* = 0$ so equation 8.11 can be simplified as

$$(Y-Y^*)_{av} = \frac{Y_o-(Y_1-Y_1^*)}{\ln(Y_o/(Y_1-Y_1^*)} \qquad (8.12)$$

Because the interfacial area is difficult to determine experimentally, a volumetric mass transfer coefficient, $K_g a_v$ has been used; which can be obtained by direct substitution, from the experimental data. The overall mass transfer coefficient is related to the film coefficients by the following relationship

$$\frac{1}{K_g} = \frac{1}{k_g} + \frac{m}{k_1}$$

In the case of absorption of ammonia into water, the rate of absorption does not depend exclusively on the resistance in the gas phase, as it has been frequently assumed. A considerable resistance to the mass transfer is due to the liquid side, this has been reported previously by Sherwood and Holloway (6) amongst others. Experimental results obtained in this work confirmed this. A considerable increase in the rate of mass

transfer was detected when ammonia was absorbed into an aqueous sulphuric acid solution instead of water.

The rate of absorption was made independent of the resistance in liquid side by absorbing the gas in an acid solution which reacts with the dissolved gas instantaneously and irreversibly. The concentration of ammonia at the interface is zero; reducing equation 8.5 to

$$r_a^{\circ} = K_g^{\circ} a_v P Y \qquad (8.14)$$

The mass balance is then reformulated as

$$G_M (Y_o - Y_1) = K_g^{\circ} a_v P Z \, Y_{av} \qquad (8.15)$$

Where Y_{av} is the log-mean mole fraction of ammonia in the gas mixture, defined by the expression

$$Y_{av} = \frac{Y_o - Y_1}{\ln(Y_o/Y_1)} \qquad (8.16)$$

Since there is no liquid side resistance, the mass transfer gas film coefficient can be obtained from equation 8.15, using the experimental data on chemical absorption. The volumetric mass transfer coefficient is expressed as

$$K_g^{\circ} a_v = \frac{G_M}{ZP} \ln (Y_o/Y_1) \qquad (8.17)$$

Assuming the resistance in the gas phase to be the same in the two sets of experiments, when the flowrate

parameters are the same, the liquid side mass transfer coefficient k_l can be estimated from equation 8.13, using the values obtained from equation 8.17 and 8.8.

8.3 Analysis and Discussion

The increase in the rate of mass transfer in a falling liquid film reactor can be explained by three different ways:

1. An increase in the interfacial area.
2. An increase in the mixing within the liquid film.
3. Turbulence in the gas stream.

The increase in interfacial area with respect to that predicted by the theory for smooth liquid films, developed by Nusselt, can be estimated from the above mentioned study on the hydrodynamics. The commonly used expression for the mass transfer coefficient, developed by Gilliland (12), has been applied to determine the theoretical volumetric mass transfer coefficient $(kg\ a_v)_t$. Gilliland defined k_c for falling films as:

$$k_c = .023\ Re_g^{.83}\ Sc_g^{.44}\ \left(\frac{P}{P_{BM}}\right)\ \left(\frac{D_g}{2R_h}\right) \qquad (8.18)$$

which can be rearranged as

$$k_g = 0.23\ Re_g^{-.17}\ Sc_g^{-.56}\ G_M/P \qquad (8.19)$$

where Sc_g is the gas phase Schmidt number, defined as

$$Sc_g = \nu_g / D_g \tag{8.20}$$

For a 3% in volume air-ammonia mixture, the Sc number is 0.74.

The interfacial area is predicted by Nusselt is

$$A_N = 2\pi(r_o - \delta_N)Z \tag{8.21}$$

The experimental interfacial area have been determined from the study of the hydrodynamics, as shown in Appendix E. The increase in interfacial area, defined as the ratio of the experimental area to the theoretical area, cannot solely explain the increase in the volumetric mass transfer coefficient, e.g. using data from the first experiment

$$\frac{k_g^{\,o}\, a_v}{(k_g\, a_v)_T} - 1 \approx .4$$

and

$$\frac{A_{ex}}{A_t} - 1 \approx 1.003$$

Since .4 >> .003, the increase in interfacial area is negligible when compared to the increase in the rate of mass transfer.

A graphical representation of the effect of the different flow parameters on the overall mass transfer coefficients is given in Figures 8.5 and 8.6.

The increase in the gas-side mass transfer coefficient as the gas velocity is increased, suggested a dependence on the gas phase turbulence. Hikita (106) and Shilimkan (14) suggested the correlation of kg to a gas-phase Reynolds number, defined in terms of the relative velocity of the gas stream to the superficial velocity of the liquid film:

$$R_e' = (\bar{u}_g - u_s)\ 2(R_h-\delta)/\nu_g \qquad (8.22)$$

Shilimkan proposed the following relationship between the Sherwood and Reynolds number

$$Sh_g = 3.29 \times 10^{-4}\ Re_g'^{.756} \qquad (8.23)$$

Where the Sherwood number is defined as

$$Sh_g = 2R_h k_c/D_g \qquad (8.24)$$

Hikita suggested the radius of gas passage, $R_h-\delta$, as the characteristic length for the Sherwood number. In Figure 8.7 the measured values of Sh_g are plotted against Re_g' and compared with the results obtained by Hikita and co-workers (106), using two columns of different sizes. As evident from this figure, the Sherwood number can be correlated as a function of the Reynolds

number, defined by equation 8.22, together with the Schmidt number. The effect of the geometry of the reactor was constant with Hikita's work and the Schmidt number was not varied in this work.

Johnson and Crynes (168) took into consideration the effect of the turbulence, by using a constant .046 in equation 8.18. instead of .023. In Figure 8.8, the measured values of kg are compared to the theoretical predictions of Johnson and Gilliland. This indicates the relationship between the effect of the gas turbulence and the increase in the relative velocity of the gas stream. It supports the use of a larger constant in equation 8.18 as suggested by Johnson.

The liquid side mass transfer coefficient, k_l, have been calculated from the volumetric mass transfer coefficients. These were measured at the same flow rates, using values for the interfacial area calculated in Appendix E.

The data indicated a dependence of k_l on the average gas velocity, which can be explained by the increase in the mixing within the liquid film. The hypothesis was supported by the decrease in the mass transfer coefficient which occurred as the liquid flow rate was decreased, keeping the gas flow constant.

Table 8.1 - Flowrates Parameter for the Mass Transfer Experiments

Run	Γ m^2/s x 10^4	Re	L_M^*	u_g m/s	G_M^*	Re_g	L_M/G_M
1	2.88	1115	45.74	8.80	36.61	65675	1.256
2	2.61	1006	41.39	8.80	36.61	65675	1.137
3	2.33	900	37.04	8.80	36.61	65675	1.017
4	1.81	725	28.76	8.80	36.61	65675	.790
5	2.88	1115	45.74	7.22	29.87	53883	1.531
6	2.61	1006	41.39	7.22	29.87	53883	1.386
7	2.33	900	37.04	7.22	29.87	53883	1.240
8	1.81	725	28.86	7.22	29.87	53883	.963
9	2.88	1115	45.74	5.47	22.63	40823	2.021
10	2.61	1006	41.39	5.47	22.63	40823	1.829
11	2.33	900	37.04	5.47	22.63	40823	1.637
12	1.81	725	28.76	5.47	22.63	40823	1.271
13	2.88	1115	45.74	4.00	16.55	29852	2.764
14	2.61	1006	41.39	4.00	16.55	29852	2.501
15	2.33	900	37.04	4.00	16.55	29852	2.238
16	1.81	725	28.76	4.00	16.55	29852	1.738

$$L_M, G_M = \frac{\text{kg moles}}{m^2 s} \times 10^2$$

Table 8.2 - Mole Fraction at the Outlet and Volumetric Mass Transfer Coefficients

Run	Y_1	Y_1°	$Kg\ a_v$ *	$Kg^{\circ}\ a_v$ *	$K_1\ a_v$ *	I
1	.0210	.0192	7.79	8.17	172.51	1.05
2	.0203	.0189	7.95	8.46	133.92	1.06
3	.0207	.0178	8.58	9.55	102.48	1.06
4	.0207	.0162	10.02	11.28	89.70	1.13
5	.0202	.0182	6.92	7.33	127.60	1.06
6	.0204	.0175	6.85	7.91	51.29	1.15
7	.0203	.0165	7.16	8.71	76.28	1.22
8	.0205	.0151	7.54	10.18	29.01	1.35
9	.0193	.0173	5.68	6.10	82.50	1.07
10	.0192	.0169	5.87	6.38	73.43	1.87
11	.0192	.0161	6.01	6.97	43.64	1.16
12	.0187	.0148	7.02	7.89	63.66	1.12
13	.0183	.0158	4.53	5.17	36.60	1.14
14	.0182	.0152	4.66	5.54	29.33	1.19
15	.0182	.0151	4.75	5.65	33.53	1.19
16	.0180	.0146	5.16	5.84	44.31	1.13

* $Kg\ a_v$, $Kg^{\circ}\ a_v$, $K_1\ a_v = \frac{\text{kg mole}}{m^3} \times 10^2$

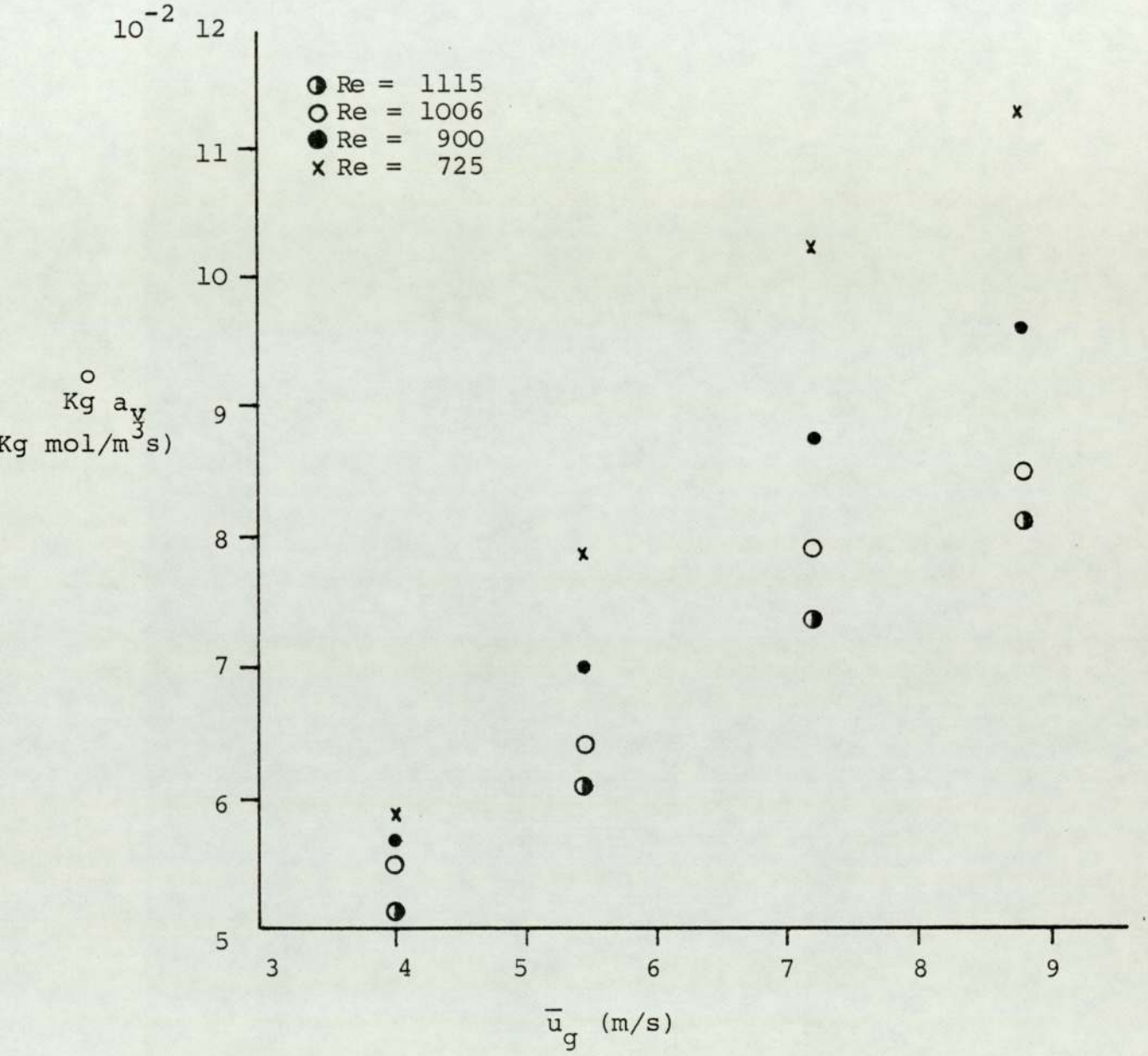

Figure 8.5 - Volumetric Gas Side Mass Transfer Coefficient vs Gas Velocity

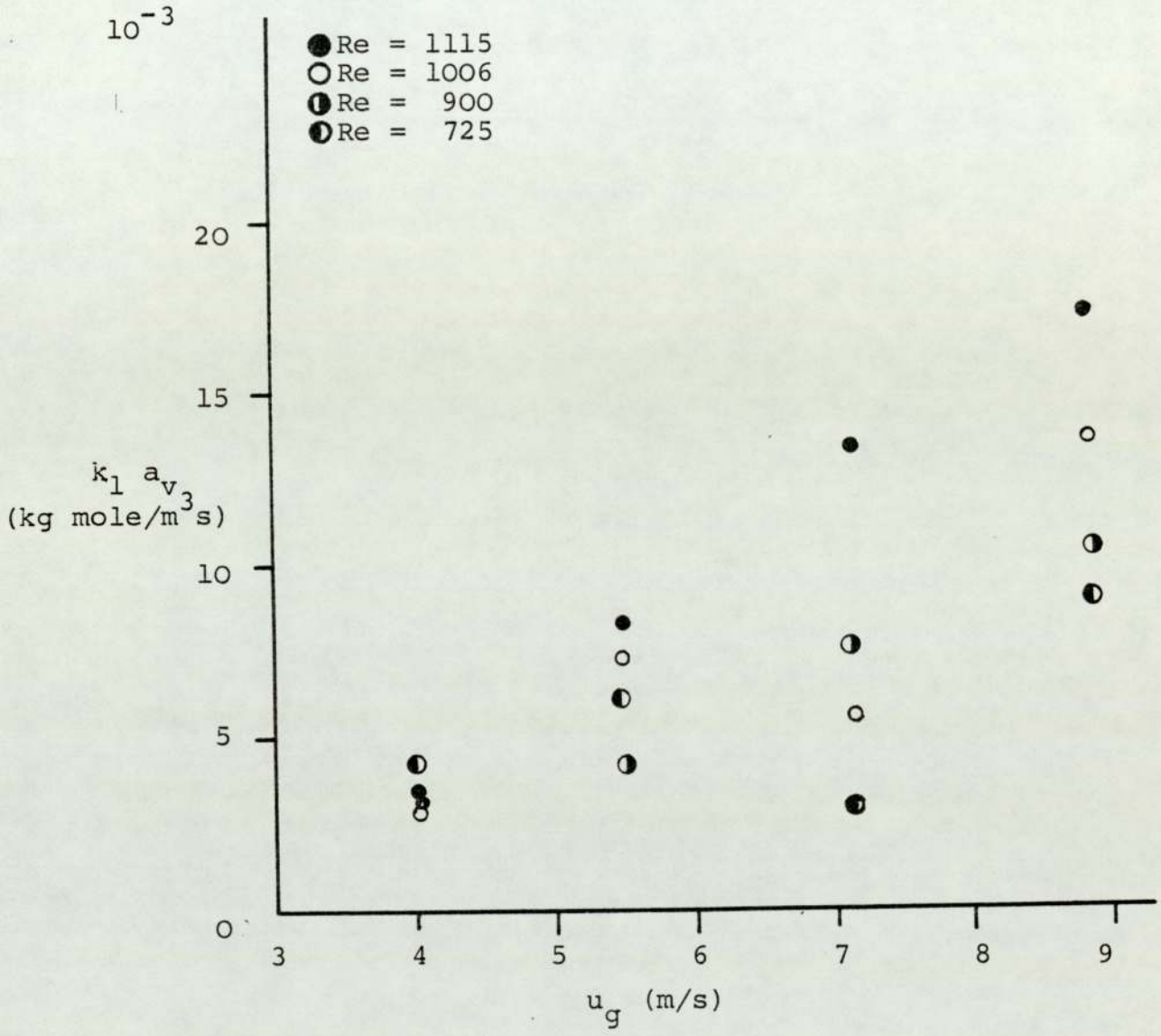

Figure 8.6 - Liquid Side Mass Transfer Coefficient vs Average Gas Velocity

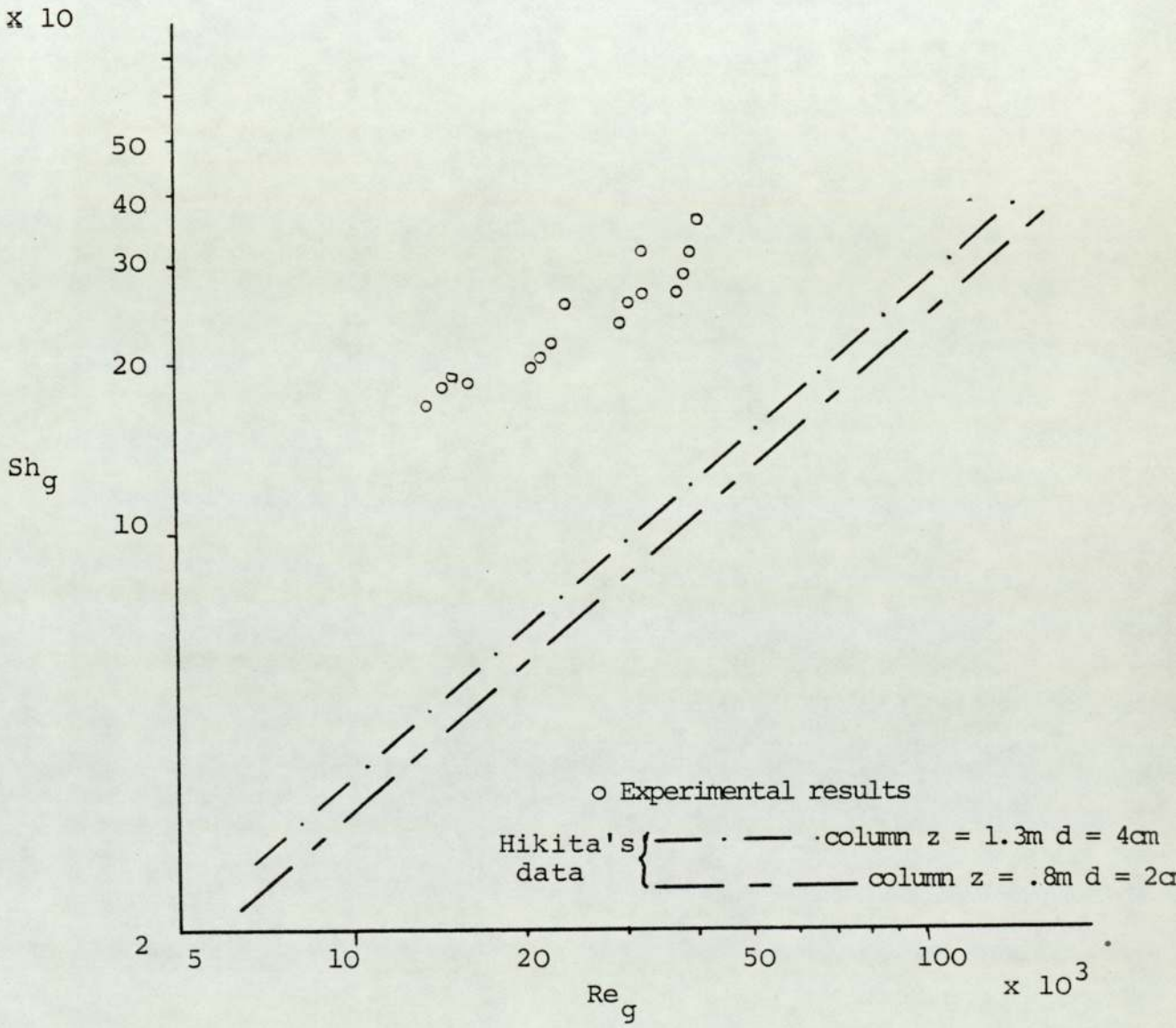

Figure 8.7 - Effect of Re_g on Sh_g

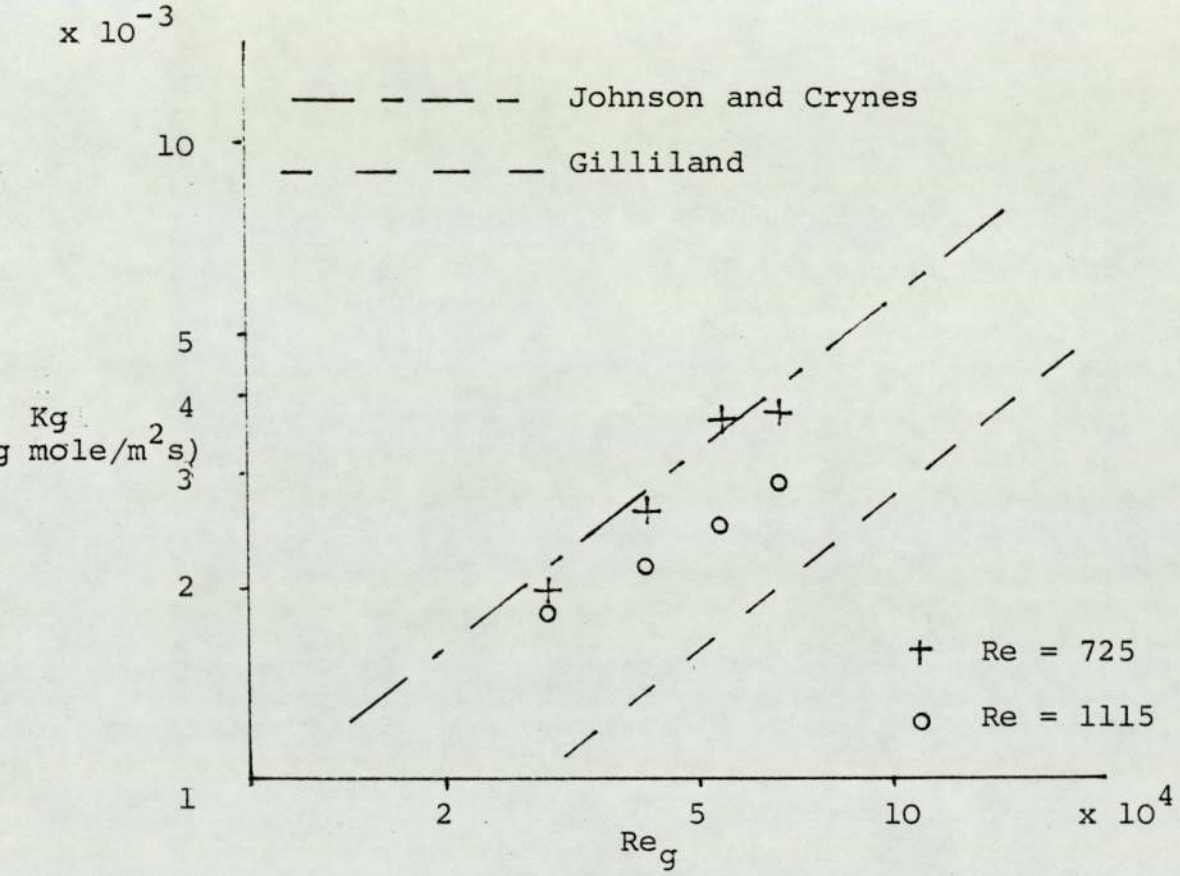

Figure 8.8 - Comparison of Gas Phase Mass Transfer Coefficients

Further experimental data would be necessary to formulate the relationship between the mass transfer coefficients. However, from the analysis of these results, the following conclusions have been drawn;

1. The mechanisms controlling the rate of mass transfer in the two-phases are different.

2. The gas-side mass transfer coefficient is affected by the increase in the turbulence, caused by the increase in interfacial shear.

3. The resistance in the liquid film increased substantially for low liquid flow rates, with high interfacial shear stress. This could be due to the thinning of the liquid film or to the existence of undetected droplet entrainment.

4. The increase in the liquid side mass transfer coefficient at higher liquid rates, can be explained by the surface motion and mixing in the liquid film.

CHAPTER IX

CONCLUSIONS

This study presents the results of an attempt to develop a better understanding of the behaviour of a falling liquid film subjected to high shear. A model which incorporates the effect of interfacial shear has been developed for an assessment of the hydrodynamic parameters. A parametric study on the effect of flowrates on the rate of mass transfer has been carried out and the conclusions drawn from the above investigation are:

1. A cocurrent turbulent gas stream decreases the thickness of the liquid film and enhances the mass transfer rate.

2. The hydrodynamics of smooth falling films are well described by Nusselt's theory, when flowing without shear at the interface and within a short distance of the interface.

3. The film thickness of the liquid film was experimentally determined by an ultrasonic probe method and the experimental data has been correlated as a function of distance along the length of the reactor, average gas velocity and the liquid flowrate and physical properties. The equation describing the flow thickness is valid for gas linear velocities above 3m/s with no droplet entrainment.

4. The hydrodynamic parameters have been predicted using the mathematical model developed in Chapter 6. A non-parabolic velocity profile has been

confirmed and the superficial gas velocity is of the order of twice the average velocity within the liquid film under these conditions.

5. In order to ensure proper distribution and development of the film experimentally certain precautions must be taken at the inlet, these are:
   (a) The distributor gap should exceed the maximum film thickness, otherwise jetting will occur.
   (b) A protective shield must be installed in order to avoid any undesirable liquid entrainment at the entry. The minimum length of the shield should be about 2cm.

6. Droplet entrainment occurs at a high gas velocity and the critical velocity is a function of the liquid flow rate. The onset of entrainment can be predicted by Andreussi's theory (138).

7. The increase in mass transfer has been related to an increase in the turbulence of the gas phase and the mixing within the liquid film. The effect of the size of the reactor have been demonstrated.

CHAPTER X

FUTURE WORK

The following recommendations for further work are:

1. The ultrasonic measuring technique could be improved, in order to obtain more information on the change in the flow pattern of the liquid film in the transition regime.

2. Measurement of the film thickness should be taken, using different size reactors, at several locations along the length of the reactor, so comparison of the data obtained in this work can be made.

3. Efforts should be directed at obtaining data from industrial absorber-reactors, which could be compared with the parameters estimated in this work.

4. Experiments involving heat transfer should be carried out in order to augment the hydrodynamic and mass transfer study.

APPENDIX A

MEASUREMENT OF GAS-FLOW RATES

A.1 Measurement of Airflow Rates

For air flow measurements, pitot static tubes are provided and these can be mounted in a transversing jig which is placed on top of the air duct and allows readings to be taken in an accurately measured pattern as required by British Standards (B.S.S. 848). See figure A.1.

The equipment for pressure reading is a standard precussion, multi-range, inclined tube manometer. When the inlet to the duct is calibrated, an inlet coefficient is obtained, which allows the single reading of static pressure drop to be converted into velocity readings for the duct.

A.1.1 Calibration of the Entry

Following the procedure specified in the British Standards (162) and the I.V.H.E. Guide (163), to test the performance of air fans:

1. Measurements of the pressure drop are taken in a specified pattern of sixteen points in the duct cross-section.

2. The average air velocity is calculated using the expression

$$\bar{U}_a = \frac{1}{16} \sum_{i=1}^{16} U_{ai} = \frac{1}{16} \sum_{i=1}^{16} \left(\frac{2\Delta P}{\rho} \right)^{.5} \qquad (A.1)$$

1. Centrifugal fan
2. Pitot tube
3. Inclined Manometer

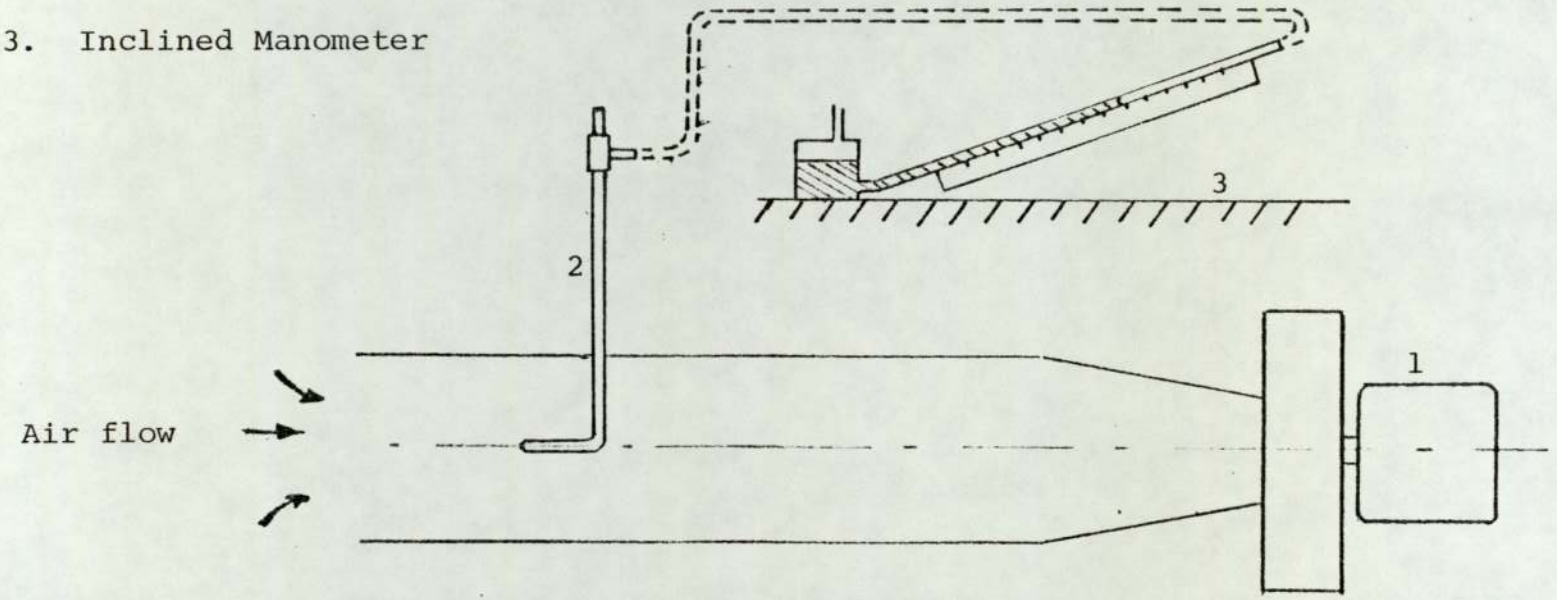

Figure A.1 - Air Duct

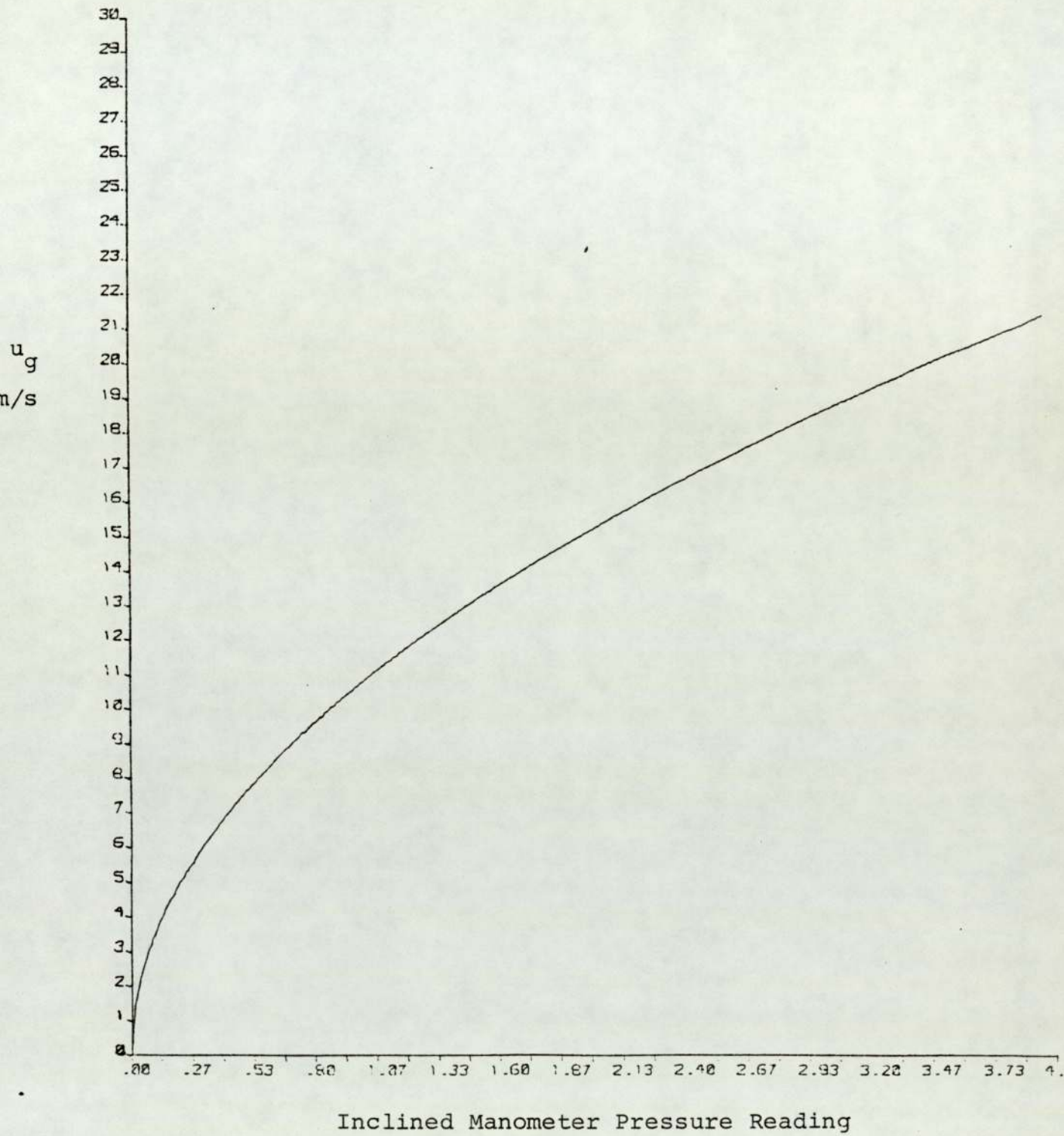

Figure A.2 - Air Flowrate Calibration

3. The volumetric air flow is obtained

$$Q_a = \bar{U}_a A_1 \qquad (A.2)$$

where A_1 is the area of the cross-section of the air duct.

4. Dividing the volumetric air flow by the cross-sectional area of tubular reaction, the air velocity is finally obtained.

$$U_a = Q_a/A \qquad (A.3)$$

5. Measurements of the pressure drop at the centre of the air duct are taken (Δp_c)

After following the above described procedure, a graph correlating the air velocity vs ΔP_c was obtained (figure A.2).

The density of air is 1.2kg/m^3 and the absolute viscosity (μ) is 1.81 x 10^{-5} kg/ms, at atmospheric pressure and 20^{o}C temperature.

A.2 Ammonia Flow Rate

The volumetric flow rate of gaseous ammonia was measured with a glass rotameter, tube size 35, fitted with a duralumin float.

A.2.1 Calibration

The method used to calibrate the rotameter is described in the manufacturer's booklet, "Calibration Data for 'Metric' Series Rotameters".

The rotameter constants are:

weight of float, ω = 27.71g

density of float, σ = 2.80g/cc

K_1 = 1.5 K_2 = 3.30

The density and kinematic viscosity for ammonia at working conditions are

ν = .1322 Stokes

ρ = .71877 x 10^{-3} gr/cc

The formulae used were,

$$I = \log \{ K_1 \quad \nu \left(\frac{\sigma \quad \rho}{\omega \quad (\sigma-\rho)}\right)^{.5} \cdot 10^4 \} \qquad (A.4)$$

$$F_T = K_2 \left(\frac{\omega \ (\sigma-\rho)}{\sigma \quad \rho}\right)^{.5} \qquad (A.5)$$

The values obtained were:

$I = 1.004$

$F_T = .0109 \ m^3/sec$

F_T represents the "theoretical" capacity. Using the chart provided by the manufacturer, we obtained the values of f (the ratio of the actual flow, F, by the "theoretical capacity". Figure A.3 contains the calculated values of F and its corresponding value in the rotameter scale, and graph showing the correlation F vs scale reading.

f	.1	.2	.3	.4	.5	.6	.7	.8	.9	1.
F, $m^3/s \times 10^{-3}$	1.09	2.18	3.27	4.63	5.45	6.64	7.63	8.72	9.81	10.09
scale reading	0	3.5	6.75	9.9	12.8	15.7	18.4	21.2	23.6	26.1

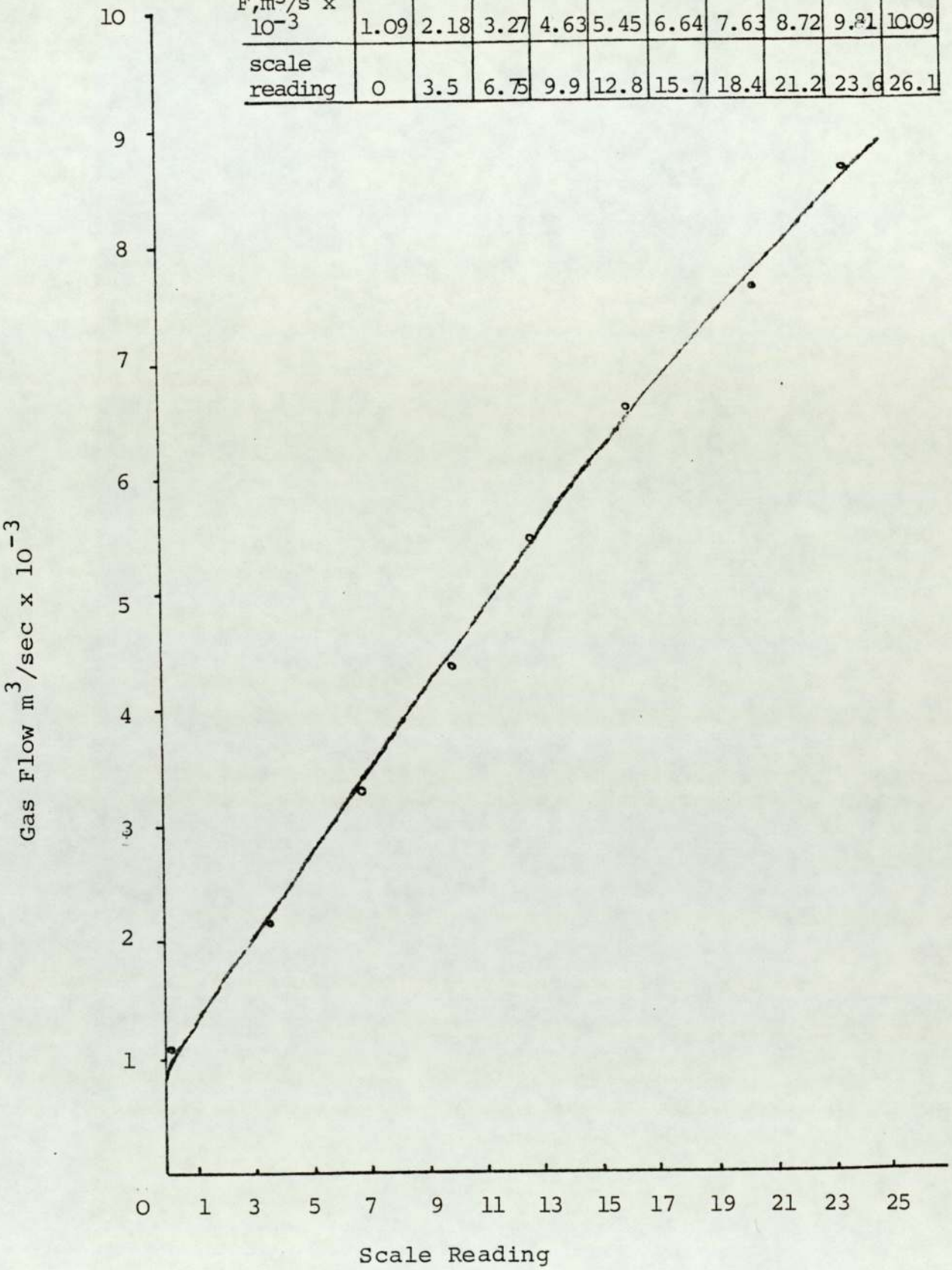

Figure A.3 - Calibration Curve, Rotameter Size 35, For Ammonia Gaseous Flow Rate

APPENDIX B

ULTRASONIC EQUIPMENT

B.1 General Specification for UFD.2M

SIZE: (with standard battery pack) 255 x 90 x 330mm)

WEIGHT: (" " " ") 6½ Kgs

TIME BASE RANGE:

10mm to 3 metres in steel (0.5 to 10ft)

FREQUENCY RANGE:

0 to 100 dB in 1 dB steps

DISPLAY:

70mm x 55mm High brilliance display with interchangeable graticules.

TIME BASE DELAY:

1000 mm on ten turn calibrated control.

PULSE REPETITION FREQUENCY (P.R.F.)

Is changed when time base range is changed.

REJECT:

More than 10 dB

LINEARITY:

Better than 1.5%

SENSITIVITY:

Full scale deflection for 130 microvolts R.M.S.

TEMPERATURE RANGE:

Equipment can be used from -20°C to +65°C temperature

(All ranges and delays given in mms of steel)

(Velocity of sound 5930 metres per second)

B.2 Additional Specification for Monitor Incorporated in UFD.2M

MONITOR SENSITIVITY:

Adjustable to respond to signals from 2mm to 50mm high on C.R.T. display.

GATE START:

Continuous delay up to 100 mm

GATE WIDTH:

Continuously variable up to 100 mm

PROPORTIONAL OUTPUT:

Approximately 2 volts output for 50mm echo on the C.R.T.

GO: NO GO OUTPUT:

Change-over relay contacts having maximum current loading of 500 ma (non-inductive & AC)

B.3 Details of Controls

TIME BASE RANGE SELECT(S):

Six position switch giving coarse selection of time base range. Approximate coverage in steel having velocity of sound of 5930 metres per second are as follows:

Range 1	7 - 25mm
Range 2	16 - 60mm
Range 3	35 - 125mm
Range 4	100 - 360mm
Range 5	300 - 1000mm
Range 6	650 - 3 metres

TIME BASE RANGE CALIBRATION (C):

Continuous control for fine adjustment of calibration with the above ranges.

GAIN CONTROL:

A switched gain control, using two ten step switches, giving 0 - 100 dB control in 1dB steps.

90dB in switched 10dB steps

10dB " " 1dB "

REJECT:

A supression control giving bettern than 10dB of cut-off on a 12 step switch. A switch is used to avoid inadvertent movement of the control. When switched out there is no "built-in" suppression in the amplifier.

FREQUENCY SELECTION:

A rotary switch allows either a 1 - 4MHz or a 3-6MHz band to be selected.

SINGLE-DOUBLE PROBE SWITCH:

This switch allows the mode of inspection to be selected, i.e. in the "SINGLE" position a single transducer, transmit/receive probe is used. In the "DOUBLE" position - combined double probes or separate Tx and Rx probes (e.g. shadow technique) may be used.

N.B. In the "SINGLE" position probes should be connected to the "Tx" socket, i.e. the left hand socket.

B4. Details of Monitor Controls

SENSITIVITY:

The MONITOR SENSITIVITY incorporates the off switch and controls the level at which the monitor will respond, from a minimum sensitivity where a full screen echo is needed to a maximum where an echo of only 2-3mm high will trigger the monitor.

START:

The MONITOR START CONTROL is the delay control which determines the position of the start of the monitor gate.

WIDTH

A continuous control which enables the monitor gate width to be adjusted from 1mm to 100mm.

VISUAL ALARM:

The lamp in the centre of the monitor control cluster is illuminated when the monitor is triggered. At the same time a high frequency audible alarm is sounded.

The monitor control also includes two switches each of which has a double function.

PHASE SWITCH:

This switch has three positions, two of which are marked + and one which is marked -. When in either of the + positions the monitor operates in positive phase, i.e. it produces an alarm signal when an echo

greater than a predetermined size appears in the gate. In the negative phase (-) the monitor gives a signal only when an echo in the gate disappears or falls below the size appropriate to the sensitivity level.

The same switch function as a

DELAY FUNCTION SELECT:

The switch has two positions which are marked "M" and one marked "P".

In the "M" position the delay control governs the TIME BASE DELAY and the start control governs the MONITOR START DELAY.

In the "P" position the delay control remains as the TIME BASE DELAY but the start control becomes a PROBE or ZERO SET DELAY and in this position the delays are additive.

The second switch functions as a

MUTE SWITCH:

In the two positions which are marked MUTE the audible alarm does not operate.

In the third switch position, which is unmarked the audible operates.

This switch also operates as a

SET & DELAY

In the SET position the time base remains undelayed but a marker pulse moves along the trace, when the delay control is moved, to indicate the delay position, i.e. the point on the trace which will move to zero when the delay is introduced.

When the switch is moved to either of the two DELAY positions, the delay operates and the time base starts at the points previously indicated by the marker pulse.

B5. PROPORTIONAL OUTPUT:

As stated in Section 2, the monitor gate will give a voltage output dependant on the height of the echo in the gate to a maximum of approximately 2 volts D.C. for a 50mm echo.

It is dependant on the trigger level of the gate and if more than one echo is in the gate the voltage output is determined by the greatest signal.

The output is between earth and Pin No. 2 on the battery charging socket at the rear of the instrument.

GO: NO GO OUTPUT

There are relay contacts provided which will switch a maximum current loading of 50mmA (non-inductive and A.C.). Connection may be made on Pin Nos. 3 and 4 on battery charging socket at the rear of the instrument.

APPENDIX C

PHYSICAL CONSTANTS

C1. Physical properties of the liquids used in the study of the hydrodynamics of the system.

Table C.1 - Entrance Region Experiments

Set	Liquid	ρ (gr/cm^3)	μ (cP)	ν (cS)	σ (dyn/cm)	t °C
1	water	.999	1.000	1.001	72.70	20
2	sugar soln. 56%	1.265	35.000	27.668	75.00	20
3	glycerol soln. 65%	1.170	15.000	12.820	67.00	20
4	glycerol soln. 80%	1.210	60.000	49.587	66.30	20

Table C.2 - Hydrodynamics Experiments

Set	Liquid	ρ (gr/cc)	μ (cP)	ν (cS)	σ (dyn/cm)	t °C
1	water	.999	1.000	1.001	72.70	20
2	glycerol soln. 63%	1.170	13.104	11.200	67.20	20
3	glycerol soln. 70%	1.180	23.718	20.100	67.00	20
4	glycerol soln. 75%	1.200	34.560	28.800	66.60	20
5	glycerol soln. 80%	1.210	60.000	49.587	66.30	20

C2. Physical properties of the sulphuric solution used in the mass transfer with chemical reaction experiments at 20°C.

Weight % H_2SO_4 in water $\simeq$ 10.0

Density = 1.027 gr/cc (Density of H_2SO_4 = 1.83 gr/cc)

Viscosity = 1.088 cPoise

Absolute Viscosity = 1.060 cStoke

Surface Tension = 73 Dyn/cm

Molarity = 1.0 grMol/lt. (Molecular weight of H_2SO_4 = 98.08 g/mol)

C3. Physical properties of gases at 1 atm, 20°C.

Gas	ρ (gr/cc)	μ (cP)	ν (cS)	Molecular weight gr/mol
Air	.001204	.01813	15.05	29.00
Ammonia	.00720	.0098	13.61	17.03
3% Ammonia-air mixture	.001190	.01788*	15.03	28.64

* The viscosity of the ammonia-air mixture was calculated, using the semiempirical formula of Wilke (164) for gas mixtures.

APPENDIX D

DEFINITION OF THE REYNOLDS NUMBERS

D1. Liquid Phase

The characteristic dimension of length in the Reynolds number equation for falling film is the average film thickness $\bar{\delta}$, and the velocity used is the average velocity $\bar{u}$, so it is written as

$$Re = \frac{4\bar{u}\,\bar{\delta}}{\nu} \tag{D.1}$$

But since

$$\Gamma = \bar{u}\,\bar{\delta} \tag{D.2}$$

So the above expressions are used to define the Reynolds number in the liquid phase

$$Re = \frac{4\Gamma}{\nu} \tag{D.3}$$

or its equivalent

$$Re = \frac{4\Gamma P}{\mu} \tag{D.4}$$

D2. Gas Phase

The characteristic dimension of length in the expression for the gas-phase Reynolds number is the hydraulic radius R_h, which is defined as the ratio of the cross-sectional area to the perimeters length.

$$R_h = \frac{\pi}{2\pi} \frac{(r_o^2 - r_i^2)}{(r_i + r_o)} = \frac{1}{2}(r_o - r_i) \tag{D.5}$$

So the following equation is used to define the Reynolds number

$$Re_g = 4\ R_h\ \bar{u}_g\ \rho_g/\mu_g \qquad (D.6)$$

of after substitution

$$Re_g = 2(r_o - r_i)\ \bar{u}_g/\nu_g \qquad (D.7)$$

APPENDIX E

APPROXIMATED AVERAGE VALUES FOR THE FILM THICKNESS, INTERFACIAL AREA AND SURFACE VELOCITY

E.1 Interfacial Area

The interfacial area can be estimated by approximating it to the curved surface area of a cone. As illustrated in the following figure.

The surface area is given by the expression

$$A = \pi (R + r) \tag{E.1}$$

where

$$r = r_o - \delta_{x=0} \tag{E.2}$$

and

$$R = r_o - \delta_{x=L} \tag{E.3}$$

The length "ℓ" can be calculated using the equation

$$\ell = \sqrt{L^2 + (R-r)^2} \tag{E.4}$$

where L is the total length of the reactor. Combining equations E.2 and E.3

$$\ell = \sqrt{L^2 + (\delta_o - \delta_L)^2} \qquad \text{(E.5)}$$

But $(\delta_o - \delta_L)^2 << L^2$, so expression E1 is rewritten as

$$A = \pi (2r_o - (\delta_o + \delta_L))L \qquad \text{(E.6)}$$

Lets assume an average film thickness $\overline{\delta}$,

$$\overline{\delta} = \left(\frac{\delta_o + \delta_L}{2}\right) \qquad \text{(E.7)}$$

now equation E6 is expressed as

$$A = 2\pi(r_o - \overline{\delta})L \qquad \text{(E.8)}$$

E.2 Surface Velocity

Using the following relationships

$$u_s = 2\overline{u}(x) \qquad \text{(E.9)}$$

$$\overline{u}(x) = \frac{\Gamma}{(x)} \qquad \text{(E.10)}$$

and E.7; an estimated value for the average velocity of the liquid at the interface is given by the following expression

$$\overline{u}_s = \frac{\Gamma}{(\delta_o + \delta_L)}$$

The film thickness at the top and at the bottom of the column is obtained by substituting into equation 7.10.

Table E.1 - Hydrodynamic Parameters for the Mass Transfer Experiments

Run	δ $\times 10^2$ m	$\bar{A}$ m^2	$\bar{u}$ m/s	$\bar{u}$ m/s	a_v $\frac{1}{m}$	Re''_g	Re'_g	τ s
1	.0378	1.9178	.7613	1.5226	28.773	42890	38446	2.68
2	.0366	1.9180	.7141	1.4282	28.776	42730	38957	2.86
3	.0353	1.9181	.6601	1.3201	28.778	43029	39541	3.09
4	.032	1.9185	.5586	1.1163	28.783	43598	40648	3.65
5	.0390	1.9177	.7381	1.4761	28.772	34233	30335	2.76
6	.0377	1.9178	.6923	1.3846	28.773	34486	31380	2.95
7	.0369	1.9180	.6401	1.2802	28.776	34773	31391	3.19
8	.0334	1.9184	.5419	1.0838	28.182	35319	32453	3.76
9	.0404	1.9175	.7138	1.4275	28.769	25110	21342	2.86
10	.0390	1.9177	.6792	1.3385	28.772	25354	21820	3.05
11	.0377	1.9178	.6189	1.2377	28.773	25629	22360	3.30
12	.0346	1.9182	.5239	1.0478	28.774	26151	23381	3.89
13	.0415	1.9173	.6948	1.3896	28.776	17445	13778	2.94
14	.0394	1.9176	.6624	1.324	28.770	17625	14127	3.08
15	.0387	1.9177	.6028	1.2057	28.772	17943	14759	3.38
16	.0355	1.9181	.5839	1.1677	28.778	18057	14972	3.49

APPENDIX F

LISTING OF COMPUTER PROGRAMS

F.1 Numerical Solution of the Mathematical Model

```
JOB JF7J5A1,:EAKXX,CP76(T20,P3000)
FTN(SL=0)
LDSET(MAP=B/ZZZZMP,PRESET=NGINF)
LGO.
####S
      PROGRAM JF7J5A1(INPUT,OUTPUT,TAPE1=INPUT,TAPE2=OUTPUT)
C        SOLUTION FOR THE MATHEMATICAL MODEL  OF THE HYDRODINAMICS
C
       COMMON/A1/RL,R
       COMMON/A4/C1,C2,C3,UD2
       COMMON/A6/UO,YO,G
       COMMON/B1/VK,VIS,DEN
       COMMON/B2/VKG,VISG,DENG
       COMMON /B3/VFLOW,VFWP
       COMMON/B4/GVF,VG
       COMMON/B5/N,A
       COMMON/C1/DNUS,B
       COMMON/A7/EFT,DR
       DIMENSION EFT(10),SV(10),YO(50),UO(50),X(50)
       DIMENSION YD(20),Y1(10,30),U(10,30),FF(10),V(20,50),VSQ(20,50)
       DIMENSION C1(50),C2(50),C3(50)
       DIMENSION  PT(50),Y(20,50),VAV(20)
       REAL HD
C        HD,HIDRAULIC RADIUS
C
       CALL RPARAM
C        INTRODUCE PHYSICAL DATA
       CALL PHYDAT
C
C        INTRODUCE FLOW PARAMETERS
       CALL FLOPAR
C
C        G=GRAVITY(980. SQ.CM. PER SEC)
       G=980.
C        HD=HYDRAULIC DIAMETER
       HD=R
       RE=4.*VFWP/VK
       REG=2.*R*VG/VKG
       WRITE(2,70)RE
       WRITE(2,71)REG
C        PD= PRESSURE DROP
       PD=.01*DENG*VG**2/HD+DENG*G
C        NS=NUMBER OF SECTIONS
C        N=NUMBER OF STEPS IN THE Y DIRECTION
       READ(1,50)N
       NP1=N+1
       A=VFWP/N
C        M=NUMBER OF STEPS IN THE X DIRECTION
       READ(1,55)M
```

```
      MP1=M+1
C        SX=STEP LENGTH IN THE X DIRECTION
      SX=RL/M
      CALL INICON
C          INTRODUCE EXPERIMENTALLY DETERMINED FILM THICKNESS
      DO 1000 IFT=1,3
      READ(1,60)EFT(IFT)
      DR=DENG/DEN
      WRITE(2,130)EFT(IFT)
 1000 CONTINUE
      YD(1)=0.0
      YD(2)=1.0/40.0
      YD(3)=0.1
      DO 99 I=4,12
      IM1=I-1
   99 YD(I)=YD(IM1)+0.1
      CALL AVEFT
      DO 2000 IFT=1,4
C
      PT(1)=DNUS
      UD=VG/2.0
      BL=UO(NP1)
      TL=VG
      DO 9 J=1,NP1
      Y(1,J)=YD(J)
      V(1,J)=UO(J)
      VSQ(1,J)=UO(J)**2
    9 CONTINUE
    1 UD2=UD**2
      DO 8 I=2,10
      IM1=I-1
      V(I,1)=0.0
      Y(I,1)=0.0
      V(I,NP1)=UD
      VSQ(I,1)=0.0
      VSQ(I,NP1)=UD2
      DO 19 J=2,N
      JP1=J+1
      JM1=J-1
      C1(J)=VSQ(IM1,JP1)-2.0*VSQ(IM1,J)+VSQ(IM1,JM1)
      C2(J)=(SX*V(IM1,J))/(2.0*(A**2))
      C3(J)=VSQ(IM1,J)+PD*SX+C1(J)*C2(J)
   19 CONTINUE
      CALL TRIDIA(X,N)
      NM1=N-1
      DO 29 J=2,N
      JM1=J-1
      VSQ(I,J)=X(JM1)
      V(I,J)=VSQ(I,J)**0.5
   29 CONTINUE
    8 CONTINUE
      DO 18 I=5,10
      DO 49 J=2,NP1
      JM1=J-1
      Y(I,J)=Y(I,JM1)+(2.0*A)/(V(I,J)+V(I,JM1))
   49 CONTINUE
      PT(I)=Y(I,NP1)
      VAV(I)=VFWP/PT(I)
   18 CONTINUE
      APT=PT(5)
      DO 28 I=6,8
      APT=APT+PT(I)
   28 CONTINUE
      FT=APT/4
      CALL COMPA1(EFT(IFT),FT,BL,TL,KS,UD)
      IF(KS.EQ.1)GO TO 1
```

```
      WRITE(2,101)FT
      AVV=VFWP/FT
      WRITE(2,120)AVV
      SV(IFT)=UD
      VR=SV(IFT)/AVV
      WRITE(2,128)VR
 128  FORMAT(//20X,'RATIO SURFACE VELOCITY TO AV. VEL.',F10.5)
      WRITE(2,2100)
      Y1(IFT,1)=0.0
      U(IFT,1)=0.0
      U(IFT,2)=V(5,2)
      Y1(IFT,2)=(Y(5,2)+Y(6,2)+Y(7,2))/3.0
      JJ=1
      DO 14 J=3,12
      JJ=JJ+4
      Y1(IFT,J)=(Y(5,JJ)+Y(6,JJ)+Y(7,JJ))/3.0
      U(IFT,J)=(V(5,JJ)+V(6,JJ)+V(7,JJ))/3.0
  14  CONTINUE
2000  CONTINUE
      WRITE(2,110)
      DO 2200 J=1,12
      WRITE(2,111)YD(J),Y1(1,J),U(1,J),Y1(2,J),U(2,J),Y1(3,J)
     *,U(3,J),Y1(4,J),U(4,J)
2200  CONTINUE
 110  FORMAT(///6X,'  Y*   ',3X,'   Y1    ',3X,'  U1    ',3X,
     *'  Y2    ',3X,'  U2    ',3X,'  Y3    ',3X,'  U3    ',3X,
     *'  YA    ',3X,'  UA    ')
 111  FORMAT(/3X,F8.5,2X,F8.5,2X,F8.4,2X,F8.5,2X,F8.4,2X,F8.5,
     *2X,F8.4,2X,F8.5,2X,F8.4)
      YD(1)=0.0
      CALL FFCAL(EFT,SV,DR,VG,4,HD)
      WRITE(2,2100)
2100  FORMAT('****************************************')
  50  FORMAT(I2)
  55  FORMAT(I3)
  70  FORMAT(//50X,'REYNOLDS NUMBER=',F12.4)
 130  FORMAT(//50X,'EXPERIMENTAL AVERAGE FILM THICKNESS',
     1F9.4,'CM')
  60  FORMAT(F12.6)
  71  FORMAT(//50X,'REYNOLDS NUMBER=',F12.4,'GAS PHASE')
 101  FORMAT(//50X,'AVERAGE FILM THICKNESS=',F9.4,'CM')
 120  FORMAT(//30X,'AVERAGE VELOCITY',3X,F9.4,'CM PER SEC')
      STOP
      END
      SUBROUTINE COMPA1(A,B,BL,TL,K,C)
       IF(A.EQ.B)GO TO 1
      K=1
      CT=1.0
      E=((A-B)/A)*100.0
      CE=ABS(E)
      IF(CE.LT.CT)GO TO 1
      IF(E.LT.0.0)GO TO 2
      TL=C
      GO TO 3
    2 BL=C
    3 C=(BL+TL)/2.0
      RETURN
    1 K=2
      RETURN
      END
      SUBROUTINE RPARAM
C
C       PARAMETERS OF THE REACTOR
      COMMON/A1/RL,R
      COMMON/A5/AREA,PERO,PERI
C       RL=REACTOR'S LENGTH(CM.)
```

```
      RL=204.
      PI=3.1415927
C       RO=OUTSIDE RADIUS(CM)
      RO=15.00
C       RI=INTERNAL RADIUS
      RI=10.9538
      R=RO-RI
C       AREA=CROSS SECTIONAL AREA (CM)
      AREA=PI*((RO**2.0)-(RI**2.0))
C       PERO=  PERIMETER UTSIDE WALL
      PERO=2.0*PI*RO
C        PERI =PERIMETER INSIDE WALL
      PERI=2.0*PI*RI
      WRITE(2,5)RL,AREA
    5 FORMAT(//50X,'REACTOR LENGTH=',F9.4,10X,'CROSS SECTIONAL AREA=
     1F9.4,'CM2')
      RETURN
      END
      SUBROUTINE PHYDAT
C       SUB-PHYDAT:INTRODUCES PHYSICAL DATA OF THE TWO PHASES
C
C       DEN:  DENSITY OF THE LIQUID PHASE
C       VK:  KINEMATIC VISCOSITY OF THE LIQUID PHASE(STOKES)
C      VIS:  ABSOLUTE VISCOSITY OF THE LIQUID PHASE(POISE)
C       DENG:  DENSITY OF THE GAS PHASE
C       VKG:  KINEMATIC VISCOSITY OF THE GAS PHASE(STOKE)
C       VISG:ABSOLUTE VISCOSITY OF THE GAS PHASE(POISE)
      COMMON/B1/VK,VIS,DEN
      COMMON/B2/VKG,VISG,DENG
       READ(1,5)DEN,VK
       READ(1,5)DENG,VKG
     VIS=VK*DEN
      VISG=VKG*DENG
      WRITE(2,10)
      WRITE(2,20)DEN
      WRITE(2,30)VIS
      WRITE(2,40)VK
      WRITE(2,50)DENG
      WRITE(2,30)VISG
      WRITE(2,40)VKG
    5 FORMAT(2F10.5)
   10  FORMAT(//50X,'**** PHYSICAL DATA ****')
   20  FORMAT(/35X,'LIQUID PHASE',20X,'DENSITY=',F7.4,'GR/CC')
   30  FORMAT(/67X,'ABSOLUTE VISCOSITY=',F7.4,'POISE')
   40  FORMAT(/67X,'KINEMATIC VISCOCITY=',F7.5,'STOKE')
   50  FORMAT(/35X,'GAS PHASE',23X,'DENSITY=',F7.4,'GR/CC')
      RETURN
      END
      SUBROUTINE FLOPAR
C
C       SUB-FLOPAR:  INTRODUCES FLOW PARAMETERS OF THE TWO PHASES
C       VFLOW:  VOLUMETRIC FLOW OF THE LIQUID PHASE
C       VFWP:  VOLUOMETRIC FLOW PER WETTED PERIMETER
C       GVF:GAS VOLUMETRIC FLOW
      COMMON/A5/AREA,PERO,PERI
      COMMON /B3/VFLOW,VFWP
      COMMON/B4/GVF,VG
      READ(1,5)KW
C       KW=1,INSIDE PIPE     KW=2,OUTSIDE PIPE
      IF(KW.EQ.2)GO TO 3
      PER=PERI
      GO TO 6
    3 PER=PERO
    6 CONTINUE
      READ(1,15)VFLOW
      VFWP=VFLOW/PER
```

```
      READ(1,15)GVF
C       VG=LINEAR VELOCITY OF THE GAS PHASE
      VG=GVF/AREA
      WRITE(2,10)
      WRITE(2,20)VFLOW
      WRITE(2,30)VFWP
      WRITE(2,40)GVF
      WRITE(2,50)VG
    5 FORMAT(I1)
   10 FORMAT(///50X,'****FLOW  PARAMETERS ****')
   15 FORMAT(F11.5)
   20 FORMAT(//35X,'LIQUID PHASE',20X,'VOLUMETRIC FLOW=',F10.4,'CC/S'
   30 FORMAT(/67X,'VOLUMETRIC FLOW PER WETTED PERIMETER=',F7.4,'CC/S'
   40 FORMAT(//35X,'GAS PHASE',23X,'VOLUMETRIC FLOW=',F10.2,'CC/S')
   50 FORMAT(/67X,'LINEAR GAS VELOCITY=',F12.4,'C/S')
      RETURN
      END
      SUBROUTINE INICON
      COMMON/A6/UO,YO,G
      COMMON/B1/VK,VIS,DEN
      COMMON /B3/VFLOW,VFWP
      COMMON/B5/N,A
      COMMON/C1/DNUS,B
      DIMENSION YO(50),UO(50),Z(50)
      DIMENSION P(5)
      G=980.0
      DNUS=((3.*VK*VFWP)/G)**(1./3.)
      B=G*(DNUS**2.0)/(2.0*VK)
      NP1=N+1
      Z(1)=0.0
      UO(1)=B
      UO(NP1)=0.0
      Z(NP1)=DNUS
      RN=N
      NM1=N-1
      DO 30 I=1,N
      IP1=I+1
      STEP=DNUS/RN
      L=NP1-I
      LP=L+1
      Z(L)=Z(LP)-STEP
      PV=Z(LP)
    3 CONTINUE
      CALL COMPA(A,Z,L,LP,UO,K)
      IF(K.EQ.1)GOTO 27
      IF(K.EQ.2)GOTO 17
      PV=Z(L)
      Z(L)=Z(L)-STEP
      GOTO 3
   17 P(1)=PV
      P(5)=Z(L)
   18 STEP=ABS((P(5)-P(1))/5.)
      DO 19 I1=2,5
      I2=I1-1
      P(I1)=P(I2)-STEP
      Z(L)=P(I1)
      CALL COMPA(A,Z,L,LP,UO,K)
      IF(K.EQ.1)GOTO 27
      IF(K.EQ.3)GOTO 19
      P(1)=P(I2)
      P(5)=P(I1)
      GO TO 18
   19 CONTINUE
   27 YO(IP1)=DNUS-Z(L)
   30 CONTINUE
      YO(1)=0.0
```

```
      YO(NP1)=DNUS
      DO 20 I=1,NP1
      C=DNUS-YO(I)
      CALL VENUS(B,DNUS,C,UO(I))
      WRITE(2,5)I,YO(I),UO(I)
   20 CONTINUE
    5 FORMAT(50X,'Y(',I2,')=',F9.6,5X,'UO',F9.4)
      RETURN
      END
      SUBROUTINE VENUS(B,D,Z,U)
      U=B*(1.-(Z/D)**2.)
      RETURN
      END
      SUBROUTINE COMPA(A,Z,L,LP,UO,K)
      DIMENSION Z(60),UO(100)
      COMMON/C1/DNUS,B
      CT=0.5
      CALL VENUS(B,DNUS,Z(L),UO(L))
      A1=((UO(LP)+UO(L))/2.)*(Z(LP)-Z(L))
      E=((A1-A)/A)*100.
      CE=ABS(E)
      IF(CE.LE.CT)GOTO 1
      IF(A1.GT.A)GOTO 2
      K=3
      RETURN
    1 CONTINUE
      K=1
      RETURN
    2 CONTINUE
      K=2
      RETURN
      END
      SUBROUTINE TRIDIA(C,N)
C       NUMERICAL SOLUTION OF THE RESULTING TRIDIAGONAL MATRIX
      COMMON/A4/C1,C2,C3,UD2
      DIMENSION A(50),B(50),C(50),D(50)
      DIMENSION C1(50),C2(50),C3(50)
      K=N-1
      KM1=K-1
      A(K)=0.0
      B(1)=0.0
      C(K)=C3(N)+UD2*C2(N)
      DO 1 J=2,K
      JP1=J+1
      B(J)=-C2(JP1)
    1 CONTINUE
      DO 2 J=1,K
      JP1=J+1
      D(J)=1.0+2.0*C2(JP1)
    2 CONTINUE
      DO 3 J=1,KM1
      JP1=J+1
      A(J)=-C2(JP1)
      C(J)=C3(JP1)
    3 CONTINUE
      DO 9 I=2,K
      IM1=I-1
      R=B(I)/D(IM1)
      D(I)=D(I)-R*A(IM1)
      C(I)=C(I)-R*A(IM1)
    9 CONTINUE
      C(K)=C(K)/D(K)
      DO 20 I=2,K
      J=K-I+1
      JP1=J+1
      C(J)=(C(J)-A(J)*C(JP1))/D(J)
```

```
 20   CONTINUE
      RETURN
      END
     SUBROUTINE APPLE(X,Y,N,B,A)
       LINEAR REGRESSION
     DIMENSION X(10),Y(10)
     SUMX=0.0
     SUMY=0.0
     SUX2=0.0
     SUY2=0.0
     SUXY=0.0
     DO 10 I=1,N
     SUMX=SUMX+X(I)
     SUMY=SUMY+Y(I)
     SUX2=SUX2+X(I)**2.
     SUY2=SUY2+Y(I)**2.
     SUXY=SUXY+X(I)*Y(I)
  10 CONTINUE
     AN=N
     XM=SUMX/AN
     YM=SUMY/AN
     B=(SUXY-AN*XM*YM)/(SUX2-AN*XM**2.)
     A=YM-B*XM
     RETURN
     END
      SUBROUTINE FFCAL(EFT,SV,RD,VG,N,HD)
      DIMENSION SV(10),EFT(10),FF(10)
      WRITE(2,10)
      DO 5 I=1,N
      FFG=0.005*(1.0+EFT(I)/(360.0*HD))
      FF(I)=FFG*(RD)*((VG/SV(I))**2.0)
      WRITE(2,20)I,SV(I),FF(I)
   5  CONTINUE
  20  FORMAT(/10X,'UD(',I2,')=',F10.5,5X,'FF',5X,F10.5)
  10  FORMAT(////////////////10X,'FRICTION FACTORS')
      RETURN
      END
      SUBROUTINE AVEFT
      COMMON/A7/EFT,DR
      DIMENSION X(10),EFT(10)
      X(1)=50.0
      X(2)=104.0
      X(3)=204.0
      CALL APPLE(X,EFT,3,B,A)
      EFT(4)=(A+EFT(3))*0.5
      WRITE(2,10)A,B
      RETURN
   10 FORMAT(/10X,'FT=',F10.5,'  +  ',F10.5,' X')
      END
####S
```

```
APPLE

UAFORTRAN
      SUBROUTINE APPLE(X,Y,N,B,A)
C       LINEAR REGRESSION
      DIMENSION X(200),Y(200)
      SUMX=0.0
      SUMY=0.0
      SUX2=0.0
      SUY2=0.0
      SUXY=0.0
      DO 10 I=1,N
      SUMX=SUMX+X(I)
      SUMY=SUMY+Y(I)
      SUX2=SUX2+X(I)**2.
      SUY2=SUY2+Y(I)**2.
      SUXY=SUXY+X(I)*Y(I)
   10 CONTINUE
      AN=N
      XM=SUMX/AN
      YM=SUMY/AN
       VARX=0.0
       VARY=0.0
       DO 20 I=1,N
       VARX=VARX+(X(I)-XM)**2.0
       VARY=VARY+(Y(I)-YM)**2.0
   20  CONTINUE
       VARX=VARX/AN
       VARY=VARY/AN
       B=((SUXY/AN)-(XM*YM))/VARX
       A=YM-B*XM
       RSQ=(VARX*(B**2.0))/VARY
       R=SQRT(RSQ)
       WRITE(2,17)B,A,R
   17  FORMAT(///20X,'SLOPE=',F10.5,'    *  INTERCEPTION=',F10.5,'
     1RESSION',F12.6)
       RETURN
       END
****
```

F.2 - Linear Regression Program

APPENDIX G

CHEMICAL ANALYSIS

G.1 Determination of Ammonia in Water

An accurately measured 100 ml of "sample liquid" were added to 100 ml of standard .1N hydrochloric acid. The excess of acid was determined by back-titrating with standard .1N sodium hydroxide. The procedure was as follows (165).

1) 10 ml of solution were placed in a 100 ml conical flask

2) Two drops of methyl red indicator were added to the sample

3) .1N sodium hydroxide solution was pipetted until the first appearance of a yellow colour

4) The number of moles of unreacted hydrochloric acid was determined by the following formula

$$C_{HC\ell} = \frac{.1 \times \text{volume of Na(OH)}}{10 \text{ ml}}$$

5) The absorbed ammonia was determined from the original concentration of hydrochloric acid

$$C_{NH_3} = 2 \times (.1 - C_{HCl})$$

G.2 Determination of Ammonia Absorbed into Sulphuric Acid Solution

The concentration of unreacted acid was determined following the same steps as above. The obtained concentration of sulphuric acid was substrated from the original concentration of sulphuric acid solution.

REFERENCES

1. Hewitt, G.F. and Hall-Taylor, N.S., "Annular Two-Phase Flow," Pergamon Press, Oxford (1970).

2. Wallis, G.B., "One-Dimensional Two-Phase Flow", McGraw-Hill, N.Y. (1969).

3. Duckler, A.E., "Characterization, Effects and Modelling of the Wavy Liquid Interface", Progress in Heat and Mass Transfer", Vol. 6, Pergamon Press, N.Y. (1972).

4. Morris, G.A. and Jackson, J., "Absorption Towers", Butterworths, London (1953).

5. Norman, W.S., "Absorption, Distillation and Cooling Towers," Longmans, London (1961).

6. Sherwood, T.K., Pigford, R.L. and Wilke, C.R., "Mass Transfer", McGraw-Hill, Tokio (1975).

7. Nusselt, W.Z., ver. dtzh. Ing., Z., 60, 569 (1916).

8. Nusselt, W.Z., ver. dtzh. Ing., Z., 60, 549 (1916).

9. Alves, G.E., Chem.Engng.Prog., 66, 7 (1970).

10. Fulford, G.D., "Advances in Chemical Engineering", 5, Academic Press, 151 (1962).

11. Hobler, T. and Kedzierski, S., Int.Chem.Engng., 7, 654 (1967).

12. Gilliland, E.R. and Sherwood, T.K., Ind.Eng.Chem., 26, 516 (1934).

13. Shilimkan, R.V. and Stepanek, J.B., Chem.Engng.Sci., 32, 1397 (1977).

14. Shilimkan, R.V., Ph.D. Thesis, University of Salford, 1975.

15. Danckwert, P.V. and Sharma, M.M., Chem.Eng., 44, 244 (1966).

16. Danckwert, P.V., "Gas-Liquid Reactions", McGraw-Hill, N.Y. (1970).

17. Astarita, G., "Mass Tranfer with Chemical Reaction", Elsevier, Amsterdam (1967).

18. Hopf, L., Am.Physik, (4), 32, 777 (1910).

19. Kapitza, P.L., Zh. Eksp. i Teor. Fiz., 18, 3 (1948).

20. Jones, L. and Whitaker, S., A.I.Ch.E.J., 12, 525 (1966).

21. Stainthorpe, F.P. and Allen, J.M., Trans.Inst.Chem. Engrs., 43, 85 (1965).

22. Tailby, S. and Portalski, S., Trans.Inst.Chem.Engrs., 40, 114 (1962).

23. Schlichting, H., "Boundary Layer Theory", McGraw-Hill, N.Y., 1955.

24. Benjamin, T.B., J.Fluid Mech., 2, 554 (1957).

25. Yih, C.S., Phys.Fluid, 6, 321 (1963).

26. Lin, C.C., "The Theory of Hydrodynamic Stability", Cambridge Univ.Press, Cambridge (1963).

27. Krantz, W.B. and Goren, S.L., Ind.Eng.Chem.Fund., 10, 91 (1971).

28. Anhus, B.E., Ind.Engng.Chem.Fund., 11, 502 (1972).

29. Solesio, J.N., A.I.Ch.E.J., 25, 185 (1979).

30. Whitaker, S. and Cerro, R.L., Ch.Eng.Sci., 29, 963 (1974).

31. Levich, V.G. "Physicochemical Hydrodynamics", Prentice Hall, N.J. (1962).

32. Bushmanov, V.K., Zh.Eks.Teor.Fiz., 39, 1251 (1960).

33. Portalski, S., Ind.Engng.Chem.Fund., 3, 49 (1964).

34. Portalski, S., Ch.Eng.Sci., 18, 787 (1963).

35. Massot, C., Irani, F. and Lightfoot, E.N., A.I.Ch.E.J., 12, 445 (1966).

36. Duckler, A.E. and Bergelin, O.P., Ch.Eng.Prog., 48, 557 (1952).

37. Von Karman, T., Trans. ASME, 61, 705 (1939).

38. Nikuradse, J., V.D.J.-Forch. 316, 1 (1933).

39. Kulov, N.N., Vorolitin, V.P., Malyusov, V.A. and Zhavorankov, N.N., Theor.Found. of Chem.Tech., 7, 717 (1973).

40. Telles, A.E. and Duckler, A.E., Ind.Eng.Chem.Fund., 9, 412 (1970).

41. Chu, K. and Duckler, A.E., A.I.Ch.E.J., 20, 695 (1974).

42. Chu, K. and Duckler, A.E., A.I.Ch.E.J., 21, 558 (1975).

43. Salazar, R.P. and Marschall, M., Ind.Engng.Chem.Fund., 13, 289 (1974).

44. Salazar, R.P., Ph.D. Thesis, Univ. of California, Santa Barbara (1976).

45. Portalski, S., Ph.D. Thesis, Univ. of London (1960).

46. Brauer, H., V.D.I. Forsch. 457, V.D.I.-Verlag (1956).

47. Duckler, A.E., Chem.Eng.Prog., 55, 62 (1959).

48. Duckler, A.E., Wicks, M. and Cleveland, R.G., A.I.Ch.E.J., 10, 44 (1964).

49. Henstock, W.S. and Hanratty, T.J., A.I.Ch.E.J., 22, 990 (1976).

50. Kulov, N.N., "Future Energy Production Systems", Vol.1, Academic Press, 245 (1976).

51. Hanratty, T.J. and Engen, J.M., A.I.Ch.E.J., 3, 299 (1957).

52. Cohen, K.S. and Hanratty, A.I.Ch.E.J., 11, 138 (1965).

53. Davies, J.T., Proc.R.Soc. London, Sor A., 290, 515 (1966).

54. Davies, E.J., Van Ourwenkerz, M. and Venkatesh, S., Chem.Engng.Sci., 26, 1979 (539).

55. Hikita H. and Ishimi , K., J.Chem.Eng. Japan, 9, 357 (1976).

56. Hikita, H., Ishimi , K. and Ikeki, H., J.Chem.Eng., Japan, 10, 375 (1977).

57. Gill, W.N. and Sheer, M., A.I.Ch.E.J., 7, 61 (1961).

58. Zhivaikin, L.Ya., Int.Ch.Engng., 2, 337 (1962).

59. Chung, H.S. and Murgatroyd, W., A201, Symp. on Two-Phase Flow, Exeter (1965).

60. Whitman, W.G., Chem.Met.Eng., 29, 146 (1923).

61. Higbie, R., Trans A.I.Ch.E., 31, 365 (1935).

62. Vyazovov, V.V., J.Tech.Phys., USSR, 10, 1519 (1940).

63. Emmert, R.E. and Pigford, R.L., Ch.Engng.Prog., 50, 87 (1954).

64. Kamei, S. and Oishi, J., Mem.Fac.Eng., Kyoto Univ., 18, No.1, (1956).

65. Nguiyen-Li, L.A., Carbonell, R.G. and McCoy, B.J., A.I.Ch.E.J., 25, 1015 (1979).

66. Whitaker, S. and Pigford, R.L., A.I.Ch.E.J., 12, 741 (1966).

67. Plevan, R.E. and Quinn, J.A., A.I.Ch.E.J., 12, 894 (1966).

68. Pigford, R.L., Ph.D. Thesis, University of Illinois, (1941).

69. Davidson, J.F. and Cullen, E.I., Trans.Int.Ch.Engrs., 35, 56 (1957).

70. Olbrich, W.E. and Wild, J.D., Ch.Eng.Sci., 24, 25 (1969).

71. Tamir, A. and Taipel, Y., Ch.Eng.Sci., 26, 799 (1971).

72. Lynn, S., Straatmeier, J.R. and Kramers, H., Chem.Engng. Sci., 4, 58 (1955).

73. Broetz, W., Chem.Ing.Tech., 26, 470 (1954).

74. Best, R.J. and Horner, B., Chem.Eng.Sci., 34, 759 (1979).

75. Kalthod, D.G. and Ruckenstein, E., Ch.Eng.Com., 7, 195 (1980).

76. Ruckenstein, E., Ch.Eng.J., 2, 164 (1971).

77. Ruckenstein, E. and Barbente, C., Int.J.Heat and Mass Transfer, 11, 743 (1968).

78. Brauer, H., Ch.Eng.Tech., 30, 75 (1958).

79. Hobler, T. and Kedzierski, S., Int.Chem.Eng., 7, 654 (1967).

80. Boyadeev, C. and Mitev, P.L., Ch.Engng.J., 14, 225 (1977).

81. Howard, D.W. and Lightfoot, E.N., A.I.Ch.E.J., 14, 458 (1968).

82. Angelo, J.B., Lightfoot, E. and Howard, D., A.I.Ch.E.J., 12, 751 (1966).

83. Yih, S.M. and Seagrave, R.C., Ch.Engng.Sci., 33, 1581 (1978).

84. Vivian, J.E. and Paceman, D.W., A.I.Ch.E.J., 2, 437 (1956).

85. Hikita, H., Ishimi , K. and Sohoa, K., J.Ch.Eng.J, 12, 68 (1979).

86. King, C.J., A.I.Ch.E.J., 10, 67I (1974).

87. Lamourelle, A.P. and Sandall, O.C., Ch.Eng.Sci., 27, 1035 (1972).

88. Sandall, O.G., Int.J.Heat Mass Transfer, 17, 459 (1974).

89. Subramanian, R.S., Int.J.Heat Mass Transfer, 18, 334 (1975).

90. Gottifredi, J.C. and Quiroga, O.D., Chem.Engng.J., 16, 199 (1978).

91. Menez, G.D. and Sandall, O.C., Ind.Eng.Chem.Fund., 13, 72 (1974).

92. Kayihan, F. and Sandall, O.C., A.I.Ch.E.J., 20, 402 (1974).

93. Yih, S.M. and Seagrave, R.C., Int.J.Heat, Mass Transfer, 23, 749 (1980).

94. Fortescue, G.E. and Pearson, J.R.A., Ch.Engng.Sci., 22, 1163 (1867).

95. Banerjee, S., Scott, D.S and Rhodes, E., Ind.Eng. Chem.Fund., 7, 22 (1968).

96. Batchelor, G.K., "The Theory of Homogeneous Turbulence", Cambridge Univ.Press., Cam. (1953).

97. Henstock, W.H. and Hanratty, T.J., A.I.Ch.E.J., 25 122 (1979).

98. Brumfield, L.K., Houze, R.N. and Theofanus, T.G., 18, 1077 (1975).

99. Chung, D.K. and Mills, A.F., Letters Heat Mass Transfer, 1, 43 (1974).

100. Chung, D.K. and Mills, A.F., Int.J.Heat Mass Transfer, 16, 694 (1973).

101. Won, Y.S., Ph.D. Thesis, U.C.L.A., California (1978).

102. Byers, C.H. and King, C.J., A.I.Ch.E.J., 13, 628 (1967).

103. Hikita, H., Kagaku Kogaku, Chem.Eng.Japan, 23, 23 (1959).

104. Hikita, H. and Ishimi , K., J.Ch.Eng. Japan, 9, 362 (1976).

105. Hikita, H. and Ishimi, K., Chem.Eng.Comm., 2, 181 (1978).

106. Hikita, H., Ishimi, K., Omotehara, Y. and Fusake, T., J.Ch.Eng. Japan, 11, 96 (1978).

107. Kasturi, G. and Stepanek, J., Ch.Eng.Sci., 29, 1849 (1974).

108. Anderson, J.D., Bollinger, R. and Lamb, D.E., A.I.Ch.E.J., 10, 640 (1964).

109. Hughmark, G.A., Ind.Eng.Chem.Fund., 4, 486 (1965).

110. Heuss, J.M., King, C.J. and Wilke, C.R., A.I.Ch.E.J., 11, 866 (1965).

111. Wales, C.E., A.I.Ch.E.J., 12, 1166 (1966).

112. Gregory, G.A. and Scott, D.S., Ch.Eng.J., 2, 287 (1971).

113. Cichy, P.T. and Russell, T.W.F., Ind.Eng.Ch.Fund., 61, 6 (1969).

114. Kasturi, G., Ph.D. Thesis, University of Salford, 1973.

115. Jepsen, J.C., A.I.Ch.E.J., 16, 705 (1970).

116. Cibrouski, J.W. and Rychlicki, R.M., Int.J.Heat and Mass Transfer, 14, 1261 (1971).

117. Lockhart, R.W. and Martinelli, R.C., Ch.Eng.Prog., 45, 39 (1949).

118. Lynn, S., A.I.Ch.E.J., 6, 703 (1960).

119. Wilkes, J.P. and Neddermann, R.M., Ch.Eng.Sci., 17, 177 (1962).

120. Cerro, R.L. and Whitaker, S., Ch.Eng.Sci., 26, 785 (1971).

121. Cerro, R.L. and Whitaker, S., J. of Colloid and Interface Sci., 37, 33 (1971).

122. Stuchèli, A. and Ozisik, M.N., Ch.Eng.Sci., 31, 369 (1977).

123. Yilmaz, T. and Brauer, H., Int.Ch.Eng., 19, 33 (1979).

124. Von Mises, R. and Friedrichs, K.O., "Fluid Dynamics", Applied Mathematical Science, 5, Springer-Verlag, N.Y. 1971.

125. Scriven, L.E. and Pigford, R.L., AIChEJ, 5, 397 (1959).

126. Bruley, D.F., A.I.Ch.E.J., 11, 945 (1965).

127. Hassan, N.A., Trans. ASME, Ser.E, 34, 535 (1967).

128. Hagen, R., Trans ASME, Ser.E, 35, 631 (1968).

129. Ito, R. and Tomura, K., J.Ch.Eng. Japan, 12, 66 (1979).

130. Ito, R. and Tomura, K., J.Ch.Eng. Japan, 12, 10 (1979).

131. Perry, R.H. and Chilton, C., "Chemical Engineers' Handbook", McGraw-Hill, N.Y., 1973.

132. Henderson, F.M., "Open Channel Flow", McMillan, London (1966).

133. Pierson, F.W. and Whitaker, S., Ind.Eng.Chem.Fund., 16, 401 (1977).

134. Hanratty, T. and Hershman, A., AIChEJ, 7, 488 (1961).

135 Zuber, N., Ge.Elec.Co. Report, 62GL, 153 (1962).

136. Brodkey, R.S., "The Phenomena of Fluid Mationss, Addison-Wesley, Massachusets (1967).

137. Ishii, M. and Grolmes, M.A., A.I.Ch.E.J., 21, 308 (1975).

138. Andreussi, P., Can.J.Chem.Eng., 58, 267 (1980).

139. Van Rossum, J.J., Ch.Eng.Sci., 11, 35 (1959).

140. Hughmark, G.A., A.I.Ch.E.J., 19, 1062 (1973).

141. Hoffman, M.A. and Potts, W., Ind.Chem.Fund., 18, 27 (1979).

142. Hartley, D.E. and Murgatroyd, W., Int.J.Heat Mass Transfer, 7, 1003 (1964).

143. Murgatroyd, W., Int.J.Heat Mass Transfer, 8, 297 (1965).

144. Hewitt, G.F. and Lacey, P.M., Int.J. Heat Mass Transfer, 8, 781 (1965).

145. Ruckenstein, E., Int.J. Heat Mass Transfer, 14, 165 (1971).

146. Ponter, A.B., Davies, G., Ross, T.K. and Thornley, P.G., Int.J.Heat Mass Transfer, 10, 349 (1967).

147. Chung, J.C. and Bankoff, S.G., Chem.Eng.Comm., 4, 455 (1980).

148. Zuber, N. and Staub, F.W., Int.J.Heat Mass Transfer, 9, 897 (1966).

149. Hobler, T. and Czajka, J., Chemia Stosow, 2B, 169 (1968).

150. Hobler, T. and Czajka, J., Chemia Stosow, 2B, 201 (1965).

151. Bankoff, S.G., Int.J.Heat Mass Transfer, 14, 2143 (1971).

152. Mikielewicz, J. and Moszinski, J.R., Int.J.Heat Mass Transfer, 19, 771 (1976).

153. Ponter, A.B. and Aswald, K.M., Int.J.Heat Mass Transfer, 20,575 (1977).

154. Norman, W.S. and McIntyre, V., Trans.Instn.Chem.Eng., 38, 52 (1968).

155. Munakata, T., Watanabe, K. and Miyashita, K., J.Chem.Eng., Japan, 8, 440 (1975).

156. Iijima, T. and Kuzouka, T., Kagaku Kogaku, 32, 52 (1968).

157. Ponter, A.B. and Boyers, A.P., J.Chem.Eng., Japan, 5, 80 (1972).

158. Ames, W.F., "Non-Linear Partial Differential Equations in Engineering", Academic Press, N.Y. (1965).

159. Mitchell, A.R. and Thomson J.Y., Z.angew. Math.Phys., 9, 26 (1958).

160. Ames, W.F., "Numerical Methods for Partial Differential Equations", Nelson London (1969).

161. C.R.C. Handbook of Chemistry and Physics, C.R.C. Press, Florida (1980).

162. British Standard 848: Part 1, 10 (1963).

163. I.V.H.E. Guide, Vol. C, p.4, section G4 (1970).

164. Bishop, R.B., Stewart, W.E., and Lightfoot, E.N., "Transport Phenomena", Wiley, N.Y. (1960).

165. Beltcher, R., Nutten, A.J. and McDonald A.M., "Quantitative Inorganic Analysis", Butterworths, London.

166. Tatterson, D.F., Dallman, J.C. and Hanratty, T.J., AIChEJ., 23, 67 (1977).

167. Tatterson, D.F., Ph.D. Thesis, University of Illinois, 1975.

168. Johnson, G.R. and Crynes, B.L., Ind.Eng.Chem., Proc.Des. Develop, 13, 6 (1974).